1979

Morphological characterization of reaction injection molded (rim) polyurethanes.

Israel David Fridman
University of Massachusetts Amherst

MORPHOLOGICAL CHARACTERIZATION OF REACTION INJECTION MOLDED (RIM) POLYURETHANES

A Thesis Presented

By

ISRAEL DAVID FRIDMAN

Approved as to style and content by:

Edwin L. Thomas, Chairperson of Committee

William J. MacKnight, Member

Richard S. Stein, Member

William J. MacKnight, Department Head
Polymer Science and Engineering

MORPHOLOGICAL CHARACTERIZATION OF REACTION INJECTION MOLDED (RIM) POLYURETHANES

A Thesis Presented

By

ISRAEL DAVID FRIDMAN

Submitted to the Graduate School of the
University of Massachusetts in partial fulfillment
of the requirements for the degree of

MASTER OF SCIENCE

September 1979

Polymer Science and Engineering

Rogelius, Gracias.

ACKNOWLEDGMENTS

I am indebted to Professor Edwin L. Thomas for his guidance, patience and encouragement throughout the course of this project. I have benefited from his knowledge and experience both personally and professionally.

I wish to thank Professor Christopher W. Macosko and Dr. L.J. Lee from the Chemical Engineering and Materials Science Department of the University of Minnesota for the preparation of the RIM polyurethanes and for numerous suggestions and valuable discussions.

Thanks also go to Dr. Richard J. Zdrahala from the chemicals and plastics division of Union Carbide Corporation for the synthesis of the special hand cast polyurethane used in this study.

My friends An-Lou Chang, Dr. Anand K. Khulshreshta and Louis E. Raboin deserve my warmest gratitude for their pleasant and beneficial association.

This study was made possible through a financial support given to me by the Department of Polymer Science and Engineering at the University of Massachusetts, and through a grant-in-aid from the Union Carbide Corporation. This contribution is gratefully acknowledged.

ABSTRACT

A relatively new polymer processing method, Reaction Injection Molding, known as RIM, can be used to manufacture polyurethane molded parts directly from liquid monomers and oligomers by fast, in situ polymerization. RIM requires lower energy and equipment costs than a comparable thermoplastic melt operation, and the restrictions regarding the shape and size of a RIM part are minimal.

The elastomeric RIM market is connected primarily to automotive applications and therefore the market potential is quite large. Yet, there is little fundamental understanding on how the RIM process influences the morphology of the polymer formed and how the morphology in turn affects the physical and mechanical properties of these materials.

RIM polyurethanes based on Poly-ε-caprolactone diol/ 4,4'-diphenylmethane diisocyanate/butane diol (PCP/MDI/BDO) with 1/6/5 mole ratio (43% weight of hard segment) were subjected to different mold temperatures and characterized using differential scanning calorimetry (DSC), wide angle x-ray scattering (WAXS), transmission electron microscopy (TEM), and polarized light microscopy. In this study we present results that show a significant effect of mold wall

temperature on the morphology and molecular weight of RIM processed polyurethanes.

The problem of hard segment domain configuration in crystalline polyurethanes is also investigated. Chemical staining of the unsaturated hard segment portion of a segmented polyurethane based on propylene oxide/MDI/butene diol permitted observation of the hard segment domains by electron microscopy. Hard segment domains are fibrillar in nature. The fibrils are arranged radially into spherulites. The concentration of the hard segment is greatest at the center of the largest spherulites, suggesting the preferential agglomeration of molecules with the longest hard segment sequences at the beginning of the phase separation process from solution.

TABLE OF CONTENTS

LIST OF TABLES

LIST OF FIGURES

Figure

C H A P T E R I

INTRODUCTION

Almost all practical polymeric materials--fibers, rubbers, coatings, adhesives, rigid and elastic foams, etc.--can be based on polyurethanes. The possibility of obtaining such diverse materials is determined by peculiarities of the chemical structure of the polyurethanes, which in turn are determined by the structure of the initial components and the conditions of synthesis. Polyurethane chemistry has been extensively characterized over the past thirty years, but only recently have investigators put emphasis on characterizing the morphological features which are responsible for the physical and mechanical properties of these materials. No studies, however, have been yet focused on characterizing the morphology of polyurethanes that are subjected to flow conditions and heat transfer at the time of polymerization. With this type of in-situ polymerized urethanes, the subject of the present study, one can expect influences from mixing-flow, monomer-polymer diffusion, and heat transfer effects on the resultant morphology and consequently on the final physical properties.

1.1 General Perspective

Polyurethanes represent a very large class of polymers, often varying widely in chemical nature and chain structure, but always containing the urethane linkage -NH-COO-. The group of polyurethanes studied here are termed thermoplastic segmented polyurethanes. They are usually prepared by a random step growth polymerization of stoichiometric amounts of an aromatic or aliphatic diisocyanate, a low molecular weight diol or diamine, and a polyester or polyether macroglycol with a number-average molecular weight of 1000 to 3000. They are linear block copolymers of the general type $-(A-B)_n-$, where one block (A) of the polymer chain, the macroglycol, is above its Tg at normal operating conditions, imparting to the material a flexible character. The other block (B), a copolymer of the low molecular weight diol or diamine and the diisocyanate, has a Tg well above ordinary operating conditions, imparting to the polymer a stiff, inflexible character. These two types of blocks are commonly referred to as "soft" and "hard" segments respectively. As a result of the random polymerization process a whole range of segment, or block lengths are produced (see Figure 1.1-1). The macroglycol blocks are accompanied in the chain by sequences comprising diisocyanate units and low molecular diols or diamines (called chain extenders, or chain lengtheners), therefore

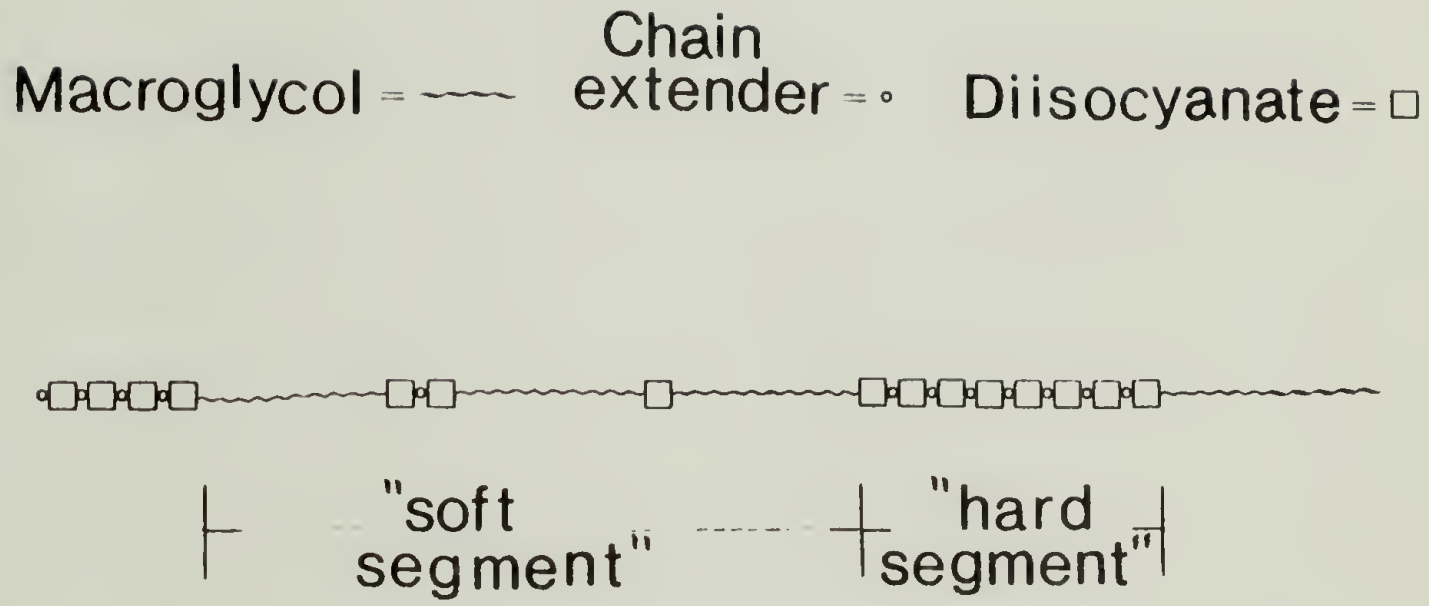

Figure 1.1-1. Schematic of segmented polyurethane structure showing soft and hard segment copolymers.

the term segmented polyurethanes. The term block polyurethanes is also applicable, but these compounds differ from traditional block copolymers in the relative small size of their blocks and block size distribution. Also, the molecular weight of these blocks is smaller than regular block copolymers, causing the number of them in the chain to be far larger.

The polar nature of the urethane group in the hard segments, and in some cases the hydrogen bonding ability, results in a strong molecular association between the hard segments. This molecular association causes the polymer to undergo phase separation into hard segment rich regions. These so-called domains act as tie points, or physical crosslinks, for the flexible soft segment phase and provide the material with practical high modulus and elastomeric properties. Segmented polyurethanes have then the properties both of thermoplasts and of elastomers, and have been termed thermoplastic elastomers (thermoelastoplasts).

A large amount of research has been aimed at a general understanding of phase separation in regular block copolymer systems,[1,2] but in the case of segmented polyurethanes, with distributions of block lengths and domain sizes, as well as the possibility of hard and/or soft segment crystallinity, rather little has been done on their morphological characterization. The distribution of block lengths will tend to increase compatibility between the hard

and the soft phases, resulting in more diffuse phase boundaries than in a regular block copolymer, and in appreciable mixing of the shorter hard and soft sequences. In the limiting case of a regularly alternating block copolymer, a single homogeneous phase is obtained. The size of inhomogeneities of phase separated systems will be a function of both the length of the individual blocks and the degree of thermodynamic equilibrium attained.

An additional element of complexity is attached to the problems mentioned above, when process variables such as flow and heat transfer are introduced during the preparation of the polymer. That is precisely the case in reaction injection molding of polyurethanes.

Reaction injection molding (RIM)--also known by such variants as liquid reaction molding or liquid injection molding--is a fully automatic process characterized by high velocity impingement mixing of low viscosity monomers or oligomers in a small chamber and immediate injection of the reacting mixture into a closed mold. A schematic diagram of the RIM process is shown in Figure 1.1-2. For urethane polymerization during RIM it is fundamental to understand how the process influences the molecular weight and sequence distributions, and the structure and properties of the polymer formed. The urethane polymerization reaction is highly exothermic and RIM parts can develop a temperature profile due to the low thermal conductivity of the polymer formed.

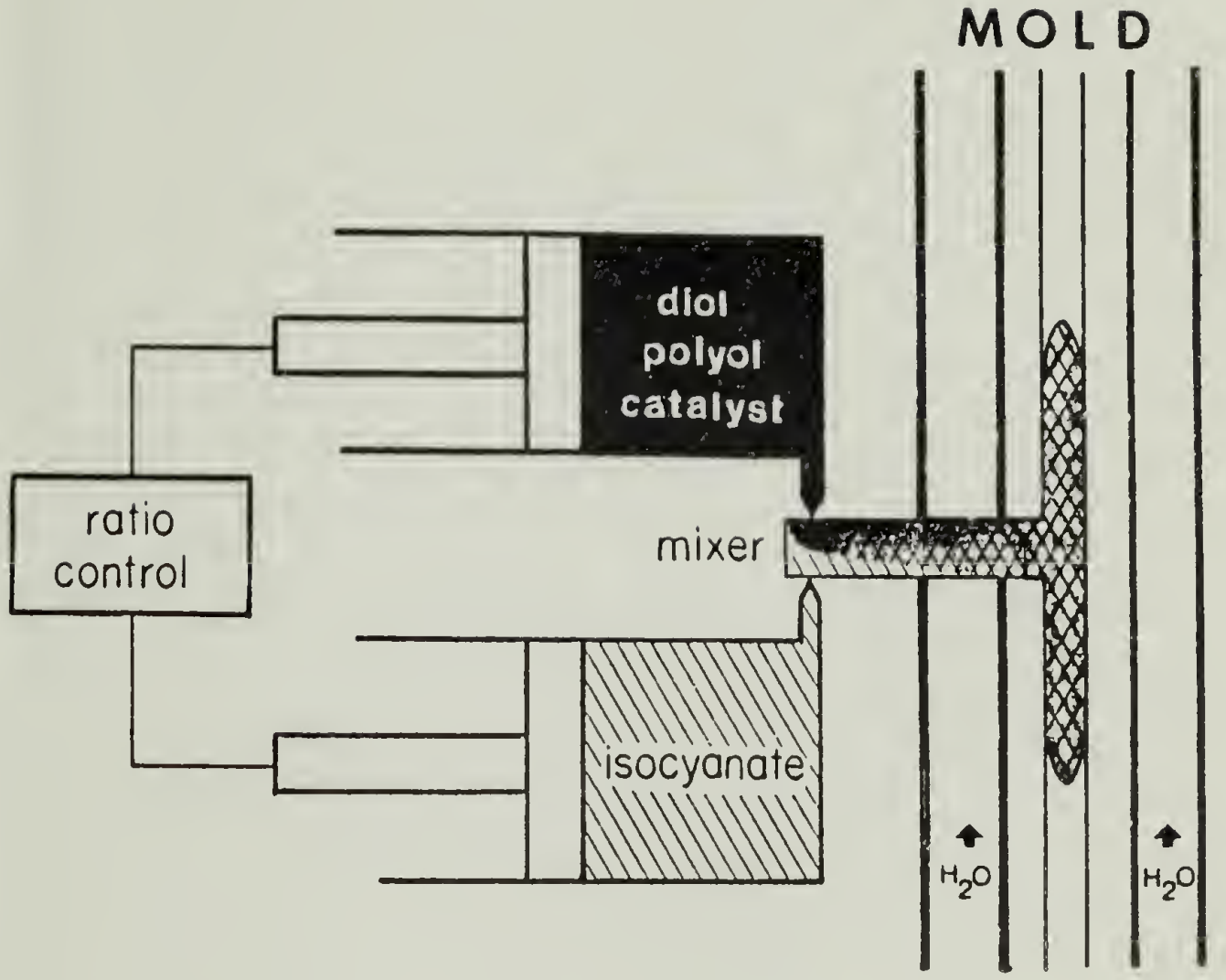

Figure 1.1-2. Schematic diagram of the reaction injection molding (RIM) process (after Lee[78]), showing impingement mixing of the polyol/diol/catalyst and di-isocyanate streams.

Temperature and conversion profiles may bring about non-uniformities in molecular weight and segment distributions, domain formation, crystallinity, etc., and these in turn will influence the final mechanical properties. When the urethane polymerization is catalyzed, the reaction is very fast. The mold must be filled within 2 to 3 seconds, and material must reach its furthest extremities before any setup occurs (usually in as little as 5 seconds). The part is then demolded and the mold reclamped. A complete cycle typically takes less than one minute.

The advantages of RIM on the industrial scale are clear: (1) the use of liquid components means that the injection step can be carried out at low pressures, resulting in lower pumping equipment cost and energy requirements than for an equivalent thermoplastic melt operation. For example, the table below compares the calculated clamp pressures in RIM vs. a comparable injection molding operation.[10]

Projected Area (sq. in.)	Calculated Clamp Pressure (tons)	
	Injection Molding	RIM
65	114	24
585	1000	60
2342	4100	88
3187	5700	120

(2) The rapid gelation time and quick buildup of mechanical properties allows relatively short mold cycle times. (3)

Restrictions regarding the shape and size of a part are minimal.

According to some estimates,[3] 200 million pounds of polyurethane RIM parts will be produced in 1980 for automotive applications alone. Due to this growth, a better understanding of the materials produced is certainly called for. A number of qualitative descriptions of RIM machinery have appeared[4-7] and some basic studies are being carried out.[8,9,11-14] However, to this date, there is no fundamental understanding on how the process influences the morphology of the polymer formed.

1.2 Thesis Problem

The present work represents a first attempt to study the morphology of RIM processed polyurethanes and to provide some insight into the problem of how the complex polymerization-phase separation-crystallization process during RIM affects the structure and properties of the materials produced. This study investigates the problems of phase separation, degree of order, and presence of superstructures as a function of relative location in the mold, processing temperatures and curing times.

For these purposes a multifaceted experimental approach was chosen. A number of RIM polyurethanes were examined using transmission electron microscopy (TEM), polarized light microscopy, differential scanning calorimetry

(DSC), and wide angle x-ray scattering (WAXS) techniques. The chemical system used consists of: (a) a polyester soft segment based on poly-ε-caprolactone diol (PCP-0200, Union Carbide Co.) with number average molecular weight of 2000; (b) a hard segment made of 4,4'-diphenylmethane diisocyanate (MDI-Mondur PF, Mobay Chemical Co.) and (c) a chain extender, 1,4-butanediol (BDO, Aldrich Chemical Co.). An especially prepared batch-polyurethane used in this work consists of atactic poly(propylene oxide)polyol endcapped with ethylene oxide (PPO, $\bar{M}_n$=2000), MDI and 1,4-dihydroxy butene-2 or butene diol (BEDO) as the chain extender.

Our attention is focused primarily on providing unambiguous visualization of domains, and on the correlation of morphology in RIM polyurethanes with processing conditions.

1.3 Thesis Organization

The thesis is organized in the following manner: Chapter I introduces the problem and states the purpose of the thesis. Chapter II reviews previous work on polyurethane morphology. Included are types of polyurethanes investigated, proposed structural models and segment crystallinity, a discussion of the block length distribution, and a compendium of RIM literature. Chapter III describes the instrumentation and experimental techniques employed, as well as specimen preparation and a detailed depiction of a

RIM machine. Chapter IV includes the experimental results and discussion sections of a chemical staining experiment done on solution cast polyurethane films, providing direct imaging of hard segment domains. The experimental results and discussion sections on RIM polyurethane samples are presented in Chapters V and VI, respectively. Chapter VIII states the main conclusions of the thesis and discusses possible extensions of the present work.

C H A P T E R I I

LITERATURE REVIEW OF POLYURETHANE MORPHOLOGY

In this chapter we present a brief review of previous morphological work on polyurethanes including structural models, segment crystallinity and domain formation. Special emphasis is on studies using MDI/BDO based systems. A compendium of RIM studies to this date is presented.

2.1 Types of Polyurethanes Previously Investigated

A large number of polyurethane systems have been previously investigated. Most morphological data for these systems is based on wide angle x-ray scattering (WAXS),[15-25] small angle x-ray scattering (SAXS),[15,21-27] optical microscopy,[15,23-25] small angle light scattering (SALS),[16,23,24,28] infrared (IR),[24,29-31] and nuclear magnetic resonance (NMR),[32,33] with relatively few direct observations of domains via transmission electron microscopy (TEM).[15,21,23,25,34-37]

A summary of the systems and their investigators is shown in Table 2.1-1.

2.2 Compatibility and Domain Formation

The thermodynamic expression that accounts for the

TABLE 2.1-1

SUMMARY OF STRUCTURAL STUDIES OF POLYURETHANE SYSTEMS

System	Investigator
1. PCP/MDI/BDO	Present study, Chang,[45] Seefried et al.[49,81,84]
2. PTMA/MDI/BDO	C. Wilkes,[22] G. Wilkes,[27] Koutsky[34]
3. PTMO/MDI/BDO	G. Wilkes,[1,27] Koutsky,[34] Clough,[16] Cooper[67]
4. EO-PO/MDI/BDO	Schneider[15]
5. PO/MDI/EO	Aggarwal[1]
6. PBA/MDI/BDO	Clough,[16,26] Cooper [29,31,50,67]
7. PEA/MDI/BDO	Miller,[55] Bonart[17-19]
8. PTMO, PBA/TDI/BDO	Schneider[30]
9. PTMO/MDI/EDA, PDA, HH, DAM	Bonart,[17-19] Kimura[24,36,37]
10. PB/TDI/HDO, HPA	Lagasse[21,25]
11. PTMO/ 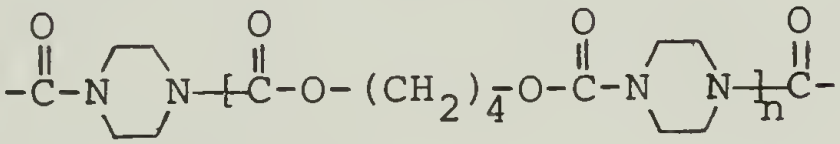	Harrell,[47] G. Wilkes[23,27,35]
12. PTMO, PCP/TODI/BDO	Lagasse[25]

Key: PCP = polycaprolactonediol; PTMA = poly(tetramethylene adipate); PEA = poly (ethylene adipate); PTMO = PTMG = (polytetramethylene oxide); EO-PO = ethylene oxide-propylene oxide; PBA = poly(1,4-butylene adipate); HDI = hexamethylene diisocyanate; TDI = toluene diisocyanate; EDA = ethylene diamine; PDA = propylene diamine; HH = hydrazine; DAM = diamino diphenyl methane; PB = polybutadiene; HDO = hexanediol; HPA = hydroxy propyl aniline; TODI = bitolylene diisocyanate

mixing of two components is:

$$\Delta G = \Delta H - T\Delta S$$

where Gibbs' free energy term ΔG is equal to the change in the enthalpy of mixing (ΔH) minus the change in the entropy of mixing (ΔS), multiplied by the absolute temperature (T). If ΔG is negative a single homogeneous phase will form. If it is positive the two components will segregate into separate phases. This thermodynamic criteria is, in principle, only applicable to equilibrium processes. The common result for the mixing of long chain polymers is that the enthalpy term dominates the free energy equation, resulting in a phase segregated system.

One definition of compatibility[38] is the presence of a single compositionally dependent Tg intermediate between the values which correspond to the pure components. Likewise, the presence of two Tg transitions belonging to the individual components, indicates a phase segregated (incompatible) system. This method, however, is not always conclusive. Clough and Schneider[39] have observed three such transitions in a block polyester-based polyurethane.

Fedors[40] and Meier[41] have studied some aspects of compatibility by deriving criteria for domain formation in block copolymers starting from thermodynamic principles. Fedors' work is based on Flory-Huggins' liquid lattice theory for the mixing of two polymer molecules, and predicts the

minimum molecular weights required for immiscibility in the styrene/butadiene system. Meier postulates expressions for the entropy and enthalpy changes upon mixing, and his prediction on the critical molecular weight for domain formation in the same chemical system is very much in line with that of Fedors'.

The rationale applied by Fedors and Meier considers spherical domains only, but in block copolymer systems layered and cylindrical phases have been reported.[42,43] These thermodynamic arguments have not yet been applied to segmented thermoplastic polyurethane systems.

2.3 Proposed Structural Models and Segment Crystallinity

Both soft and hard domains in polyurethanes can be amorphous or partially crystalline depending on molecular architecture and thermal history. In addition, the overall domain morphology--for which both bicontinuous[44] (see Figure 2.3-1) and discrete-isolated[34] arrangements have been suggested--is a function of block lengths and volume fraction of each type of segment. For many polyurethane systems, besides domain microstructure, spherulitic superstructure is also present[28,35,45] (see Figure 2.3-2).

Hard segment. Bonart and his coworkers[17-19] investigated the domain structure of urethane elastomers by x-ray scattering and proposed two-dimensional and three-

Figure 2.3-1. Schematic representation of proposed two-phase model domain structure (Cooper[31]).

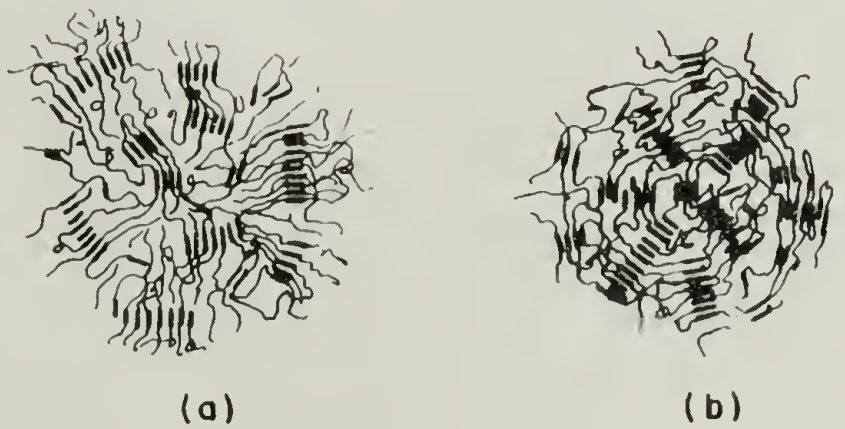

Figure 2.3-2. Two proposed models to account for the spherulitic structure present in segmented urethanes. (a) Chain orientation tangential as hard segments crystallize radially; (b) chain orientation radial as hard segments crystallize tangentially (Samuels[35]).

dimensional models for the MDI/BDO copolymer crystals (see Figure 2.3-3,(a),(b)). They considered the possible alignment of chains to form hydrogen bonded networks and proposed a paracrystalline arrangement of the hard segments. The chains are staggered to allow hydrogen bonding of the urethane groups in either a coplanar or three-dimensional array. Recently, Blackwell and Gardner[46] have determined by x-ray methods a new model for the chain conformation and packing of MDI/BDO hard segments, which consists of a triclinic unit cell. The unit cell parameters are a=5.2Å, b=4.8Å, c=35.0Å, α=115°, β=121°, γ=85° and are the subject of ongoing refinement. They have considered the stereochemistry of the MDI/BDO repeat unit, and found the MDI unit to be "V"-shaped with the two phenyl groups angled 90° at each other (Figure 2.3-4a). The butanediol units are assumed to have a planar zig-zag configuration. Figure 2.3-4b shows a view of the chain packing that allows urethane hydrogen bonding between adjacent chains.

A summary of WAXS data of the MDI/BDO copolymer as found by different authors appears in Table 2.3-1. The differences in intensity of scattering (d-spacings 4.58, 4.07 and 3.77 Å) may be attributed to different degrees of aggregation of hard segments, since the soft segment is different in each system.

Koutsky et al.[34] found that the hard domain size for a polyester based urethane containing 38% hard segment was

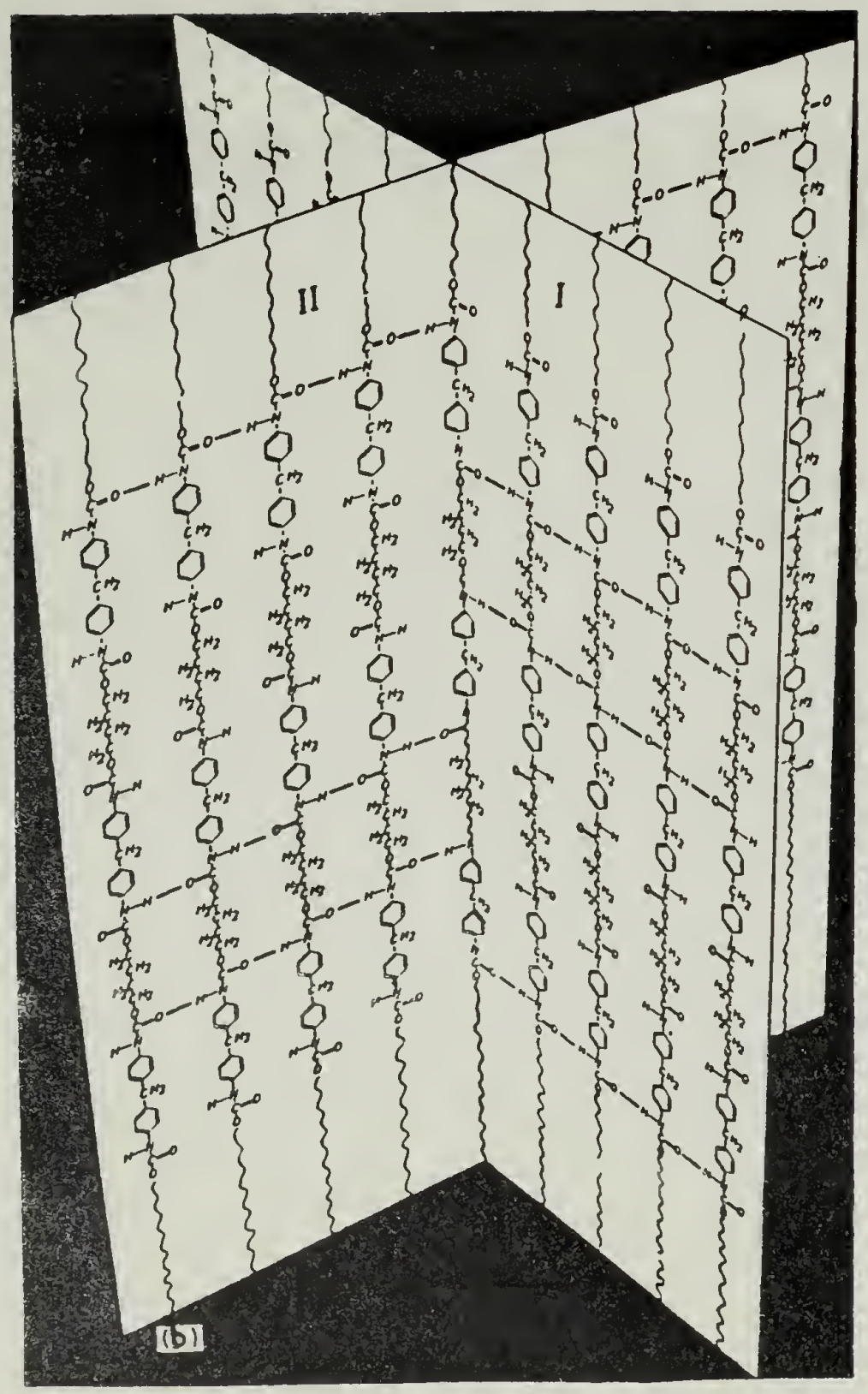

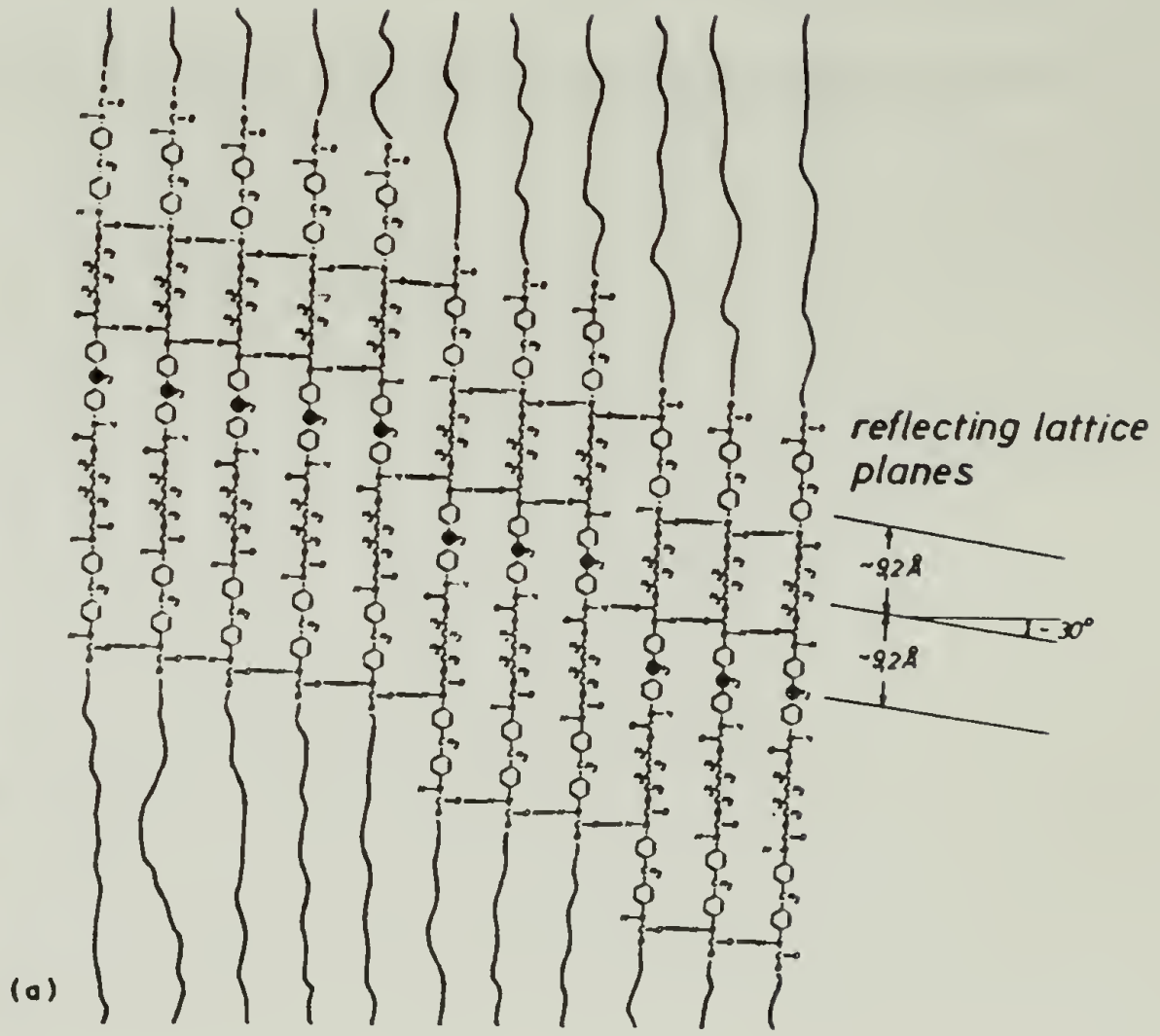

Figure 2.3-3. (a) Physical structure of crosslinking in purely two-dimensional hard segment aggregates; (b) diagrammatical representation of the three-dimensional crosslinking structure [extended with butane diol] (Bonart[18]).

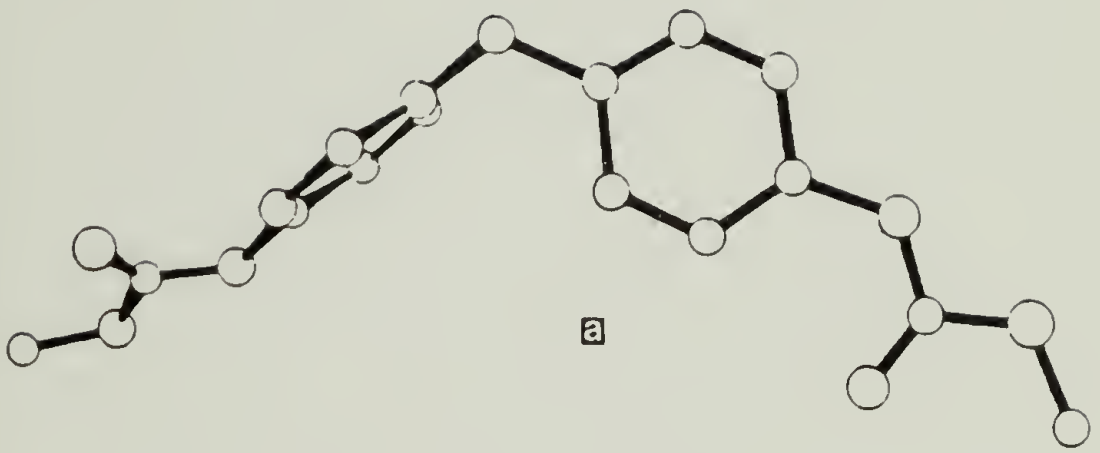

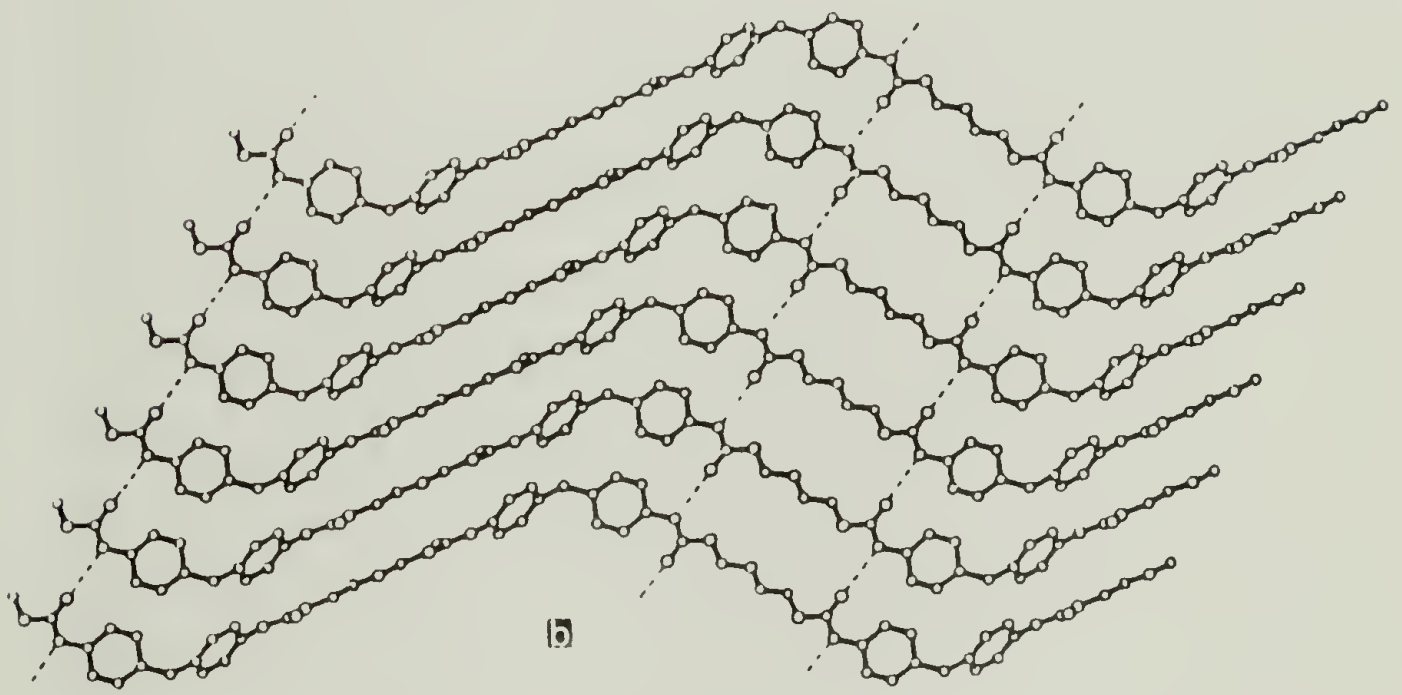

Figure 2.3-4. (a) Stereochemistry of MDI unit with phenyl groups angled 90° at each other. (b) Proposed MDI/BDO chain packing allowing interurethane hydrogen bonding (Blackwell[46]).

TABLE 2.3-1

WAXS DIFFRACTION DATA OF MDI/BDO COPOLYMER

Huh and Cooper[67]	C. Wilkes and Yusek[22]	Schneider[15]
	16	15.9
	8.22	8.32
	4.86	4.87
4.55	4.60 (I)	4.58 (1)
4.05	4.08 (III)	4.09 (2)
3.78	3.75 (II)	3.77 (3)
	3.51	3.45
	2.68	2.24

NOTE: I, II, etc., indicate strongest reflections.

about 30 to 100Å, and that for polyether based MDI/BDO urethanes was 50 to 100Å, with no evidence of spherulitic superstructure. Ordered hard segment domains and stress crystallized soft segment models have been reported by Wilkes and Yusek[22] (Figure 2.3-5) for highly oriented MDI/BDO based polyurethanes. The diffraction patterns of undeformed specimens show a weak reflection (~8.0Å) corresponding to an interplanar spacing of 12Å which is suggested to be a consequence of intermolecular packing of hard segments (see Figure 2.3-3a). Stretching the specimen from 200 to 300% results in the oblique orientation of hard segments to the draw direction, while soft segments are oriented in the direction of deformation, as shown in Figure 2.3-6. Further stretching leads to reorientation of hard segments parallel to the draw direction. Heat treatment followed by stretching results in almost complete disorientation of soft segments but does not affect the orientation of the ordered hard segment domains.

Schneider and coworkers[15] studied the domain structure of MDI/BDO based polyurethanes by electron, optical microscopy and x-ray scattering. They found poorly organized hard segment spherulites with an open fibrous texture with intervening soft segment phase. They proposed a model in which the hard segment phase was thought to be composed of fringed lamellae domains of thickness (dimension parallel to chain axis) equal to the hard segment length, and lateral

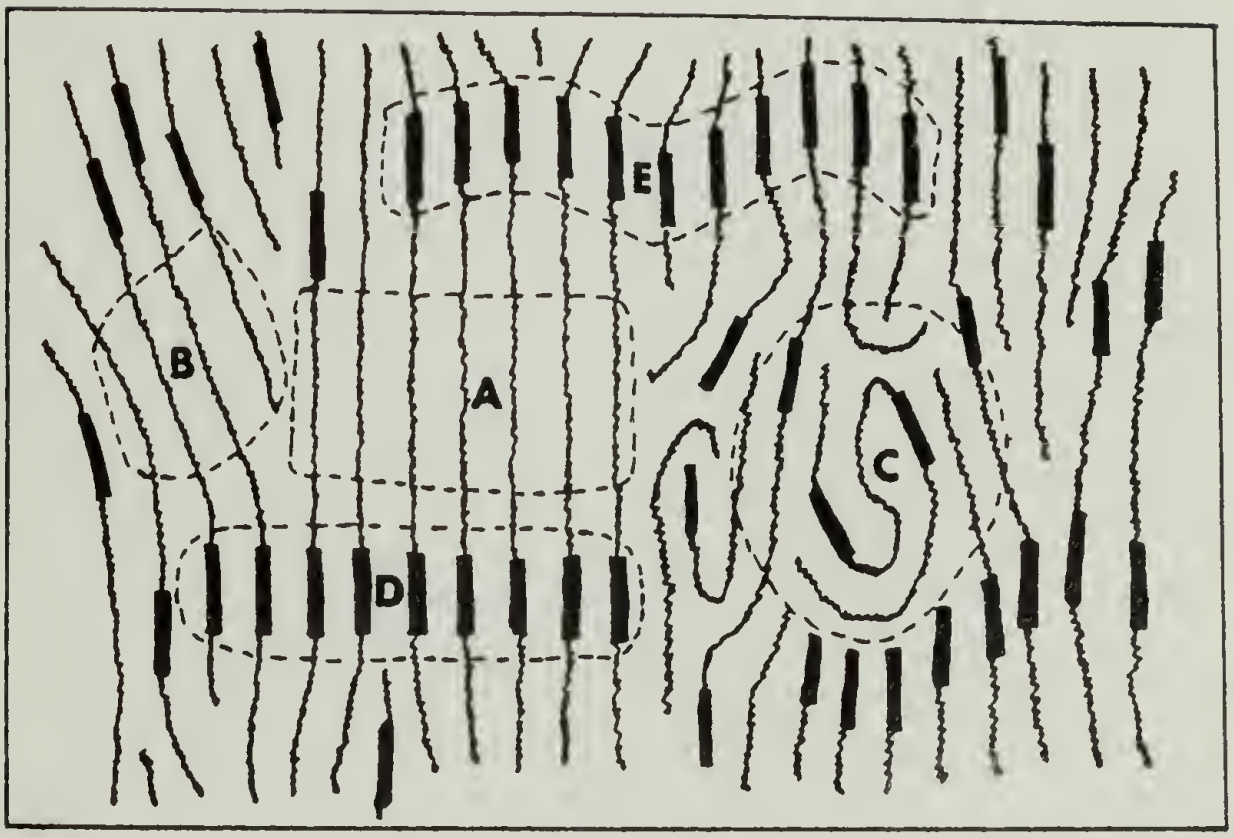

Figure 2.3-5. Model of highly oriented segmented polyurethane. (A) Stress-crystallized polyester or polyether; (B) ordered but noncrystalline polyester or polyether; (C) amorphous "solution" of hard and soft segments; (D) crystalline hard-segment (urethane) domains; (E) ordered but noncrystalline hard-segment domains. Black bars represent hard segments consisting of the products from the reaction of the diisocyanate and a low molecular weight glycol (C. Wilkes[22]).

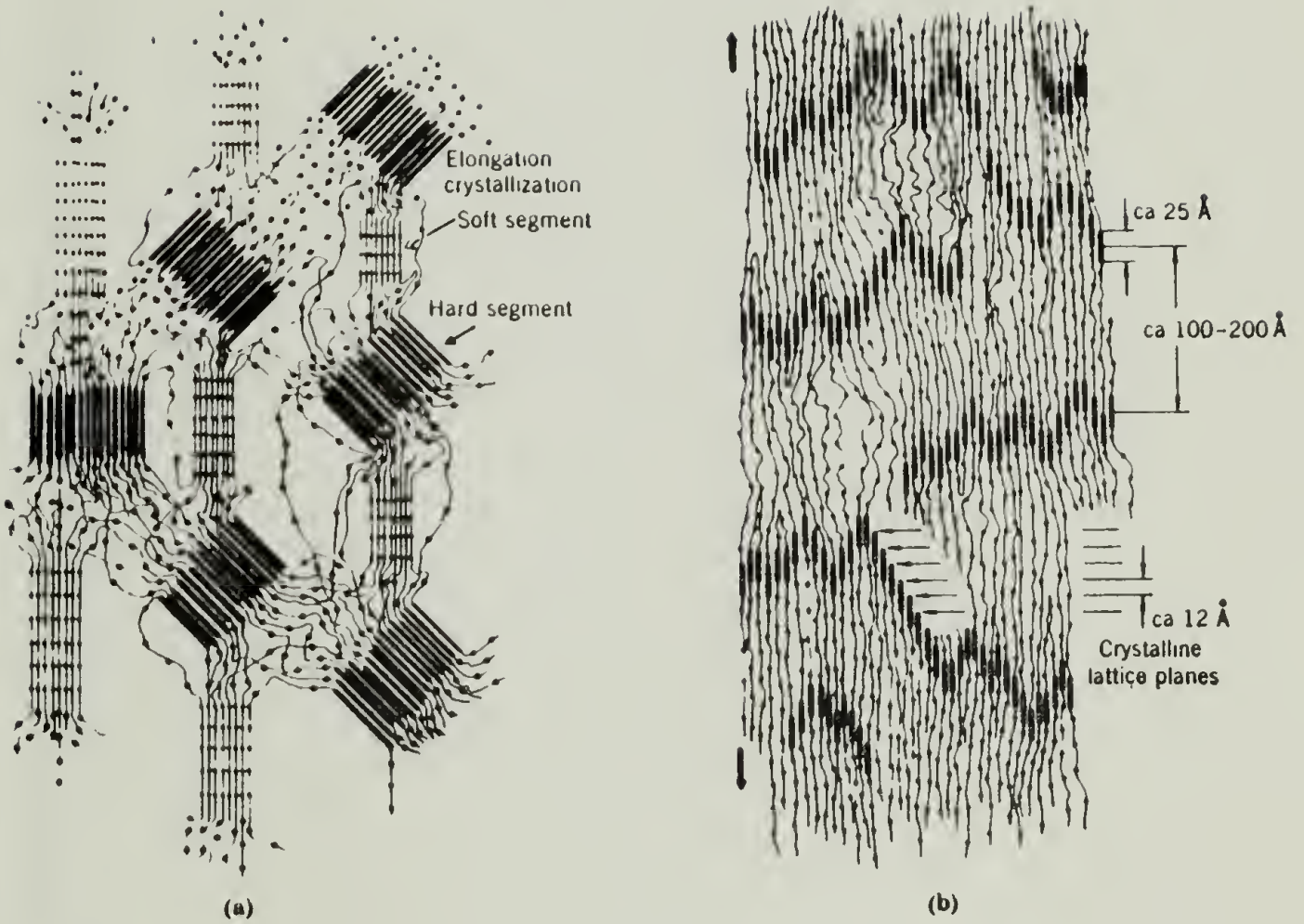

Figure 2.3-6. (a) Schematic drawing of the structure in a polyurethane block polymer stretched approx. 200%. The thick strokes represent hard segments and the thin strokes soft segments. (b) Schematic drawing of the structure in material stretched approx. 500% and subsequently fixed in water at 80°C (Bonart[17]).

width (dimension normal to chain axis) of a few hundred angstroms (see Figure 2.3-7). They suggested that dispersed hard segment domains existed which indicated that the polymer must be considered as a three-phase material consisting of soft segment matrix, dispersed (unorganized) hard segment domains, and organized crystalline hard segment fibril structure.

The domain structure of the special piperazine polyurethanes prepared by Harrell[47] was investigated by Wilkes and coworkers.[23,28,35] They showed the existence of spherulitic superstructure in these segmented urethanes devoid of hydrogen bonding, and the dependence of the size of hard segment domains and superstructure on the length of the hard (crystallizable) segment. They also proposed two models which incorporated domain formation, optical anisotropy, hard segment crystallinity, and large spherulitic superstructure (see Figure 2.3-2). Interestingly, Harrell[47] reported that increasing the hard segment length did not appreciably affect the degree of order within the hard domains, though the melting point of the hard segment phase was raised. Wilkes also found that longer hard segment sequences resulted in larger hard segment domains.

Soft segment. Poly-ε-caprolactone (PCL) has been extensively studied. Its crystal structure, reported by Chatani et al.,[48] consists of an orthorhombic unit cell with parameters a=7.47Å, b=4.98Å, and c (fiber axis)=17.05Å.

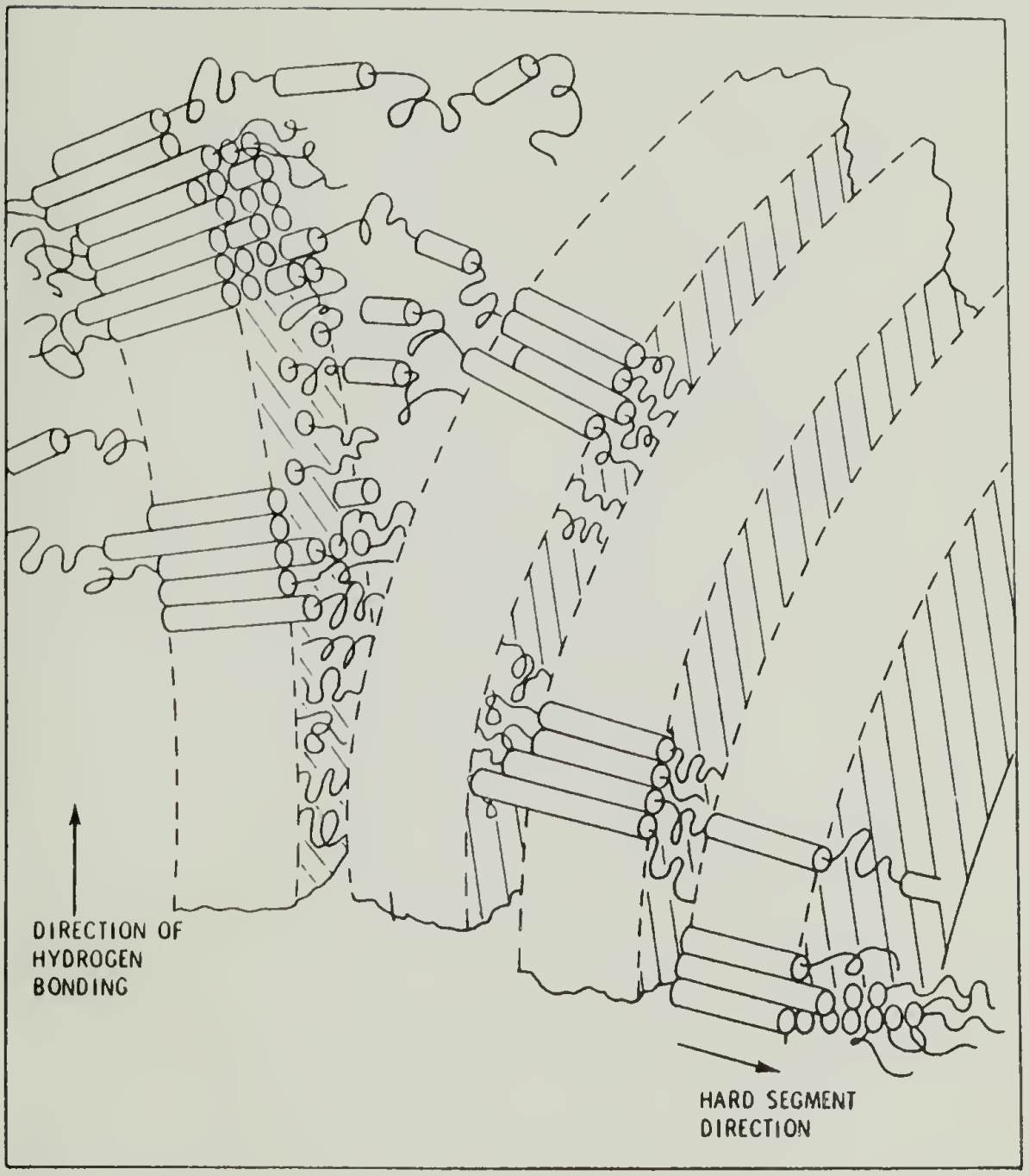

Figure 2.3-7. Suggested organization of crystalline hard segment strands. The average orientation of the strands is in the spherulite radial direction (Schneider[15]).

The molecular chains are arranged side by side and the carbonyl groups of the two chains in the unit all are staggered by an amount of 3/14 c along the fiber axis. The PCL interplanar d-spacings and relative intensities corresponding to various h, k, l values, are shown in Table 2.3-2. No crystal structure for the PCL/MDI copolymer is available, but if we consider MDI links between PCL molecules as defects, then for sufficiently long PCL segments, these segments will be excluded from the crystal lattice. Seefried et al.,[49] reported that crystallization for the PCP/MDI soft segment copolymer occurred only for $\bar{M}_n$=3000 or higher for the PCP prepolymer.

2.4 Domains and Spherulites

There are relatively few direct TEM studies of domain structure in polyurethanes[15,16,34,35,37] and none of them has reported observation of distinct micelle lamellar platelets. Instead, the domain structures observed generally appear as isolated equiaxed grains of 30-500Å diameter[21,25,34] or as randomly oriented fibrils with lateral dimensions of 30-600Å.[1,15] It is still not clear what relation the equiaxed grains and the fibrils observed by TEM have with the micelle lamellae structures inferred from WAXS and SAXS.[22,23]

Several SAXS studies on polyurethanes have shown a discrete small angle maximum in the 200Å range.[15,23,26,50]

TABLE 2.3-2

INTERPLANAR d-SPACINGS AND RELATIVE INTENSITY OF POLY-ε-CAPROLACTONE HOMOPOLYMER

h	k	l	d_{hkl}	I_{rel}
1	0	2	5.618	.02
0	0	4	5.262	.01
1	1	0	4.144	1.00
1	1	1	4.026	.06
2	0	1	3.648	.05
0	1	3	3.746	.01
2	0	0	3.735	.78
1	1	2	3.727	.01
2	1	0	2.988	.06
2	1	1	2.943	.01
0	0	6	2.842	.01
0	2	0	2.490	.08
1	2	1	2.340	.01
1	0	7	2.316	.01
3	1	0	2.227	.10
0	1	7	2.188	.09
1	1	7	2.100	.02
2	2	0	2.072	.05
2	0	7	2.040	.05
2	1	7	1.888	.01
4	0	0	1.867	.04
1	2	7	1.696	.02
3	1	7	1.644	.01
1	3	0	1.620	.01
4	2	0	1.494	.01
4	0	7	1.482	.01
5	1	0	1.431	.01
3	2	7	1.427	.01
0	3	7	1.372	.01
2	3	7	1.288	.01

The poly-ε-caprolactone (PCL) interplanar d-spacings and relative intensity corresponding to different h, k, l values. The intensity was calculated by using observed structure factors reported by Chatani.[48] The data with relative intensity less than 2% were omitted.

This maximum has been attributed to the average center to center spacing of the hard segment domains. One would expect a systematic variation of this maximum with composition, but this has not always been observed.[15,22]

The influence of soft segment hydrogen bonding ability and hard segment block size on phase separation have been clearly shown in SAXS studies.[26] For the same molecular weight polyol, a 1/2/1 polyester/MDI/BDO system (15% weight of hard segment) was shown to be single phased, while a polyether/MDI/BDO system with the same molar composition was phase separated. An examination of the efficiency of hydrogen bonding in similar systems by IR quantitative spectroscopy[51-54] shows that NH moieties in urethane groups are hydrogen bonded, with 60% bound to urethane carbonyls and the remaining 40% to ether oxygen. Whereas the presence of hydrogen bonds between urethane groups indicates the type of association that forms hard segment domains,[50] the higher the content of hydrogen bonds involving ether oxygen, the stronger is the evidence for phase mixing. It is important, however, to underline that piperazine based polyurethane systems for which hydrogen bonding is absent[23,28,35,47] also exhibit the presence of domains, indicating that domain structures in segmented polyurethanes are not a consequence solely of the presence of polar groups capable of forming hydrogen bonds.

In addition to microphase structures, several poly-

urethane systems[16,20,30,45,57] have exhibited spherulitic superstructure. The ability of the system to form spherulitic superstructure depends on its composition and the solidification conditions.

2.5 Block Length Distribution

Sequence length and sequence length distribution in multiblock copolymer systems have been investigated theoretically by several researchers.

Frensdorff's study[56] was directed at determining the amount of polymer which could undergo phase separation by calculating the weight fraction of chains containing blocks greater than some minimum size. Cella[57] employed Frensdorff's method to calculate both the differential and integral hard segment block length distribution for polyester based thermoplastic elastomers. From such distributions the weight and the volume fractions and the size of hard segment domains can be inferred, starting from the assumption that a minimum hard segment length is required for phase separation.

Peebles[58] calculated the number average sequence length based on statistical arguments. He developed the weight fraction distribution for polyurethanes as a function of the length of the hard segment block for single and two-stage polymerization schemes. Figure 2.5-1 shows the resulting distributions for a single stage polymerization

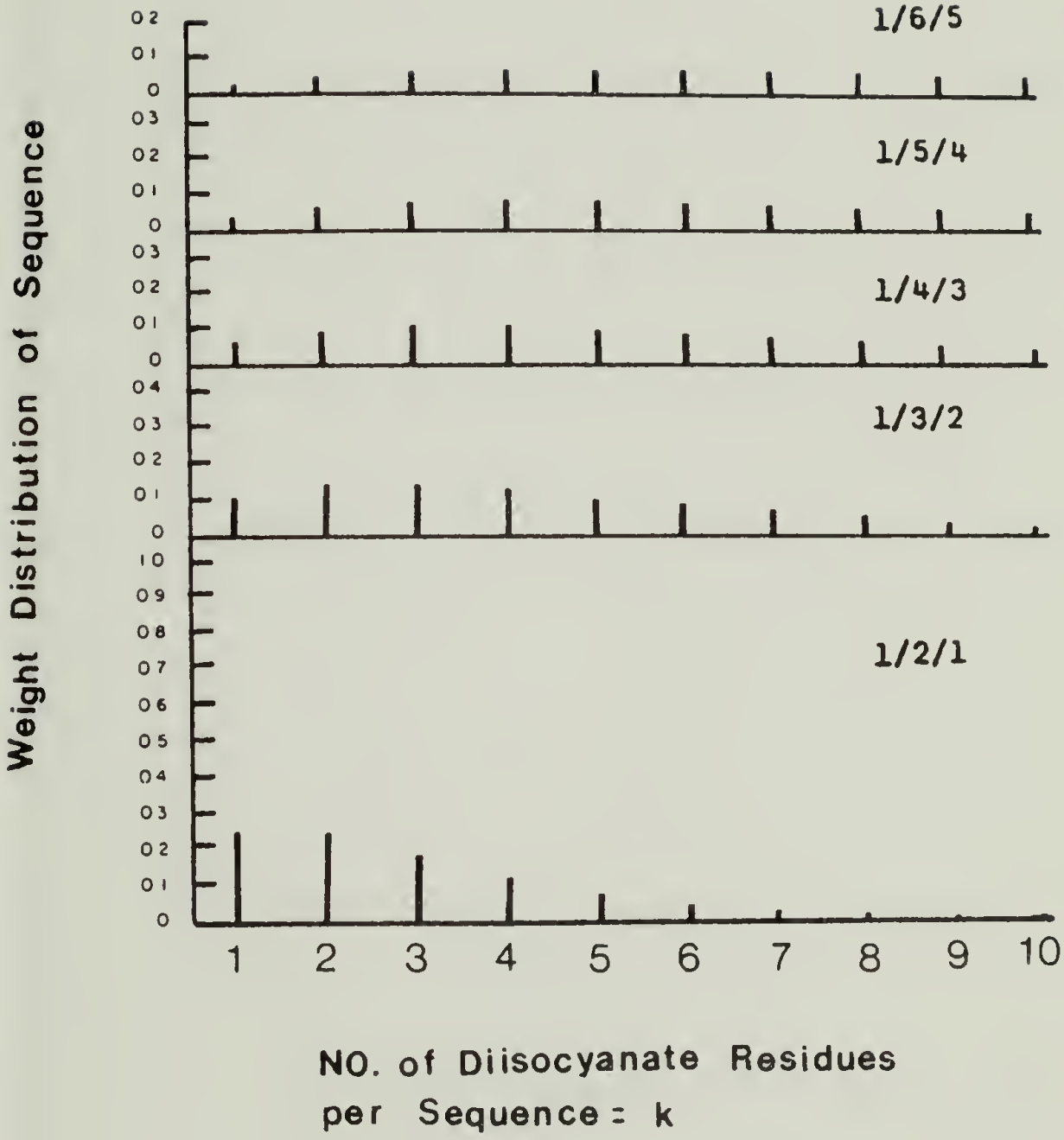

Figure 2.5-1. Weight fraction of sequences containing k diisocyanate units between two consecutive macrodiol units (Peebles[58]).

with polyurethane mole ratios varying from 1/2/1 to 1/6/5 of polyol/diisocyanate/diol, and a reactivity ratio (μ) equal to unity. μ is defined as the ratio of the first reaction rate constant of an isocyanate group to the second reaction rate constant for a number of diisocyanates with aliphatic alcohols. It can be seen that as the hard segment content increases, the number of long hard segments slowly increases. For samples with a very broad length distribution, a large variation in domain size is expected, as well as a higher degree of phase mixing. It is important to point out that RIM processed polyurethanes undergo a single stage polymerization, and sequence length and molecular weight distribution is expected to be broader as compared to a two stage polymerization scheme.

2.6 Compendium of RIM Studies

RIM designates a process which results in a finished product, rather than a specific chemical system, and can be applied for the preparation of microcellular, rigid[4] and elastomeric products. The elastomeric product which will be the area of emphasis of this work, was among the first materials researched by Professor D. Bayer and coworkers in Farbenfabriken Bayern during the 1940s as a response to the invention of nylon by Carothers at DuPont in the late 1920s. Although the idea and implementation of RIM has been in the mind of European researchers a relatively long time, its

history in the United States can be traced back only a little more than a decade.

The RIM process and its applicability to automotive usage was demonstrated by Mobay Chemical Corporation during 1968. After a period of seemingly little growth, Cacciotti[4] in 1973 presented the advantages of urethane elastomers in automotive energy absorbing parts (i.e., bumpers and fascia), and described the types of machinery needed for the "one-shot reaction-injection process." A year later, Rogers and Sassman[60] underscored the advantages of RIM-urethane elastomers over the traditional vulcanized rubber parts, and they described several applications of elastomeric urethanes in industrial products. In 1972 the impetus for RIM development came from the Motor Vehicle Safety Standard 215 Federal Regulation, which requires that the front and rear ends of an automobile be able to withstand a 5 mph impact without impairment of functional parts.[7] In order to fulfill the requirement it was natural for engineers to look toward elastomeric materials. Because the elastomeric RIM market is connected primarily to automotive applications the market potential is quite large. Market estimates show 30 million pounds of consumption during 1976, and as much as 150 to 200 million pounds for 1980.[6]

In contrast to the large literature on melt processing-property studies, there appears to be very little basic work relating in-situ polymerization to resultant properties.

Professor C.W. Macosko and coworkers at the University of Minnesota have concentrated on this issue and produced, starting in 1976, a number of papers aiming at developing a model that includes the process, molecular structure, and physical property aspects of the urethane RIM process. A detailed description of the laboratory scale RIM machine designed by Macosko and Lee,[61] and used to manufacture some of the samples used in this study, will be given later in section 3.9. Critchfield and coworkers[73] at Union Carbide Corporation have done work correlating RIM processing conditions and chemical systems with modulus and relaxation properties. A cooperative research effort is under way with the University of Minnesota and Union Carbide groups and samples for the present study have been provided by both sources.

The Minnesota group has investigated,[62] together with other authors,[12,14] the critical problem of impingement mixing and postulate that polymer layers form and isolate local pockets of reactants. The average distance between these layers is called "striation thickness," <s>. A correlation between <s> and Reynolds' number, Re (based on polyol nozzle velocity) is proposed:

$$\langle s \rangle \alpha [Re]^{-3/4}$$

and it is found that in adiabatically polymerized systems, initial temperature rise increases with an increase in Re,

for values of Re up to 200 (see Figure 2.6-1), above which the reaction is kinetically, and not diffusion, controlled. Utilizing the adiabatic temperature rise method, Macosko[64,65] has developed a method for quickly obtaining overall kinetics and a model for curing and heat transfer processes in RIM isothermal (heated) molds.[9] Work at Minnesota is being carried out on developing a model for step growth copolymerization with phase separation[66] that will hopefully contribute to the understanding of molecular weight and sequence distributions.

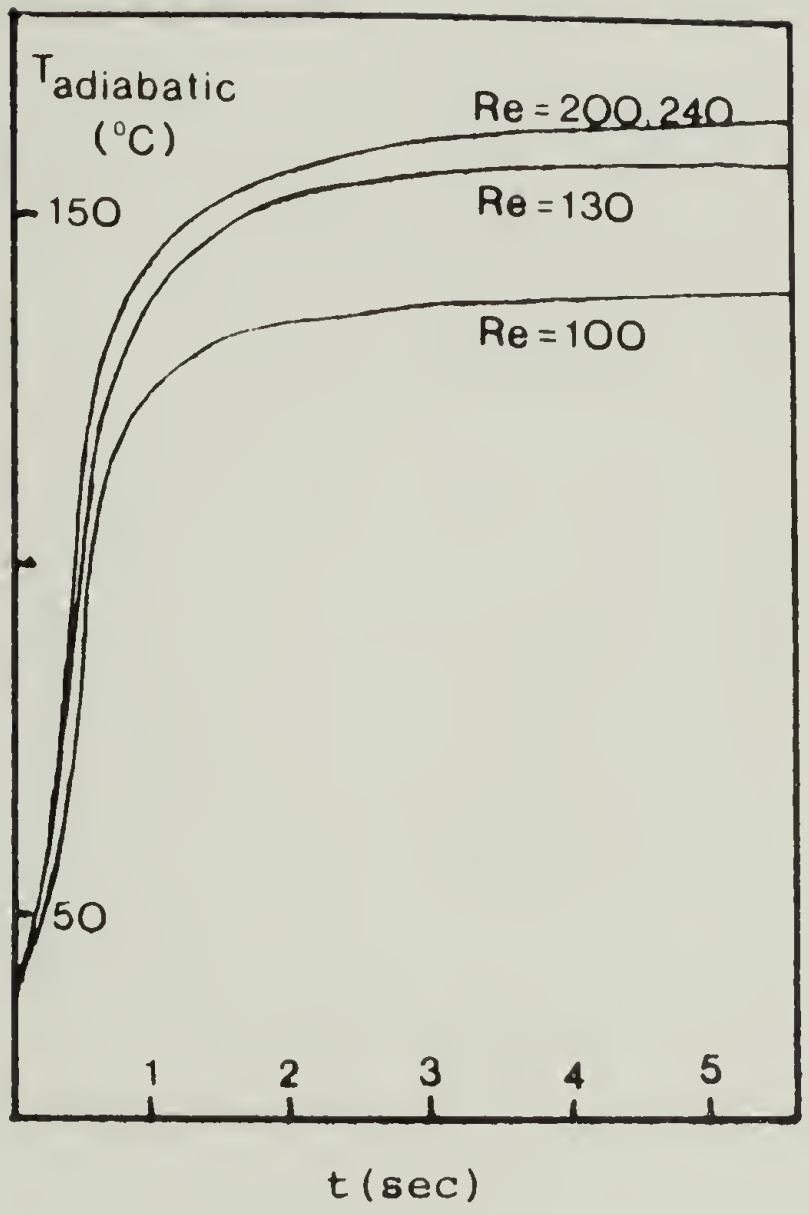

Figure 2.6-1. Adiabatic temperature rise for a fast urethane polymerization at several nozzle (polyol) Reynolds numbers (Macosko[8,78]).

C H A P T E R I I I

EXPERIMENTAL TECHNIQUES

A description of the instrumental techniques employed is given in sections 3.1 through 3.5. Great detail is devoted to explain the cryo-microtoming technique. Sections 3.6 through 3.9 describe the different polymer preparation methods used, with emphasis on the RIM machine employed.

3.1 Wide Angle X-Ray Scattering

WAXS scans of scattering intensity vs. scattering angle (2θ) were obtained by means of a General Electric XRD-5 unit which generated nickel filtered CuK_α radiation of $\lambda = 1.542\text{Å}$. The radiation was obtained from a CA-7 Coolidge x-ray diffraction tube operated at 35 kV and 14 mA. An SPG spectrogoniometer was used to measure intensity vs. scattering angle at a scan rate of 2 degrees per minute. The intensity output was recorded on a Leeds and Northrup Co. Speedomax-type G chart recorder unit. Samples of thickness 2 to 3 mm. were cut manually. Scattering angle calibration was done with a polyethylene standard.

3.2 Differential Scanning Calorimetry

A Perkin-Elmer DSC-II was used to investigate the thermal properties of RIM-urethane materials. Samples used weighed 10 to 20 mg. The instrument was set at a heating rate of 20°C/min. and a range of 2 millicalories/sec. Both the heat input and the temperature scale of the DSC were calibrated with the heat of fusion and the melting transition of pure Indium standards.

3.3 Cryo Ultra-Microtomy

A morphological study of RIM polymerized materials calls for a sample preparation technique that will not alter the existing structures. More traditional techniques, like solution casting or melt pressing, for the preparation of thin films provide valuable information, but they do not reflect the true in-situ morphology which is a product of the processing conditions utilized to form the polymer. Thus, microtoming, or thin sectioning is the only alternative. Furthermore, due to the elastomeric character of the materials involved and the need to eliminate plastic deformation during sample sectioning, temperatures far below the vitrification point of the soft segment are needed.

Due to the lack of previous studies the whole microtoming technique had to be developed and implemented. Below we present a description of the cryo ultra-microtoming

technique that was employed.

3.3-1 General recommendations. Microtomy equipment may vary in shape and style, but the principle of operation of any such device is basically mechanical cutting. Therefore, disturbances such as vibrations or temperature changes, sometimes casually overlooked, are of critical importance. Ideally the experiment should be performed inside a booth, or in a closed room without draft. The very fine stability required for the instrument is easily disrupted by draft, heavy steps, and loud conversations.

A typical microtoming session took not less than four hours. Time has to be allowed for all preliminary preparations (making knives and troughs, trimming block faces, etc.) and for the equipment to reach stable operating conditions.

3.3-2 Equipment description. A Sorvall MT2-B Porter-Blum ultra microtome with frozen thin sectioning attachment was used. The controls for operation shown in Figure 3.3-2a belong to the front panel of the instrument, and it includes a pushbutton switch for the motor drive which overrides the manual handwheel motion, separate pushbuttons for re-setting the advance system of the moving arm and for by-passing the knife on the cutting stroke. It also includes dials for setting the cutting speed and the desired thickness, and the upper knob (pivot) for setting the coarse thickness.

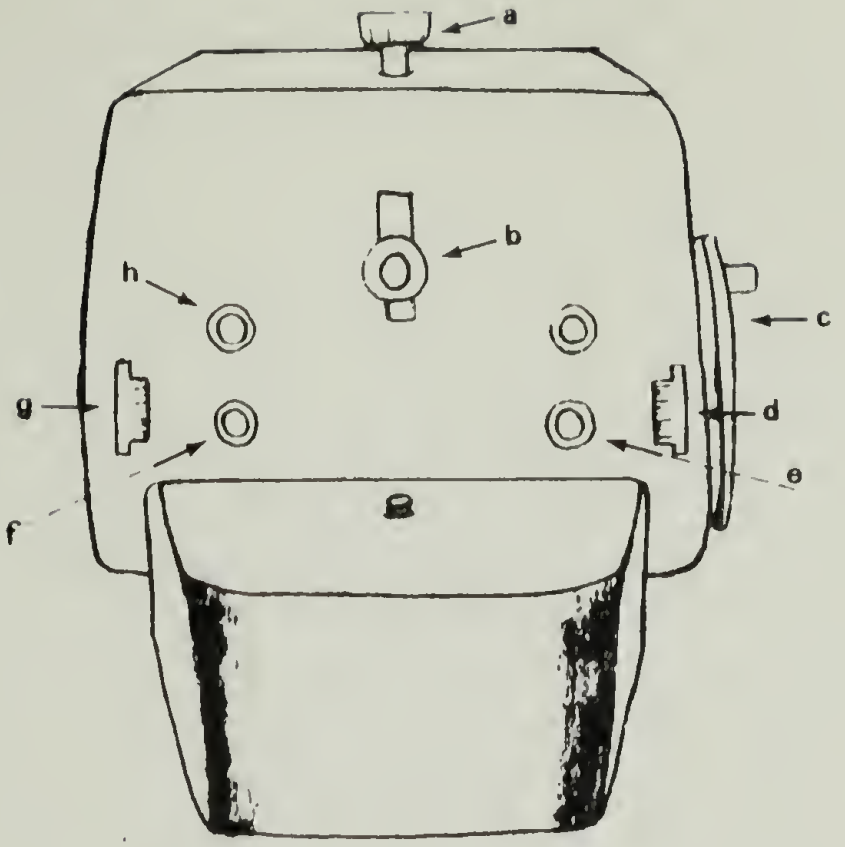

Figure 3.3-2a. Front panel of MT2B ultra microtome. (a) Upper thickness control, (b) cantilever arm, (c) hand-wheel, (d) speed control dial, (e) reset, (f) by-pass, (g) thickness control dial, (h) motor switch.

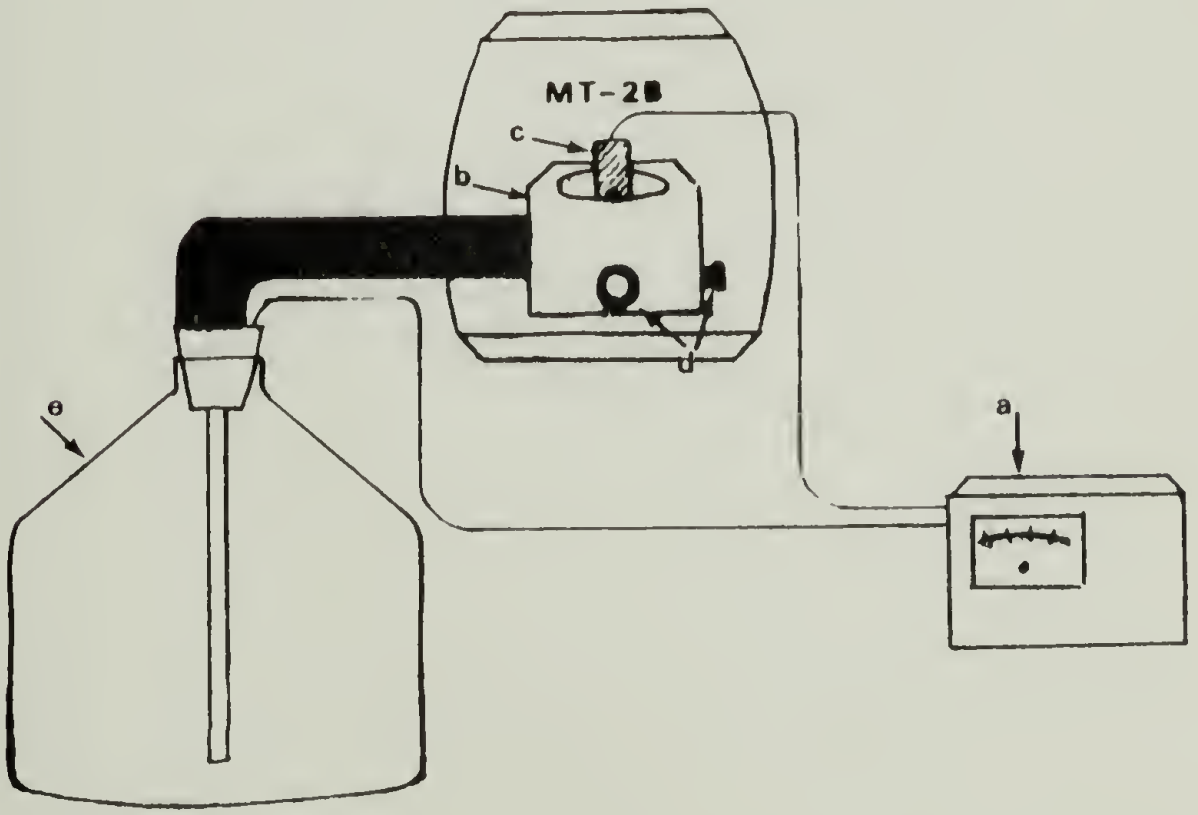

Figure 3.3-2b. MT2B ultra microtome cryo-sectioning attachments. (a) temperature control, (b) knife stage, (c) sample holder, (d) positioning controls, (e) liquid nitrogen reservoir.

Figure 3.3-2b shows the cryo sectioning attachment which comprises the thermally insulated knife stage with positioning controls, the sample holder and temperature sensor, the liquid nitrogen reservoir, and the temperature control unit.

3.3-3 Knife preparation. An KLB-type 7801B knife maker was used to prepare 45° angle knives of the following approximate dimensions: height and length 2.5 cm, thickness 0.7 cm. Satisfactory knives have to show a cutting face similar to those described in Figure 3.3-3a, where area I (the sharpest) is used for fine sectioning, area II is used for trimming, and area III is discarded because of edge effects (whiskers).

After a satisfactory knife has been prepared, a trough is constructed to collect the sections. The common wax and polyester tape arrangement is inadequate for cryomicrotoming and has been successfully replaced by aluminum foil and rubber or silicone cement. A strip (dimensions 3.0 by 0.7 cm approximately) of aluminum foil is wrapped from one side to the other of the cutting edge and glued onto the glass knife with cement. The lower edge of the strip should be parallel to the lower edge of the knife, and its upper edge must reach exactly the edge of the knife's cutting face. This is illustrated in Figure 3.3-3b. The region of the heel and sides of the trough are sealed with

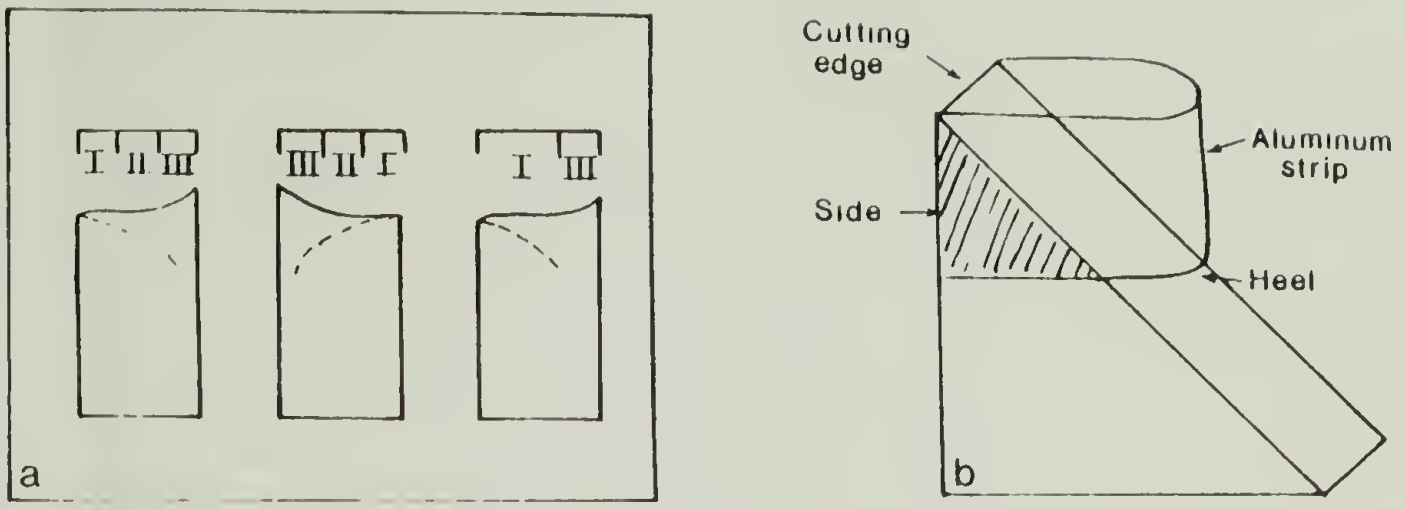

Figure 3.3-3. (a) Diagram showing the different configurations of the cutting edge of glass knives and the approximate length of the usable parts. I. fine sectioning, II. fine trimming, III. discardable. (b) Illustration of finished trough.

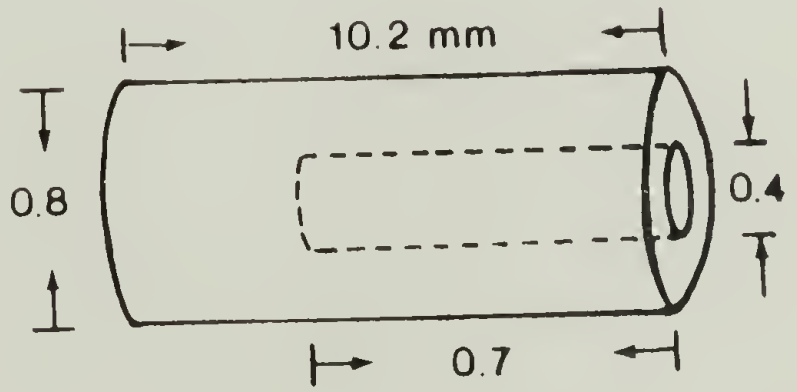

Figure 3.3-4. Schematic of copper cylinder.

additional cement. The trough should be leak tested (H_2O is suitable) before its implementation.

3.3-4 Sample preparation. Instead of the epoxy embedded samples normally used, a copper cylinder with an internal channel (see Figure 3.3-4) that accommodates a cylinder of the polymer to be sectioned, was found to be of simpler use and yielded better results.

The block face of the cylindrically cut polymer (of dimensions diameter = 0.35 to 0.40 cm, maximum length = 0.8 cm, minimum length = 0.3 cm), is cut in the shape of a truncated pyramid with its base at least twice as long as its height. This particular shape, as will be seen later, is of great importance in avoiding the problem of section curl-up. The cutting of the block face is performed with a clean, sharp razor blade at an angle of approximately 45°.

The internal channel of the copper cylinder is filled with glycerol, and the polymer cylinder (with the block face already prepared) fitted in. The use of glycerol, which solidifies at 14°C, strongly fixes the polymer to the copper cylinder at normal cryo-sectioning temperatures and permits its removal at room temperature. The cantiliever arm of the polymer cylinder should not exceed 1 mm in length.

3.3-5 Cutting procedure. The copper cylinder with the sample is accommodated in the sample holder, and the knife in the knife holder, maintaining a 5° sectioning angle.

The trough is filled with an inert (to the polymer) fluid having a melting temperature 10 to 20°C below the cryo-sectioning temperature. Propyl alcohol was found to be adequate (melting point -127°C). The fluid level in the trough should be kept below the upper edge of the trough. This will aid in preventing the fluid from "jumping" onto the block face as it passes the knife.

The temperature is set in the control unit starting the flow of nitrogen, and 15 to 20 minutes are allowed for the system to reach a temperature of -70 to -90°C. Liquid nitrogen should not be poured inside the knife holder stage since this drastic cooling can break the glass knife and cause thermal stress cracking of equipment parts and unnecessary vibrations. Once the system is temperature stable, one can proceed to fine trim the block face (section II of knives, see Figure 3.3-3(a)) turning the handwheel manually and approaching the knife with the fine advancement micrometer drum (Figure 3.3-2(b)) at about 1 μm for every cutting cycle, until the first thick section is sliced. The knife is then translated to permit cutting with the sharpest area, and the automatic advancement mechanism reset. All the levers and locks on the stage should be tightly fastened, and the controls on the front panel should read: thickness control dial 10 (Å), speed control dial 3.2 (mm/sec), and upper thickness control 10 (100Å). Fine sectioning can then begin:

1. The handwheel is turned manually until the first section is cut. The section is then taken out of the knife's edge with a hair (attached to a conveniently long handle).

2. The motor switch is turned on, and within a few cycles slices of medium thickness (circa 3000Å) will start appearing on the edge of the knife. These sections are again removed.

3. The speed control dial is set at 1 mm/sec. Faster speeds will result in excessive chatter marks on the section.

4. The thickness control dial is lowered 2 or 3 units every 10 cutting cycles (removing all accumulated sections) until it reads 8Å. For thicknesses below this level the instrument needs greater conditions of stability than those normally attainable in a common laboratory, and the production of sections will be inconsistent.

5. Sections within the acceptable thickness range (thickness is calculated by multiplying the thickness control dial times the upper thickness control), are picked up with a 300 or 400 copper mesh grid.

3.3-6 Problems encountered.

1. Most of the polymers microtomed following the above procedure showed a tendency to release sections that curled up at the time of cutting. A number of remedies were tried:

(i) preparation of block faces with short and wide shape;

(ii) lowering the temperature level to the maximum permissible, which is limited by the equipment setup and the freezing temperature of the fluid in the trough;

(iii) work at highest possible thickness (within allowable TEM range);

(iv) increase the fluid level in the trough without causing the wetting of the block face.

For reasons that are not fully understood, for every 10 or 20 curled-up sections one comes out flat. Then, if other measures have failed, it becomes a matter of patience and concentration to spot and recover the flat sections, removing all others continuously from the edge of the knife.

2. Excessive water condensation inside the system can spoil an entire microtoming session. Ice crystals deposit on the knife's cutting edge, sample block face, floating liquid, etc., making it impossible to follow the sequential sectioning of the sample. In order to avoid this problem:

(i) keep a steady stream of nitrogen gas flowing inside the stage. Replenish the nitrogen reservoir frequently;

(ii) keep the stage covered, with a glass or plastic plate, as long as possible;

(iii) do not breathe or speak directly into the stage;

(iv) avoid passers-by.

3. When the advancement mechanism appears not to be working, one should check the following:

(i) all locks and clamps should be securely fastened;

(ii) temperature should be below 0°C to insure solidification of the fastening agent (glycerol, inside the copper cylinder);

(iii) thickness control dial should be set at, or above, 8Å;

(iv) moving parts, especially the cantilever arm, should be free from friction.

3.4 Transmission Electron Microscopy (TEM)

A JEOL 100-CX TEMSCAN was used to carry out bright field TEM observations. This instrument provides a high vacuum of 10^{-7} torr in the specimen chamber, and is equipped with a liquid nitrogen anti-contamination trap that keeps the contamination rate below 1Å/min.

TEM experiments were carried out at 100 keV using magnifications of 2000x to 3000x only, though the instrument can provide up to 3.4Å resolution under optimum conditions. Solution cast films (see sections 3.7 and 3.8) and thin microtomed sections (see section 3.3) were directly observed

on 400 mesh copper grids.

Contrast was enhanced by using objective apertures of 40 and 60 m in diameter. A decrease in the size of the objective aperture results in an increase in the contrast. The number of scattered electrons blocked out by the aperture is larger, forming a less intense but better contrast image.

Electron beam damage affects the morphology of the specimen by causing ionization and subsequently crosslinking and/or chain scission.[74] Diffraction contrast from a polymer may be completely destroyed in a very short time of irradiation, leaving only mass thickness contrast. The mass thickness contrast comprises the original mass thickness variation in the specimen, and thickness variations induced by radiation damage.

Standard irradiation tests were routinely conducted on the materials studied, in order to assess the magnitude of mass loss due to the electron beam exposure.[75] The screening tests were carried out on the pure segments (e.g., PPO/MDI copolymer and MDI/BDO copolymer) to determine if differential etching does occur during TEM observations. This was done using the reduced raster mode of the scanning unit, which allows the irradiation of a chosen area leaving adjacent areas undamaged.

In order to minimize electron dose, the habit was kept to make preliminary observations and focus on a given

area, and quickly translate to an undamaged area before recording a micrograph.

3.5 Polarized Light Microscopy

Solution cast films, and manually sectioned specimens were observed directly on glass slides between crossed polars, using a Zeiss microscope equipped with a Mettler Hot-stage. Magnifications used varied between 40 and 200 times, using different combinations of oculars and objectives. Black and white (400 ASA) pictures were taken using a green light filter.

3.6 Batch Reacted Polyurethane Samples

A specially prepared (Union Carbide Corporation) polyether based thermoplastic polyurethane having 45% weight of hard segment was used for solution casting of thin films. This polyurethane was batch reacted (hand cast) and not RIM processed. It consists of: (i) poly(propylene oxide)diol with $\bar{M}_n$=2000 (PPO), capped on each end with poly(ethylene oxide) blocks, (ii) 4,4'-diphenylmethane diisocyanate (MDI) and (iii) 1,4-butenediol (BEDO). The structure of the soft segment is:

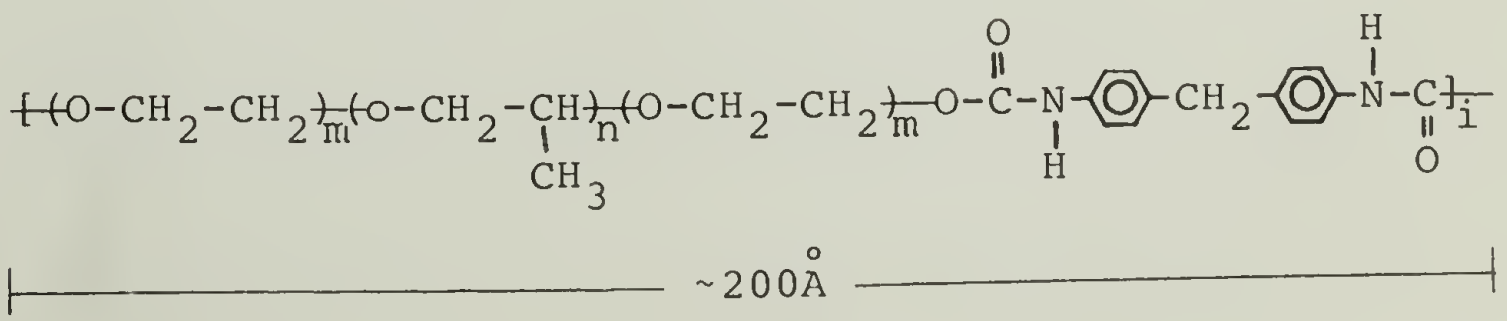

where $n/(2m+n) \cong 0.7$ and $2m+n \cong 35$. The structure of the hard segment is:

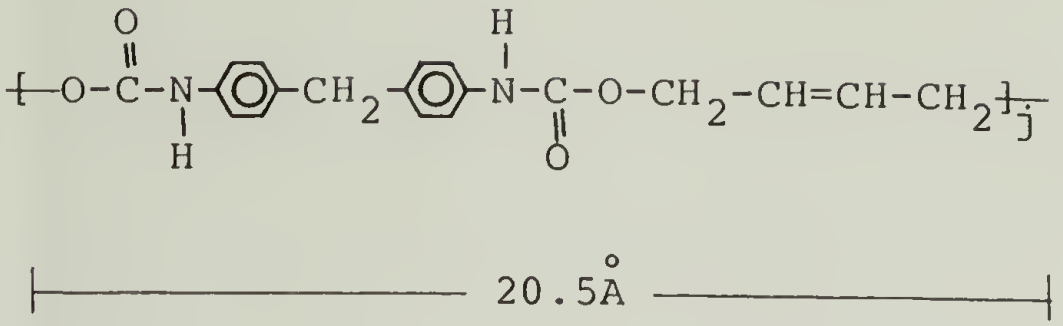

The reactants PPO and BEDO are stored over molecular sieves (A-5) to be kept dry, and molten MDI (50°C) is purified by filtering prior to use. The catalyst dibutyltin dilaurate (Tl2) is used as received.

The polymer was prepared by R.J. Zdrahala at Union Carbide Corp. with the following procedure:[49]

1. 107.5 g of polyol, 24.4 g of BEDO and 0.02 g of T-12 were charged into a three-neck round bottom, 500 ml reactor equipped with rigid stirring device, thermometer, and vacuum inlet.

2. The reaction mixture was degassed for 30 minutes at a vacuum of approximately 1 torr.

3. The stirring was stopped, the vacuum broken, and 86.5 g of freshly filtered MDI were quickly introduced into the reactor.

4. The vacuum was reapplied, the stirring started and the reactor content was rapidly stirred for 12 seconds.

5. The stirring and vacuum were stopped, the reactor assembly quickly opened (gel time 22 seconds), and the

reaction mixture poured into a glass mold treated with mold release agent. The glass mold consisted of two plate-glass sheets separated by a teflon spacer of the desired thickness.

6. The polymer was cured in the mold for 16 hours at 100°C.

3.7 Solution Cast Films

Thin films (~500-1000Å) were cast with the following procedure:

(i) Preparation of a dimethylformamide (DMF) solution of the polymer with concentrations of 0.3 to 0.5% by weight.

(ii) Immersion of clean microscope slides in a solution of the polymer.

(iii) Slow drying of the microscope slides inside a vacuum oven for 3 hrs. at 50°C.

3.8 Osmium Staining of Solution Cast Films

Several procedures for osmium tetroxide (OsO_4) staining of polymers appear in the literature.[68,69] However, important variables like exposure times and concentration of staining agent are not clearly indicated. The staining procedure used in this study was determined by a method of trial and error.

Films solution cast on microscope slides were

exposed to the vapors of a 2% aqueous solution of OsO_4 for increments of 20 min. Staining took place inside a dessicator at room temperature. The films were then removed from the glass by careful immersion in distilled water. The films lying on the surface of the water were mounted on 400 mesh copper grids and dried overnight at room temperature.

3.9 Nonisothermal, Slowly Reacted RIM Samples

RIM samples that experienced a temperature gradient across their thickness were prepared. The polyurethane used to study the effects of such a nonisothermal RIM process consists of: (a) a polyester soft segment based on poly-ε-caprolactone diol (PCP-0200, Union Carbide Corp.) with a number average molecular weight of 2000, and the structure:

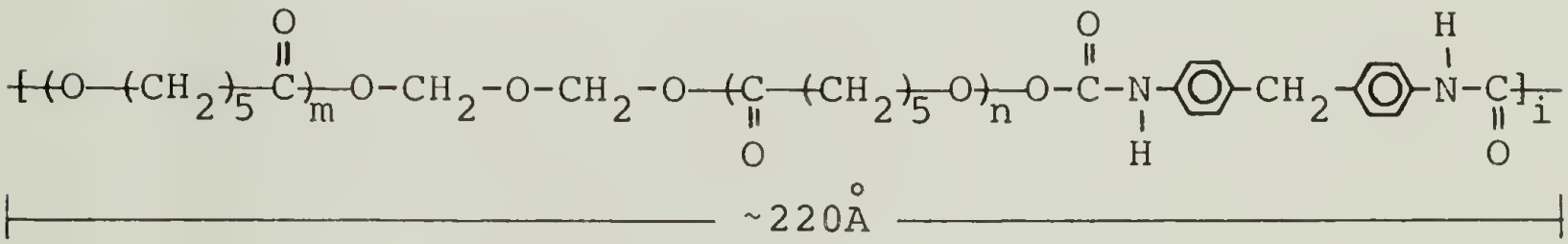

where m+n≅17, (b) a hard segment made of 4,4'-diphenylmethane diisocyanate (MDI-mondur PF, Mobay Chemical Co.), and (c) a chain extender 1,4-butanediol (BDO, Aldrich Chemical Co.). The hard segment has the structure:

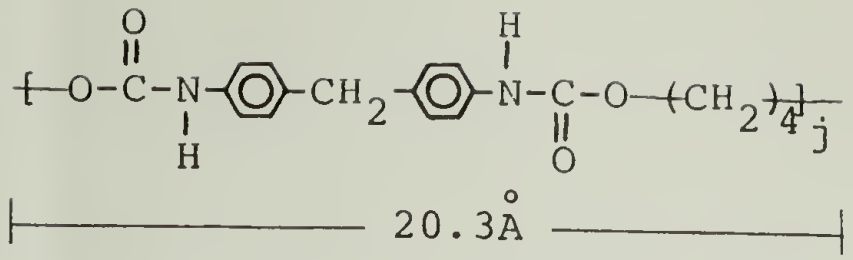

These components are degassed by heating at 60°C for two hours followed by filtering. The catalyst, dibutyltin dilaurate (DBTDL-T12, M&T Chemicals) was used as received in concentration of 0.01 weight percent. This catalyst concentration causes gelation to occur at about 1 minute which is considerably longer when compared to typical gel times of 5 to 10 seconds in commercial RIM materials (0.05-0.1% catalyst). The purpose of preparing RIM samples with longer gel times was to attain better temperature control.

The nonisothermal RIM polymerization was carried out in a laboratory scale RIM machine developed, designed and operated by L.J. Lee and C.W. Macosko at the University of Minnesota.[61] Figure 3.9-1 shows a side and top schematic of this machine, while Figure 3.9-2 shows a front view. The two reactants are dispensed from hydraulic-type reactant cylinders into the mixing head where impingement mixing occurs. Power is supplied to the reactant cylinders by a drive cylinder either pneumatically or hydraulically and transmitted directly through the clevis joints to cylinder A. Cylinder B is driven by a level arm through another clevis joint. The stoichiometric ratio between these two reactant

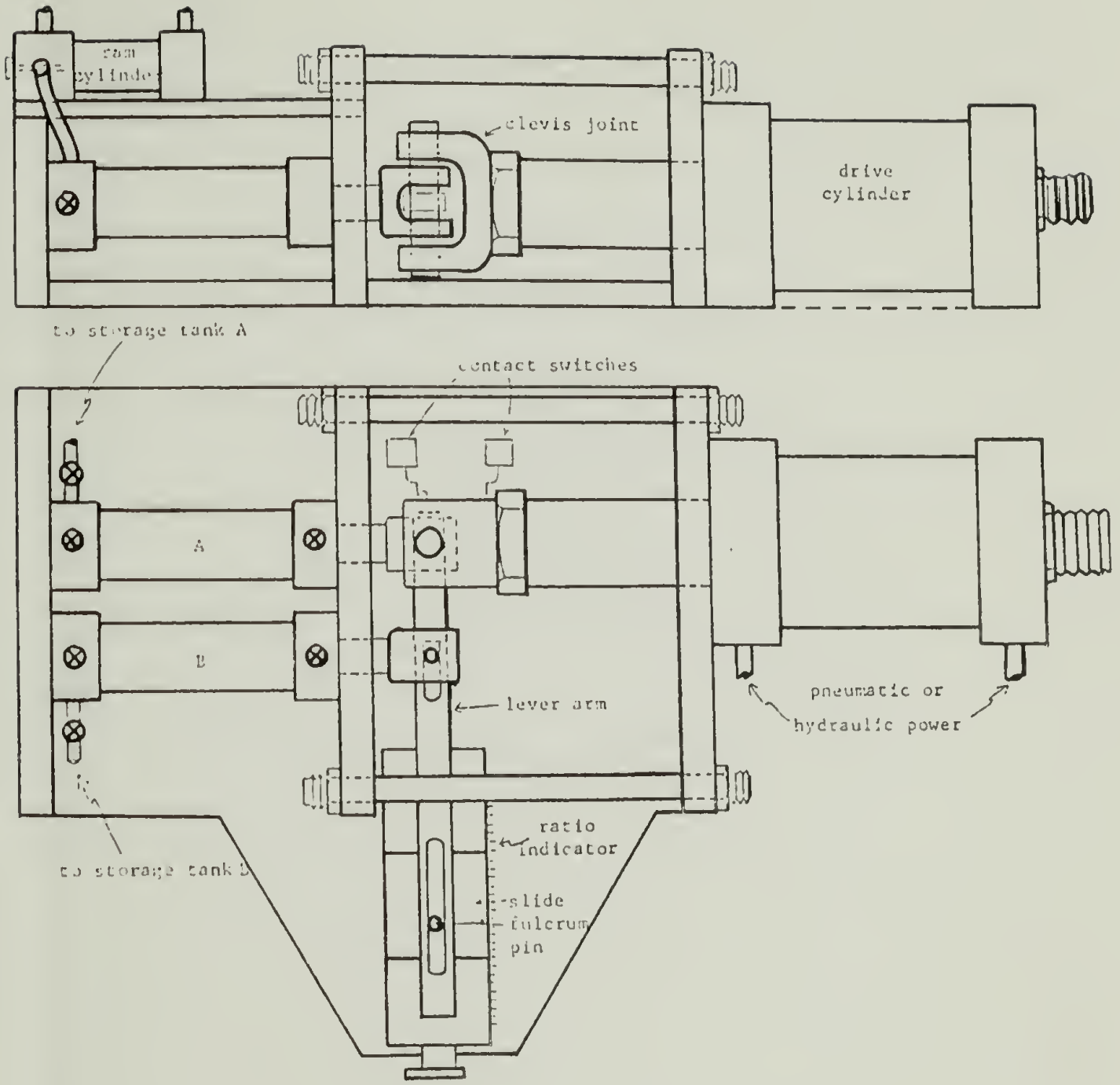

Figure 3.9-1. Schematic diagram of a laboratory size RIM machine (Lee[61]). Side and top view showing the lever arm metering system.

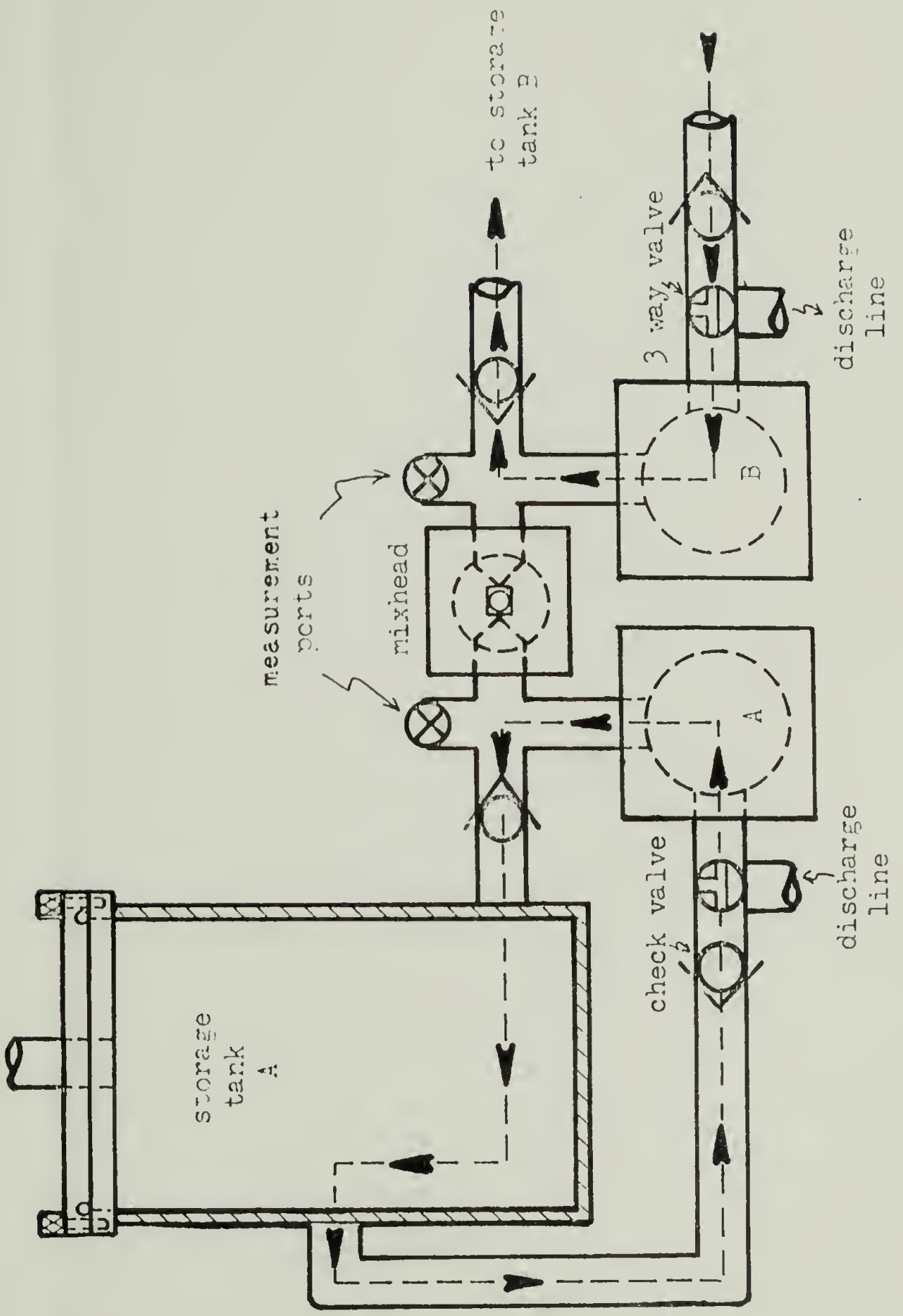

Figure 3.9-2. Schematic front view of RIM machine and reactant circulation path (Lee61).

cylinders is controlled by the position of the movable fulcrum pin which can be adjusted continuously by a slide.

A small pneumatic cylinder is actuated by a solenoid valve which controls the location of the mixhead ram. When this ram is in the forward position, the impingement nozzles are blocked and flow is prevented. When reactant cylinders are pressurized the ram moves backwards after a delay time which is preset on the control panel. Fluids then move through impingement nozzles into the mixing chamber. At the end of the shot, the mixhead returns to the forward position, stopping the shot and cleaning the mixhead.

The shot to shot reproducibility was found to be within the accuracy of the measurement method,[61] ±0.5%. The overall stoichiometric ratio was found to be within 1% of the theoretical ratio at low pressures. For high pressure operation, trial and error adjustments were necessary.

The reactants were impingement mixed at 50°C and injected into a mold that consists (see Figure 3.9-3) of two 1/8 inch thick steel plates placed 1/2 inch apart. The mold is cored for water cooling or heating.

Two runs were conducted using different mold temperatures, 85 and 37°C, designated as N1 and N2 respectively. Both nonisothermal runs were carried out with a 1/6/5 molar ratio of PCP/MDI/BDO corresponding to 43% by weight of hard segment. The measured temperature profiles[78] for both samples are shown in Figure 3.9-4. It is seen that the

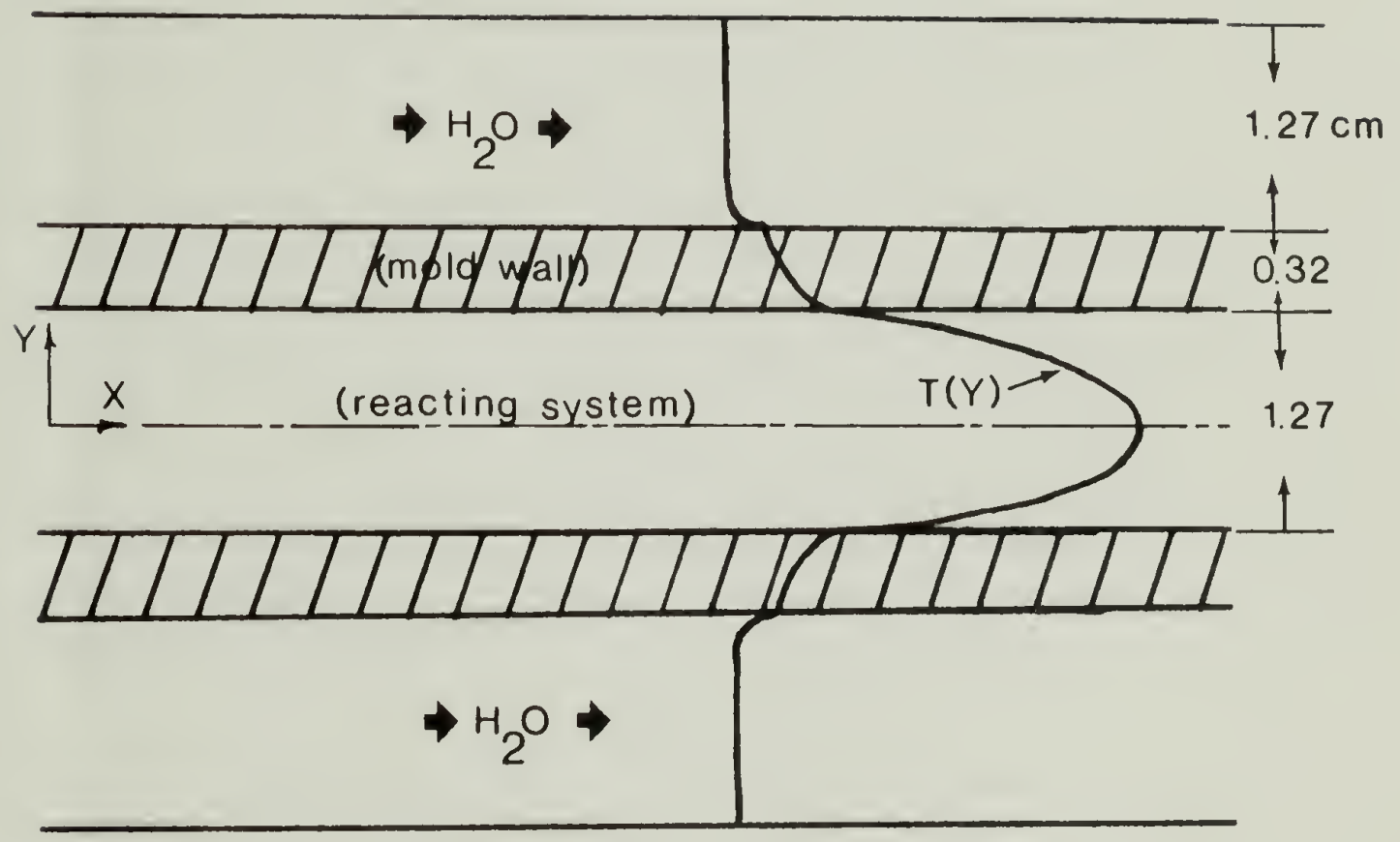

Figure 3.9-3. Schematic diagram of nonisothermal (water cooled) RIM mold showing assumed temperature profile.

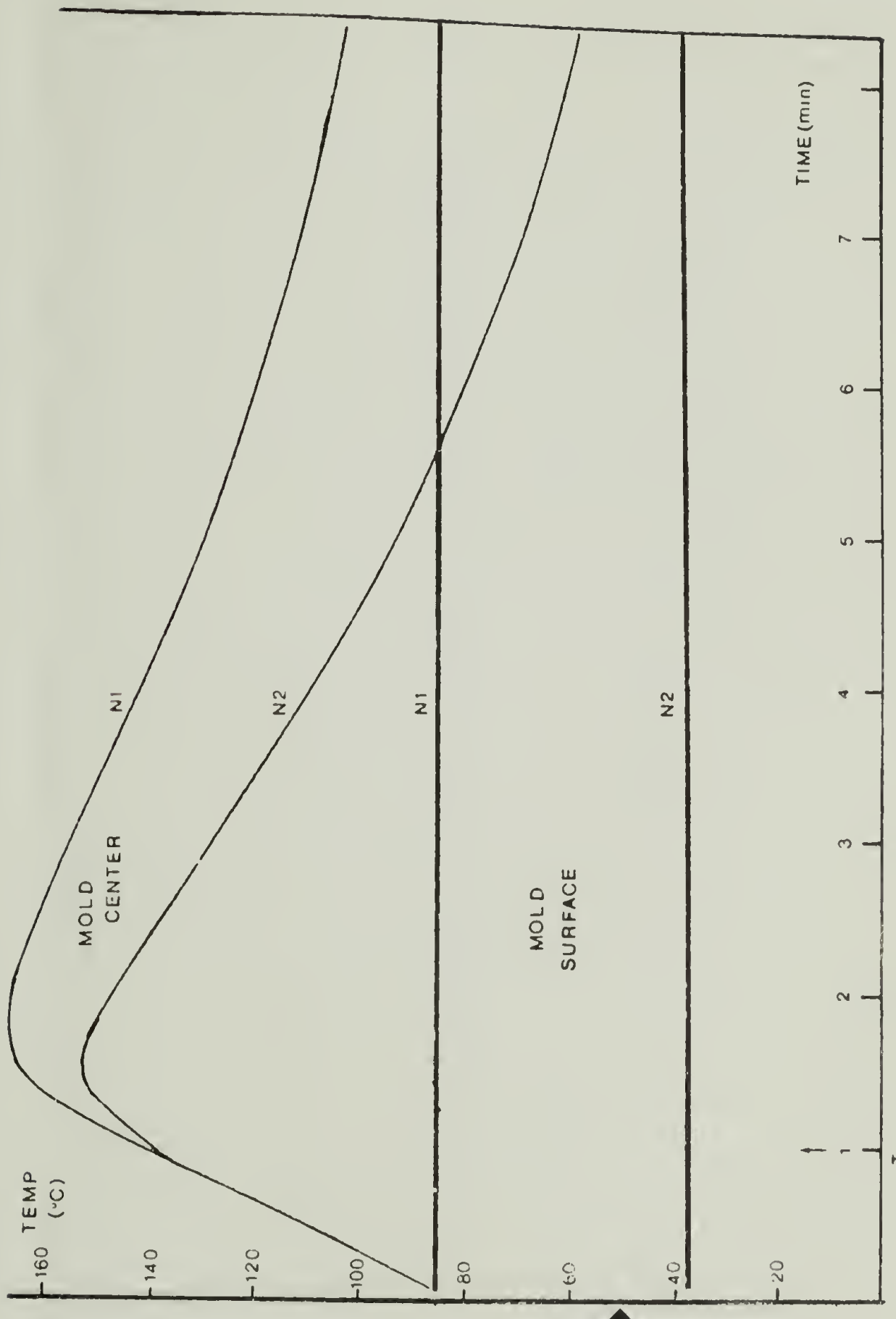

Figure 3.9-4. Time-temperature history for samples N1 and N2 during RIM nonisothermal molding (Lee[78]). Gel time for these samples is approximately 1 minute.

reacting polymer at the mold center behaves adiabatically due to the fast reaction and extremely low heat conductivity of the polymer. The mold surface remains close to isothermal. It is also seen that for sample N1 (wall temperature 85°C) the polymer near the wall rises in temperature due to heat conduction from the hot wall--the temperature at the time of impingement is 50°C. But the heat of polymerization quickly begins to dominate, and soon after (about 10 seconds) the centerline temperature is the hottest. Clearly, a temperature profile develops across the thickness of the part. Samples studied are termed N1-C or N1-S indicating the sample is taken from the center or the surface of the mold, respectively.

C H A P T E R I V

RESULTS AND DISCUSSION ON OSMIUM STAINING OF SOLUTION CAST FILMS

The present chapter is divided into two sections. In the first section we present the experimental results of a heavy atom staining experiment done on solution cast PPO/MDI/BEDO films. In the second section we present a discussion of the observed results.

4.1 Experimental Results

By choosing an atactic material for the soft segment of the polymer, namely poly(propylene oxide), one is limiting the appearance of crystallinity to the hard segment phase, greatly simplifying the study of the system. By using an unsaturated chain extender, the hard segment phase can also be provided with additional electron density by heavy atom staining. The chemical behavior of the staining agent osmium tetroxide (OsO_4) has been thoroughly studied by Criegee[70] who suggested the formation of the following products in the oxidation of a double bond by OsO_4:

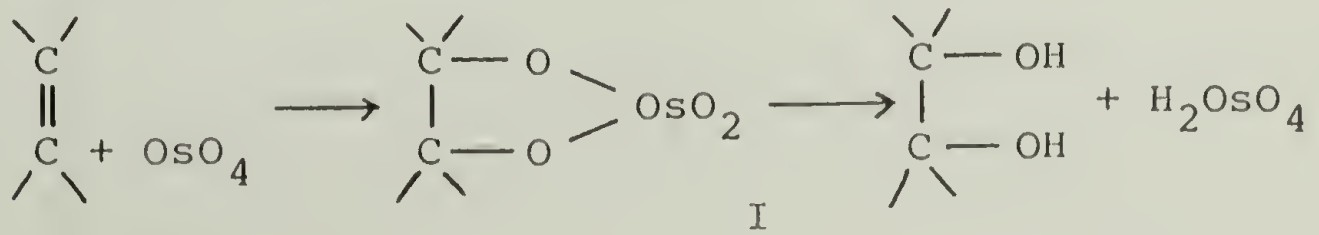

I

Compound I (monoester) is not very stable and is easily hydrolized, but the resulting glycol can react with I to give:

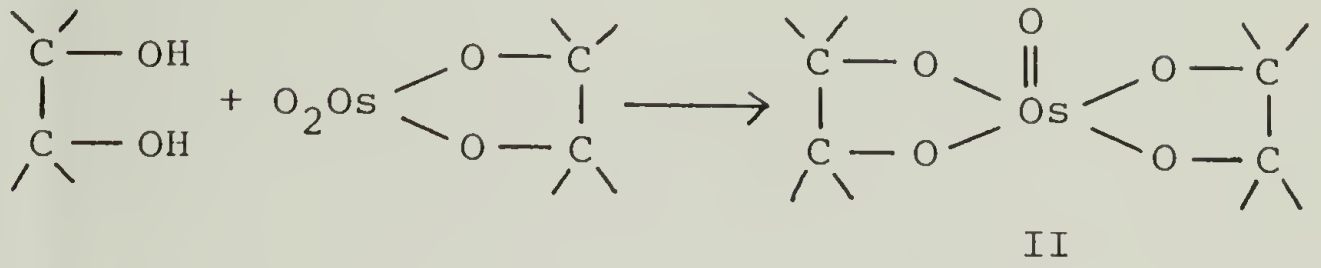

II

Compound II (diester) is very stable and explains satisfactorily the fixation effect of OsO_4. A polymer of compound I for which the following structure was tentatively proposed:[71]

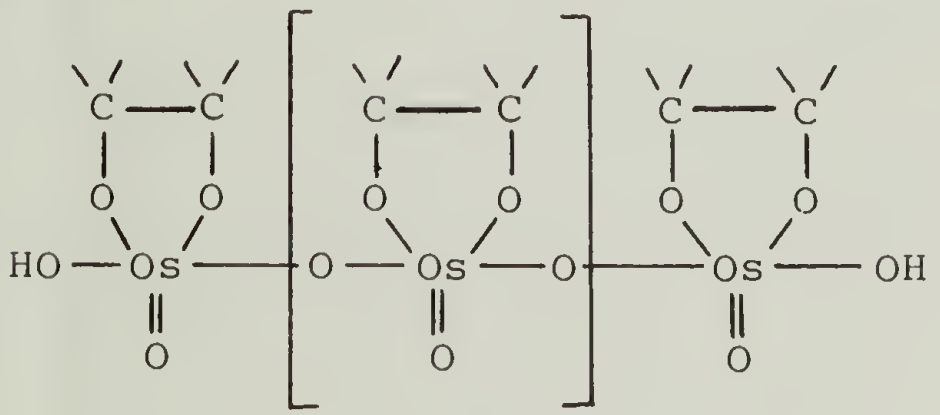

III

would also account for the fixation effect of OsO_4. Unfortunately, so far there is no direct evidence for the formation of compounds II and III.

Figure 4.1-1a shows a bright field micrograph of a PPO/MDI/BEDO unstained film as it appears after the solution casting procedure. One sees volume filling spherulites outlined by bright (thin) spherulite boundaries. At higher magnifications (Figure 4.1-1b) the coarse radiating structure shows some intensity variations most likely due to small

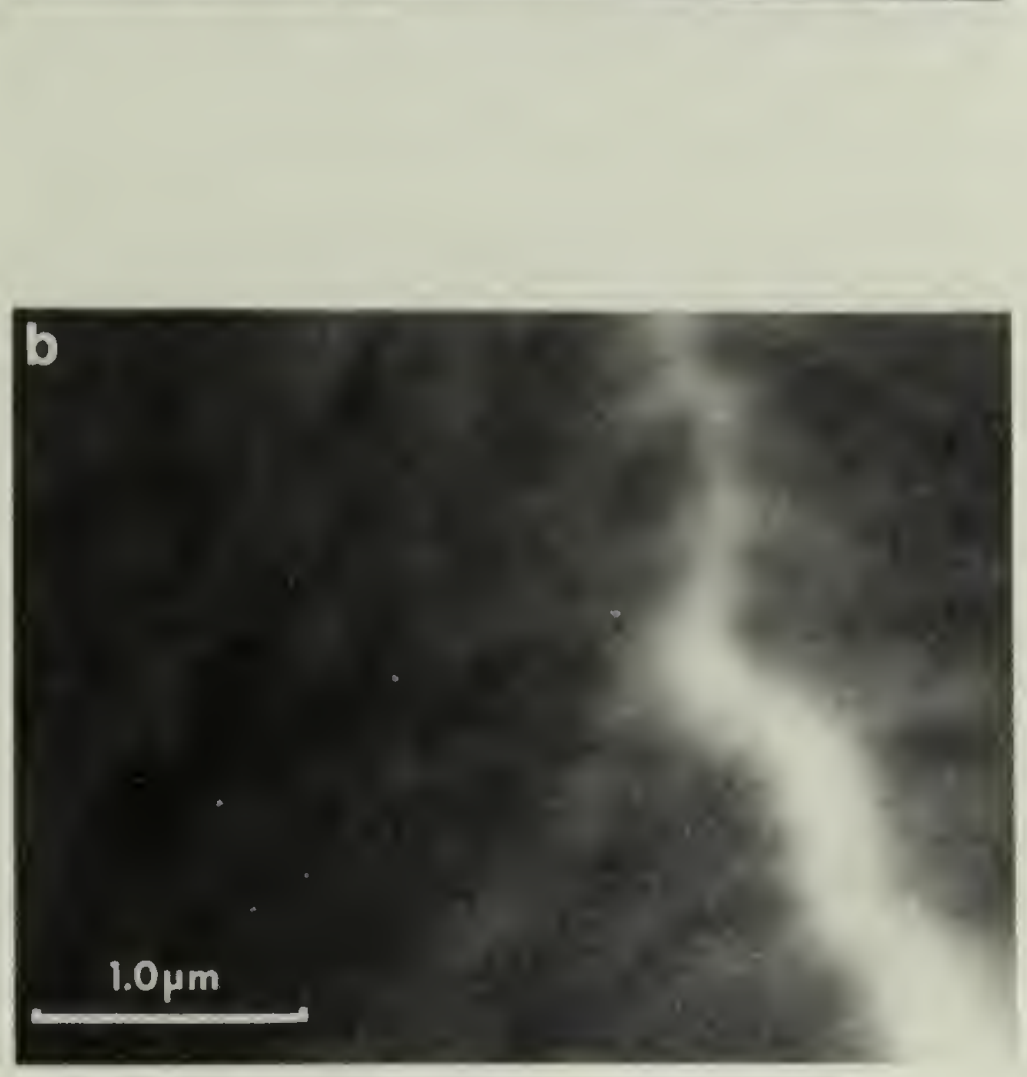

Figure 4.1-1. Unstained PPO/MDI/BEDO film (45% hard segment) as it appears after the casting procedure. (a) 5000X, (b) 25,500X (an enlargement of the upper right portion of the center spherulite).

thickness variations and local compositional changes but does not show any distinct features on the 100Å scale.

After an OsO_4 vapor exposure of 40 minutes (Figure 4.1-2) the centers of the largest spherulites have become noticeably dark. The dark region extends out several microns in the radial direction.

The small dark spheres of about 500Å in diameter that appear randomly throughout the films exposed to OsO_4 have been determined to be osmium rich particles lying on the surface, by x-ray microanalysis in combination with secondary electron imaging.

Figure 4.1-3a shows that the film is less electron transparent after 60 minutes of OsO_4 vapor exposure. The centers of the largest spherulites have darkened considerably. The dark regions extend several microns along the radial direction before diminishing gradually. An enlargement (see Figure 4.1-3b) shows the presence of dark fibrils arranged in bundles, branching out in "palm-leaf" configurations oriented along the radial direction of the spherulites. The branched fibrils are on the order of 0.5 μm in length and the smallest cross section is about 60Å with aggregates of fibrils forming bundles of up to 0.5 μm in diameter. The radiating branching fibrils surround regions of lower electron density. The brightest regions are between branches where the electron density is lowest.

An 80 minute exposure to OsO_4 vapors (Figure 4.1-4)

Figure 4.1-2. PPO/MDI/BEDO film after 40 minutes of exposure to osmium tetroxide vapors showing slight darkening of large spherulites' centers.

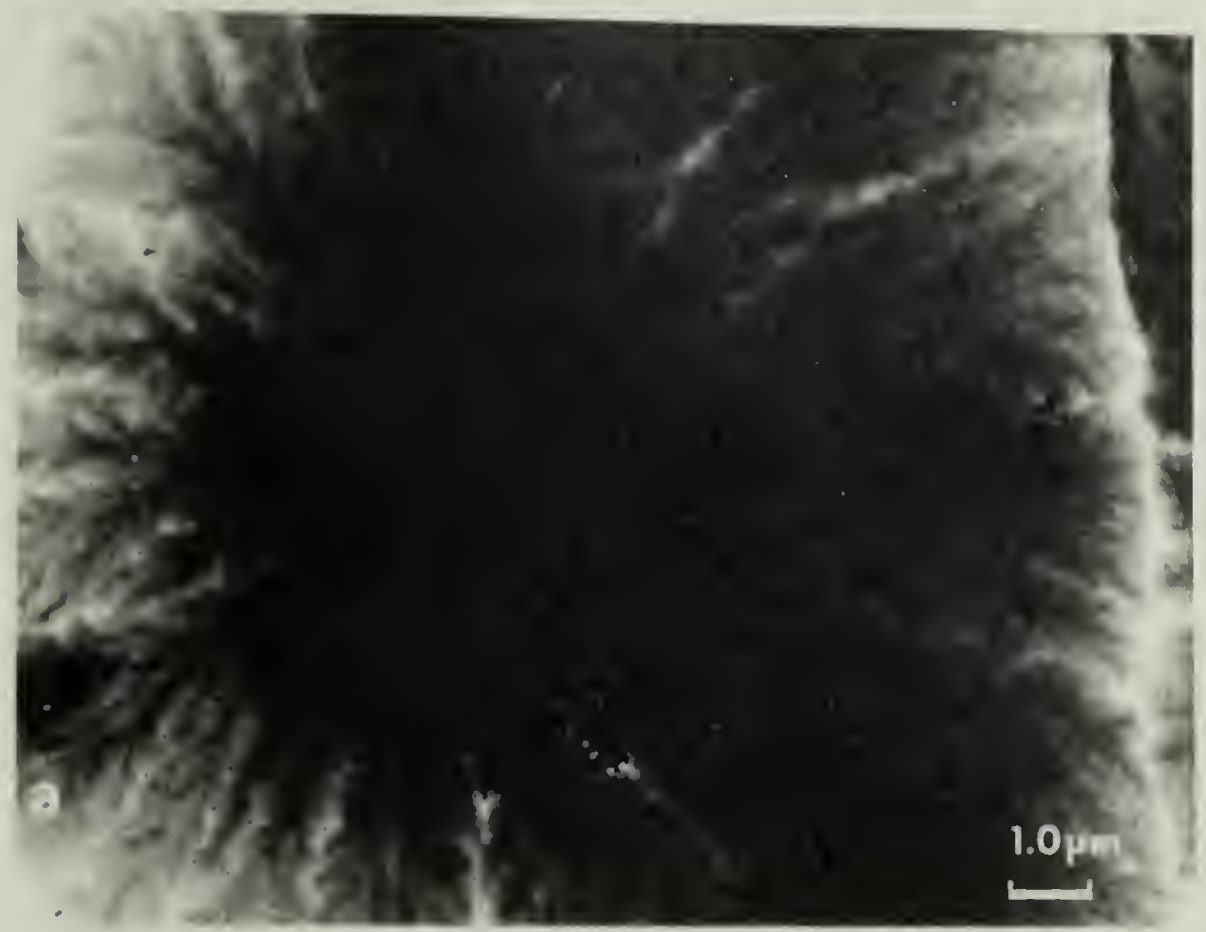

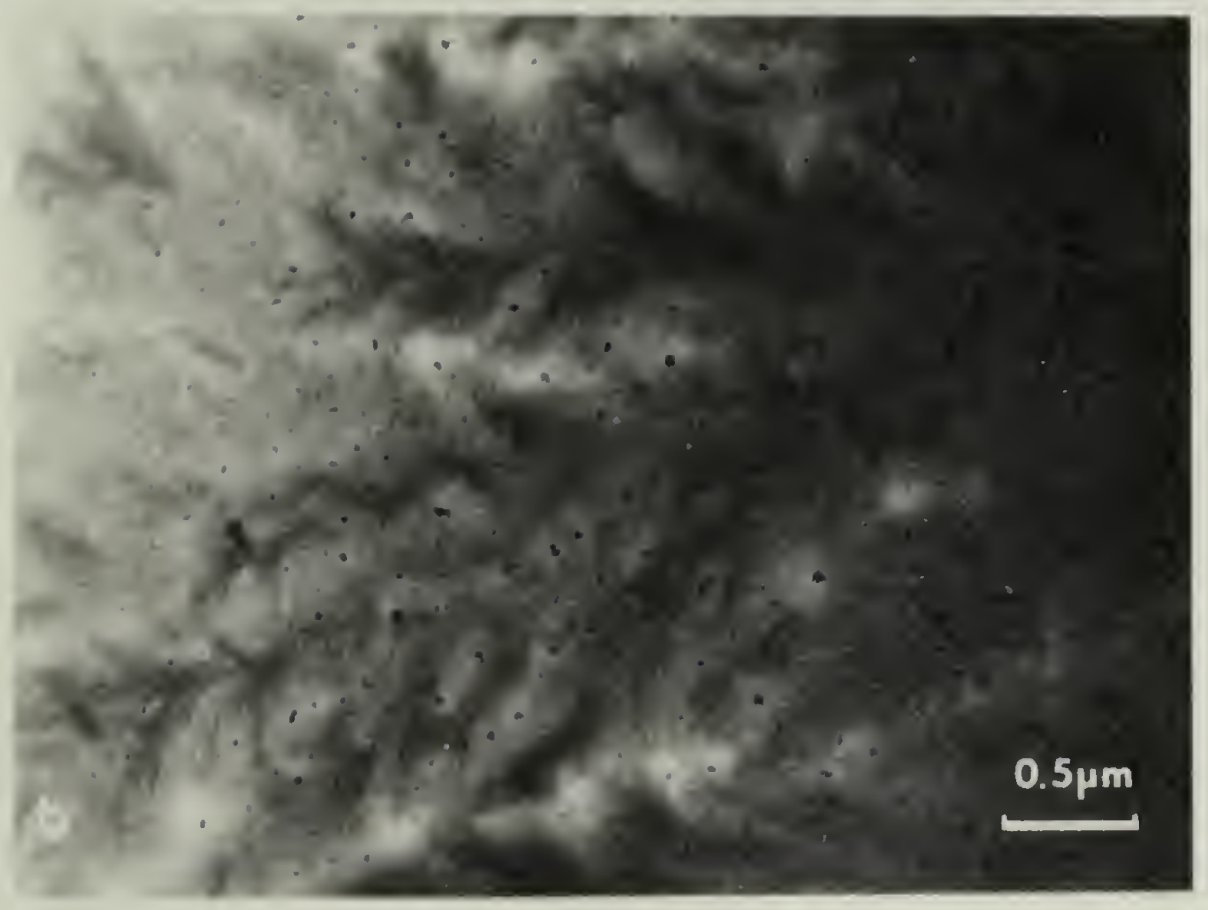

Figure 4.1-3. PPO/MDI/BEDO solvent cast film after 60 minutes of OsO_4 vapor exposure (a) 7500X, (b) radial fine structure discernable from left central portion of spherulite (25,500X).

Figure 4.1-4. PPO/MDI/BEDO film after 80 minutes of OsO_4 vapor exposure. Note large spherulite (about 40 µm in diameter) dark covered over, roughly 70% of its area.

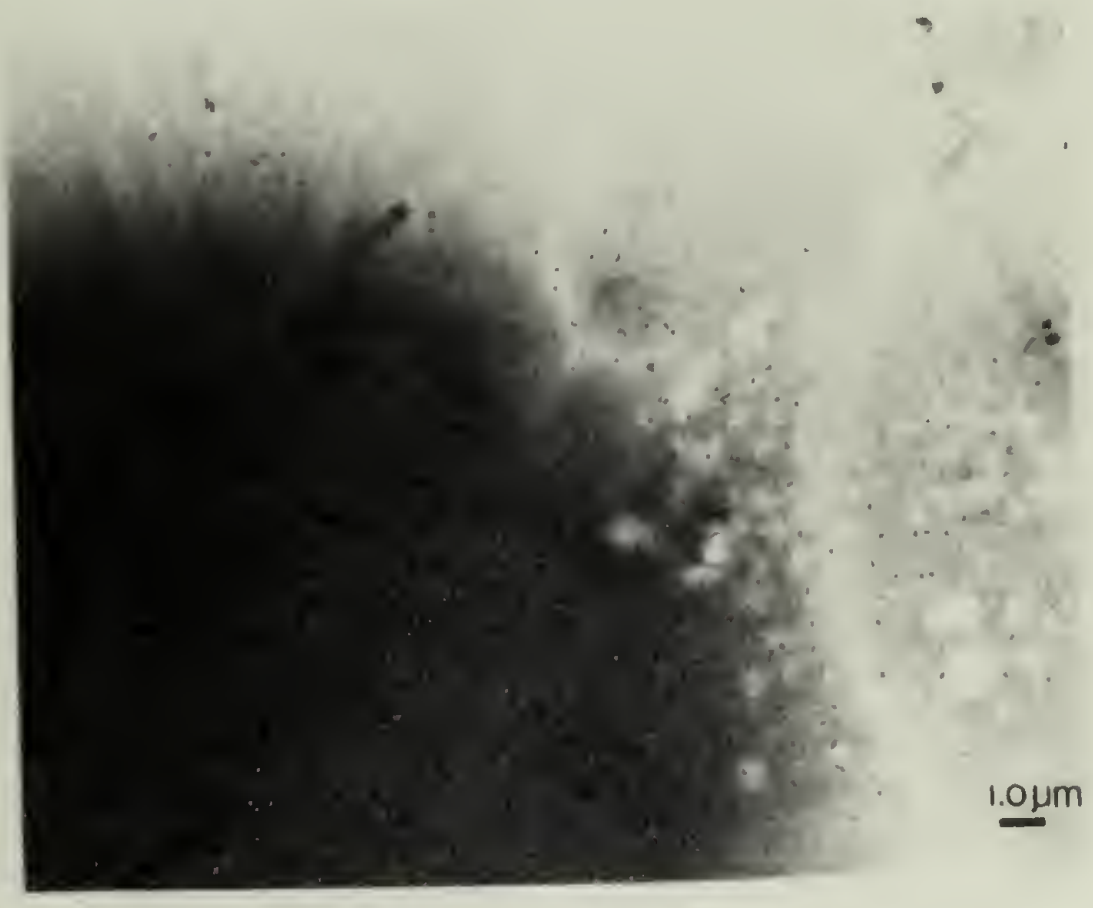

Figure 4.1-5. PPO/MDI/BEDO film after 250 minutes of exposure to OsO_4 vapors. Note abundant osmium nucleation on the film surface.

exhibits a dark covered spherulite over roughly 70% of its area and the radius of the dark region has extended further. The fibrillar region is now very noticeable and occupies the area from the limits of the dark region up to the spherulite boundary.

Finally, Figure 4.1-5 shows the effect of exposing the film to very long staining times (250 minutes). The drastically darkened region has covered the spherulite almost in its entirety, and there is copious nucleation of osmium on the surface of the film.

It is important to point out that not all the spherulites displayed the same extreme dark region development (see Figure 4.1-6). There is a difference on the basis of spherulite size, i.e., larger spherulites are much more heavily stained than smaller spherulites in the same sample. Also, as shown in Figure 4.1-7, the size of the extreme dark center region increases with increasing staining time.

DSC of the solution cast films (Figure 4.1-8b) indicates a Tm of the hard segment phase of approximately 195°C. The heat of fusion value (3.9 cal/g of hard segment) if compared to that of the MDI/BDO hard segment,[76] suggests a low degree of hard segment ordering in the (para) crystalline fibrils. For comparison, the experimental heat of fusion of the original PPO/MDI/BEDO hand cast material is 9.8 cal/g of hard segment (see Figure 4.1-8a). The present degree of ordering of the butenediol based hard segment

Figure 4.1-6. 60 minute OsO_4 stained film showing difference in osmium uptake between large and small spherulites.

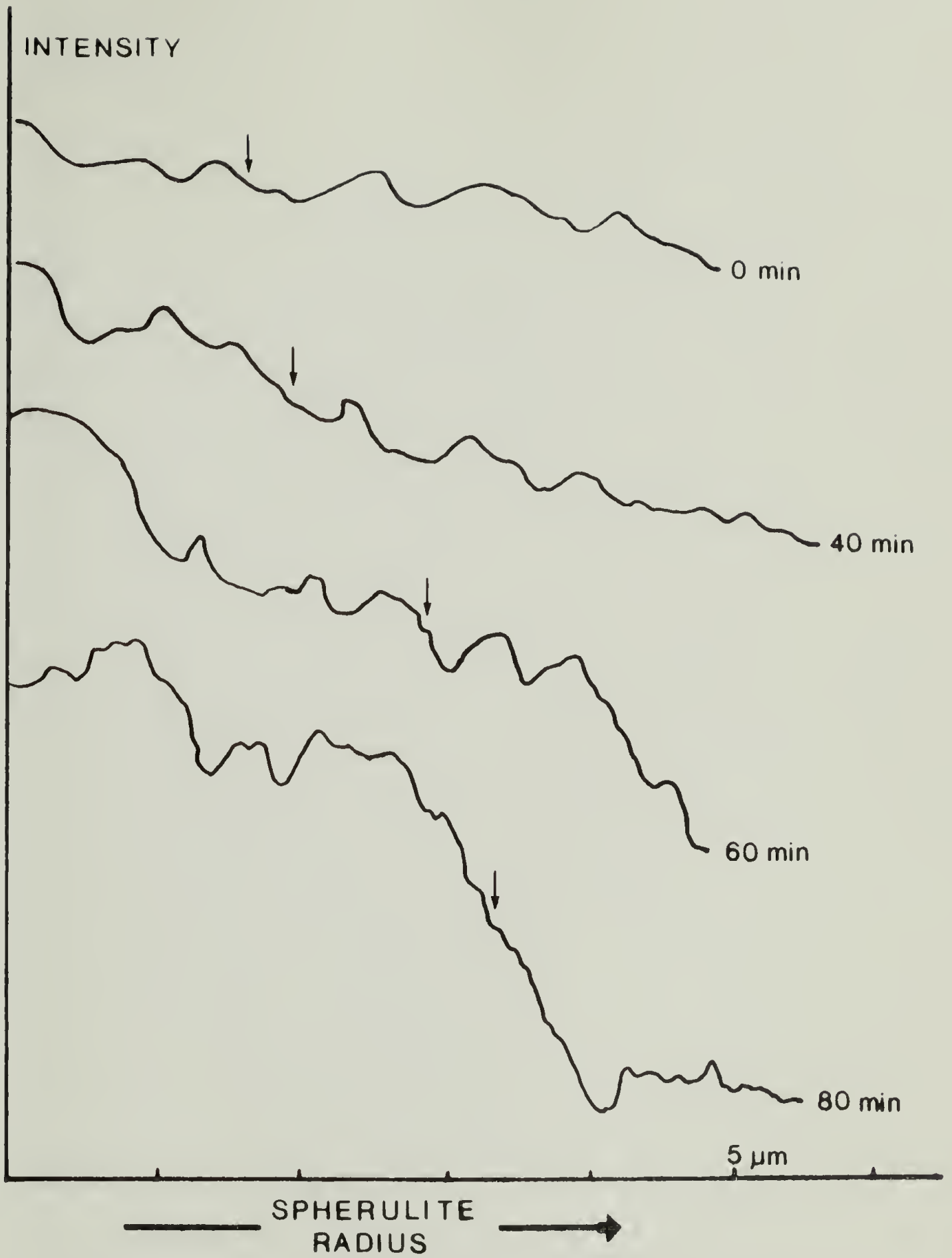

Figure 4.1-7. Microdensitometer scans across approximately 10 μm diameter spherulites showing the radial position for 50% intensity decrease as a function of OsO_4 vapor exposure time. Intensities are not normalized.

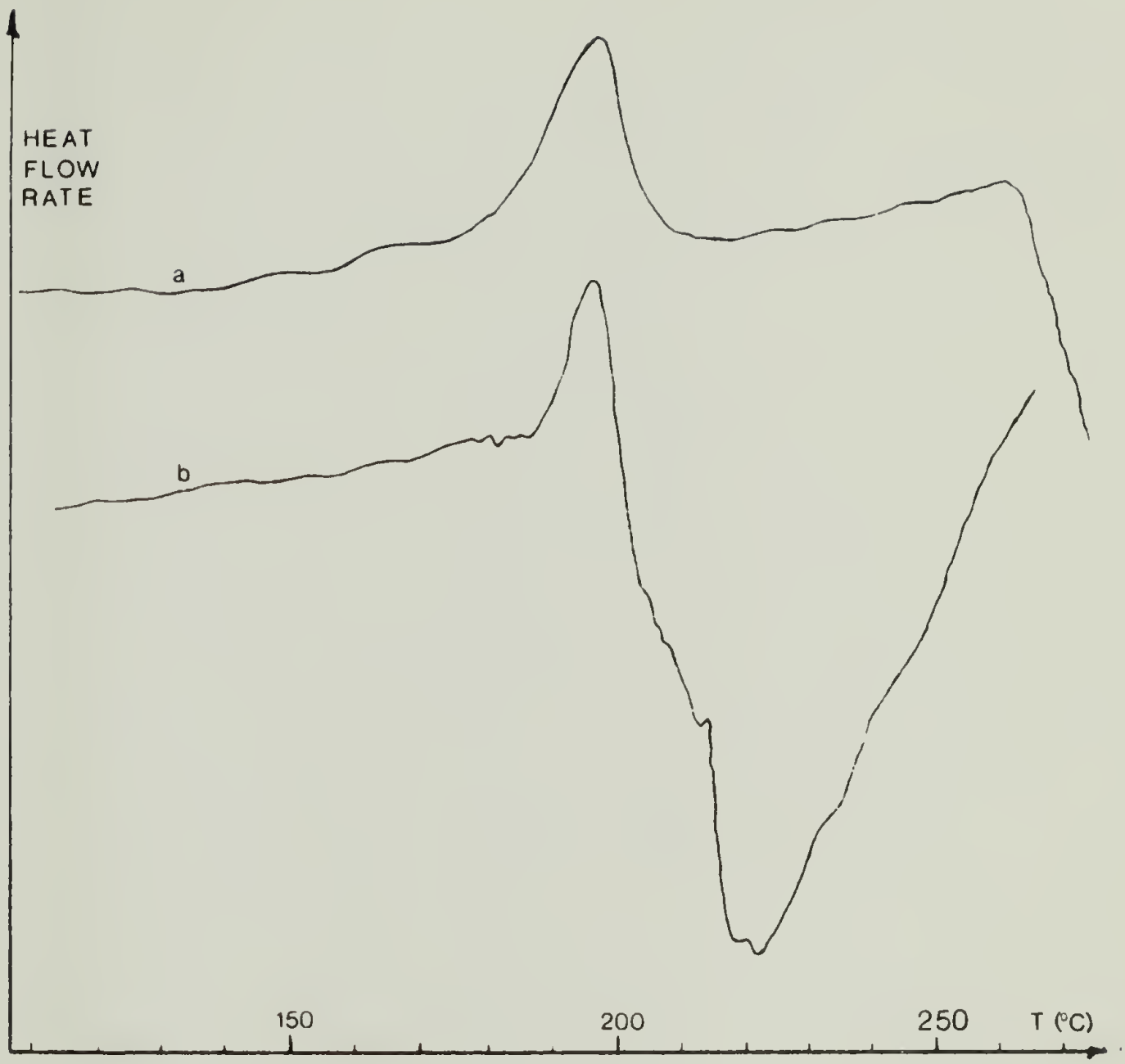

Figure 4.1-8. DSC scans of PPO/MDI/BEDO polyurethane. (a) As-received sample. Sharp exotherm onset (circa 260°C) possibly due to double bond opening. (b) Solution cast (DMF) sample. Broad exotherm may be due to reaction of the polymer with remaining DMF.

phase is very similar to that of the butanediol based hard segment phase in films cast from DMF under comparable conditions.[45]

4.2 Osmium Staining: Discussion

Film casting from solution is a separation process between a solvent and its solute, carried out at approximately constant pressure. The course of solidification of the film can be best appreciated by referring to Figure 4.2-1. The sample starts at point A in the single phase liquid solution region of known composition, and as the solvent slowly evaporates in an open system we approximately follow an isothermal path enriching the system with solute. The evaporation must take place very slowly in order to be close to equilibrium in the condensed phase at any point along the path. At point B we enter the biphasic region where a liquid phase coexists in equilibrium with the first formed solid phase. This solid phase consists of those portions of the polyurethane molecules having the highest potential for hydrogen bond formation (i.e., the longer hard segment sequences). The relative amount of each phase as one moves towards point C can of course be calculated by the lever rule. As one transits from point B to point C, more solute molecules come out of solition on the basis of their ability to crystallize, namely chains possessing predominantly long hard segment sequences, followed by chains with on the

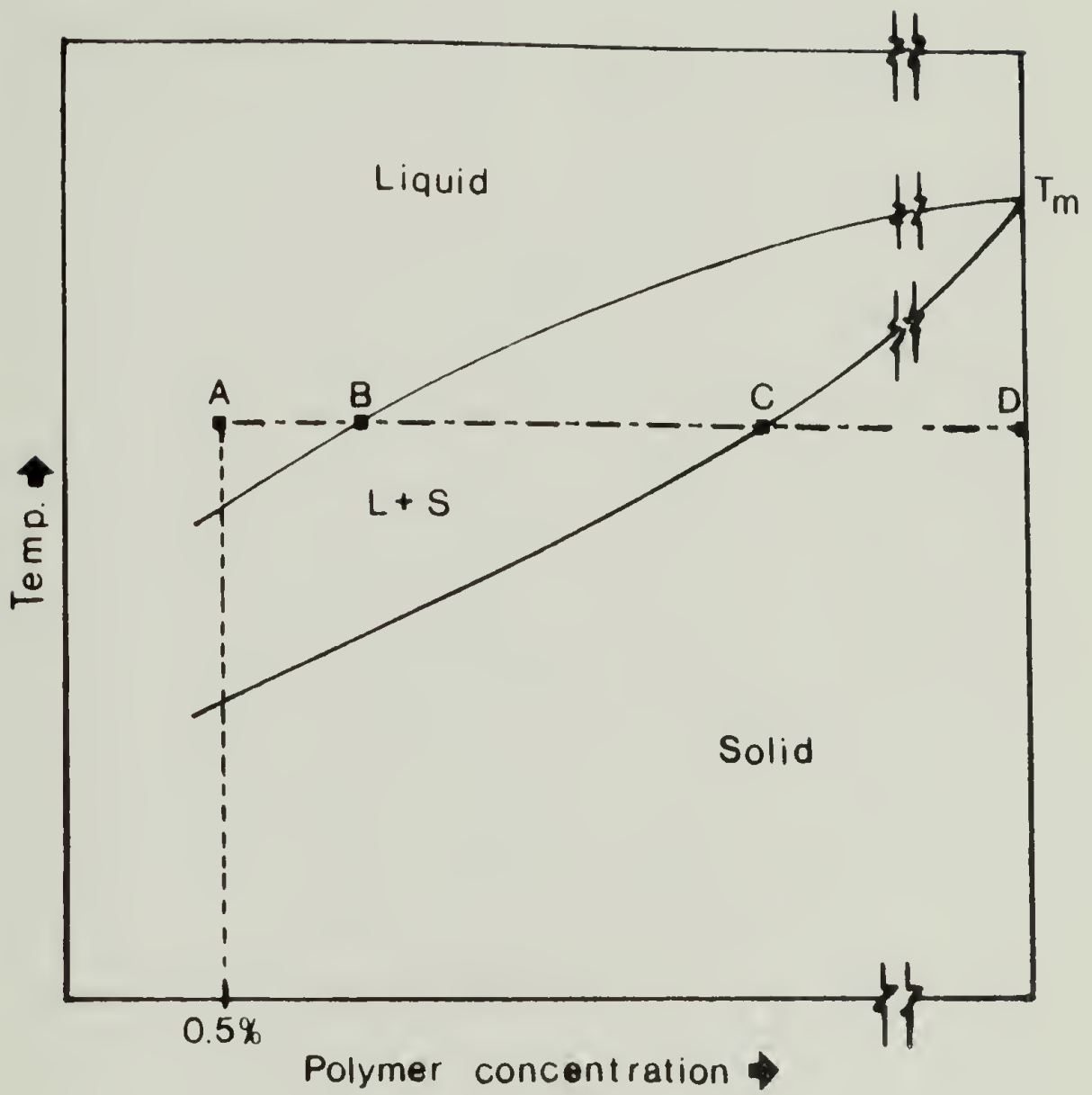

Figure 4.2-1. Assumed phase diagram of polymer-solvent.

average shorter hard segment sequences. From point C and on the polymer is essentially in swollen solid phase. With further drying one arrives at the solid polymer film, represented by point D.

This rationale suggests that the centers of the largest spherulites are composed primarily of molecules with long hard segment sequences, inasmuch as nucleation is expected to initiate with the most easily precipitated species. The polymer molecules with the fewest and shortest hard segment sequences remain in solution longest and eventually form the peripheral regions of the spherulites. By the same token, the population of stainable double bonds will be highest at the center of the largest spherulite and decrease with spherulite radius. Since at any time during solvent evaporation the remaining liquid phase can be assumed homogeneous, then the centers of the later nucleating spherulites should have approximately the same hard segment content as a region of an already growing spherulite (e.g., compare points x and y in Figures 4.2-2a,b).

At longer staining times (see Figures 4.1-4 and 4.1-5) the darkening of the central portion of the spherulite becomes progressively larger (see Figure 4.1-7) and increasingly darker. The extreme degree of darkening seems far beyond what would be expected by addition of osmium tetroxide to double bonds only. It might involve some additional autocatalytic mechanism allowing collateral attach-

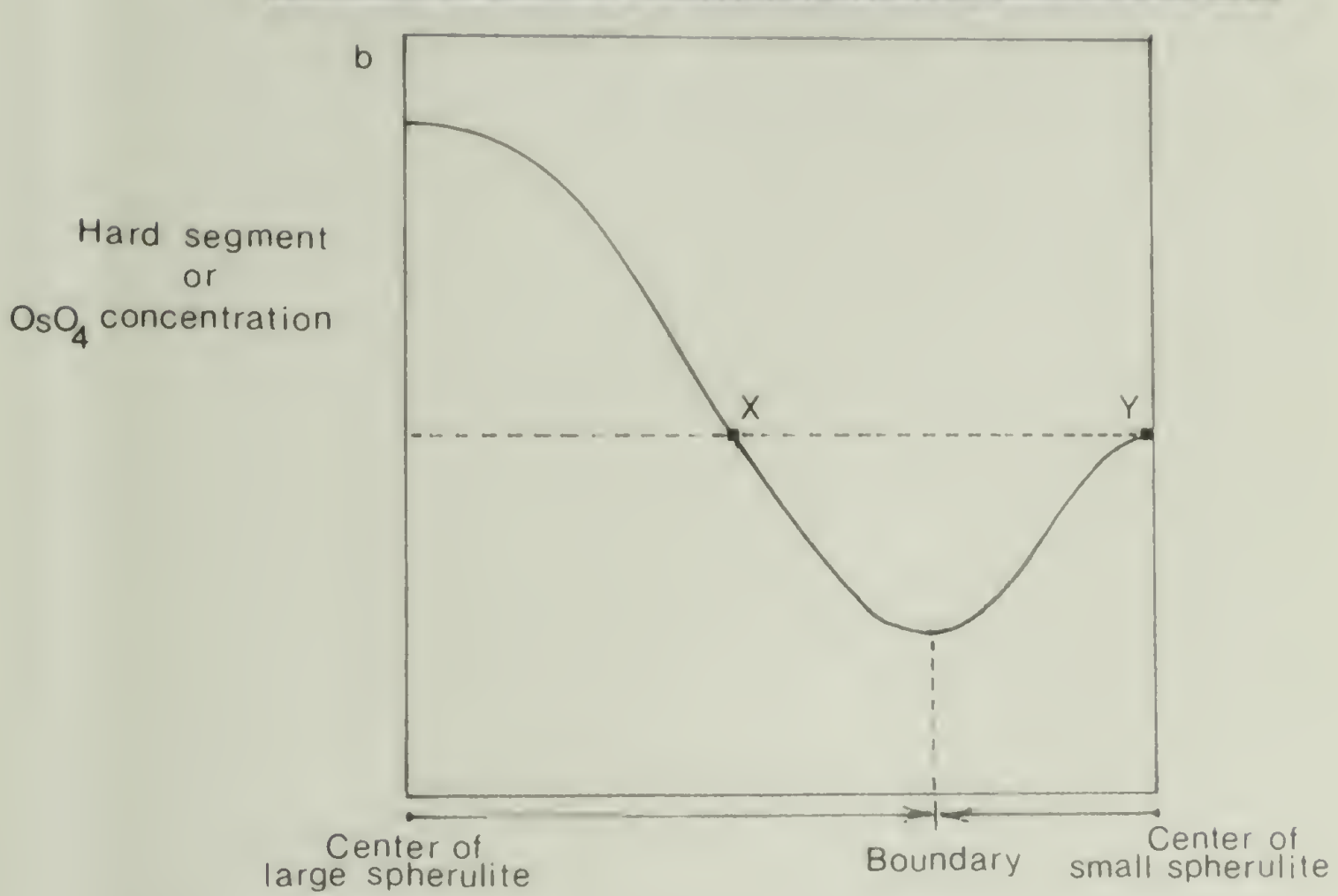

Figure 4.2-2. (a) PPO/MDI/BEDO after 80 minutes of OsO_4 vapor exposure. (b) Diagram showing points of equal hard segment concentration (x,y) in large and small spherulites.

ment of OsO_4 in the previously stained regions.

Careful observation of the micrograph series (Figures 4.1-1 through 4.1-4) yields a detailed morphological picture of this polyurethane that is in good agreement with Schneider's model for crystalline spherulite forming hard segment urethanes.[15] Overall there are three levels of intensity discernable: (i) dark branched structures, (ii) uniform areas of intermediate intensity with no distinct features, and (iii) small, very light areas. These three structures seem to correspond well to the previously proposed (i) crystalline hard segment fibril domains, (ii) unorganized mixed hard (presumably short sequences) and soft segment phase, and (iii) a soft segment rich phase with low hard segment content. Such correspondence seems reasonable since Schneider's polyurethane is essentially the same, only with butanediol as chain extender.

The smallest fibrils previously observed were somewhat thicker (200-300Å diameter) and formed an open network containing material of lower electron density but while part of a spherulitic superstructure, the fibrils did not show a pronounced radial orientation.[15] This difference is ascribed mainly to the different solidification conditions used in each study as well as to the nature of the different chain extenders employed.

Solution casting promotes the partitioning of the polyurethane molecules on the basis of hard segment sequence

length, resulting in a radial dependence of the hard segment concentration in the spherulites. The reported increase in the melting point[47] and the sharpening of x-ray reflections[23] with volume fraction of hard segment is accepted to imply an increase of domain size with increased hard segment content. Thus, a distribution of domain sizes along the radius of a solution cast spherulite follows for a given sample possessing both molecular weight and length distributions.

A further feature of the present experiment indicates a definite branching tendency of the fibril structures. This can be understood by noting that as hard segment solidification-crystallization proceeds, the incorporation of hard segment units into the growing fibril requires accommodation of the intervening connecting soft segment units which results in the need for fibril branching (see Figure 4.2-3a,b). The minimum observable fibril diameter of about 60Å corresponds to about 3 consecutive hard segment units (20.51Å for a single MDI/BEDO repeat unit). This suggests a minimum crystallizable MDI/BEDO hard segment block size of 3 units. An earlier study[56] postulated a minimum hard segment block size for phase separation. Some fibrils appear to have diameters up to a large fraction of a micron. Such structures are very likely agglomerates of smaller fibrils although the techniques employed cannot distinguish substructure within these bundles. The fibril volume fraction in

Figure 4.2-3a. High magnification of 80 minute OsO_4 stained film showing fine fibrillar texture. Volume fraction of fibrils approximately 14%.

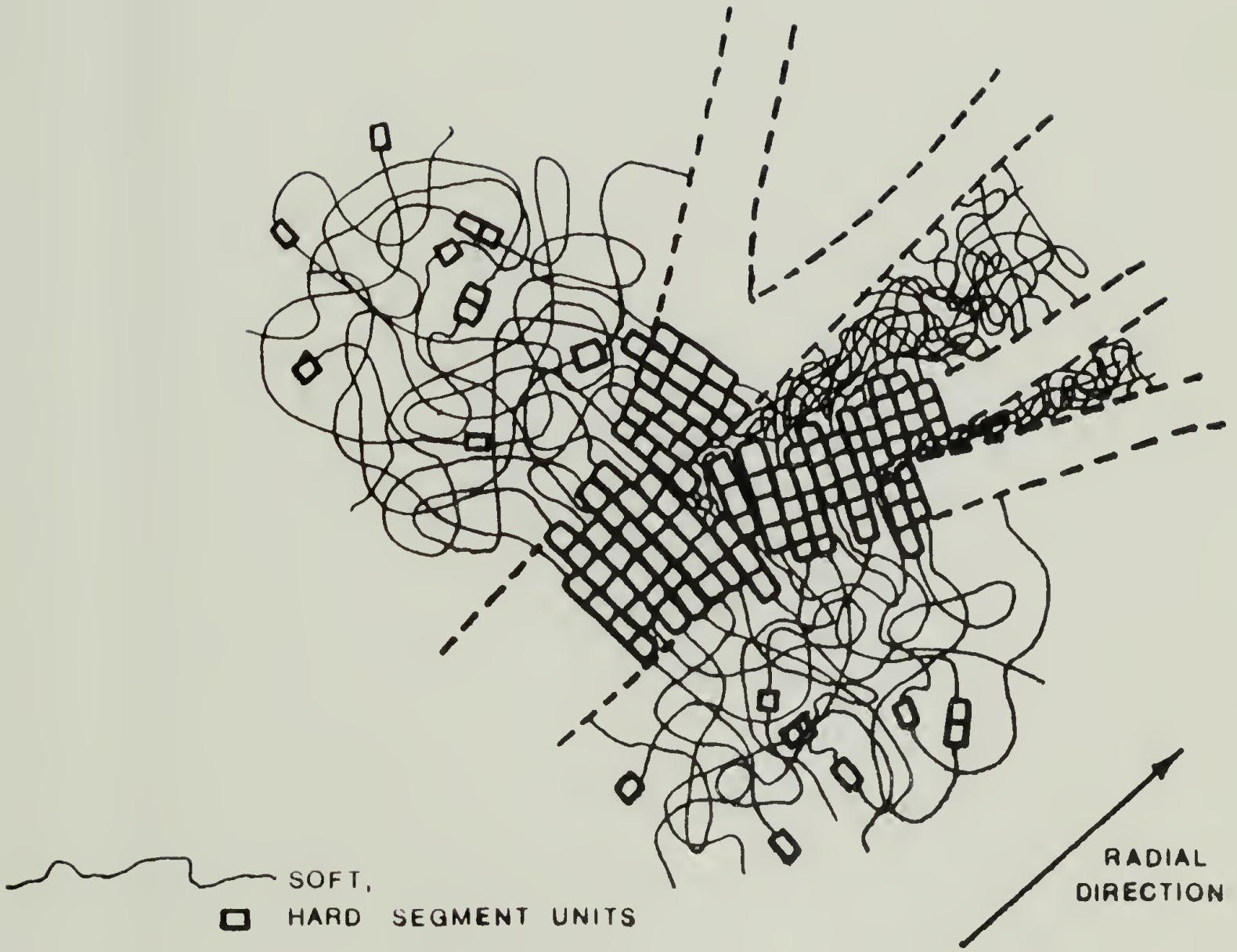

Figure 4.2-3b. Proposed structure of hard segment domains. Branching occurs to allow accommodation of soft segment units. Approximate 10:1 ratio of soft segment to hard segment length is drawn.

Figure 4.2-3a measured using the grid point fraction method[82,83] is approximately 14%. This supports considerable phase mixing of shorter hard segment sequences in the surrounding matrix which is in good agreement with the uniform OsO_4 staining of the matrix.

C H A P T E R V

EXPERIMENTAL RESULTS

This chapter presents the experimental results of morphological differences between mold centerline and mold surface as investigated by DSC, WAXS, optical and transmission electron microscopy.

5.1 Differential Scanning Calorimetry

DSC thermograms for the samples N1 and N2 are shown in Figure 5.1-1a,b. Two clear transition regions are observed: (a) a soft segment melting endotherm at about 53 to 58°C, and (b) a hard segment melting transition at 200 to 220°C. In addition N1-S and N2-S samples show an exotherm centered at 180°C. The hard segment glass transition could not be detected by DSC. Tg of the pure hard segment is in the range of 110 to 125°C.[15,81] The Tg of the pure soft segment was taken at -70°C.[49,84] Note that the soft segment melting point and the hard segment Tg occur in the temperature range of the RIM process (see Figure 3.9-4). The importance of this fact will become evident in further discussion.

The measured crystalline heats of fusion of both types of segments are shown in Table 5.1-1. In comparing

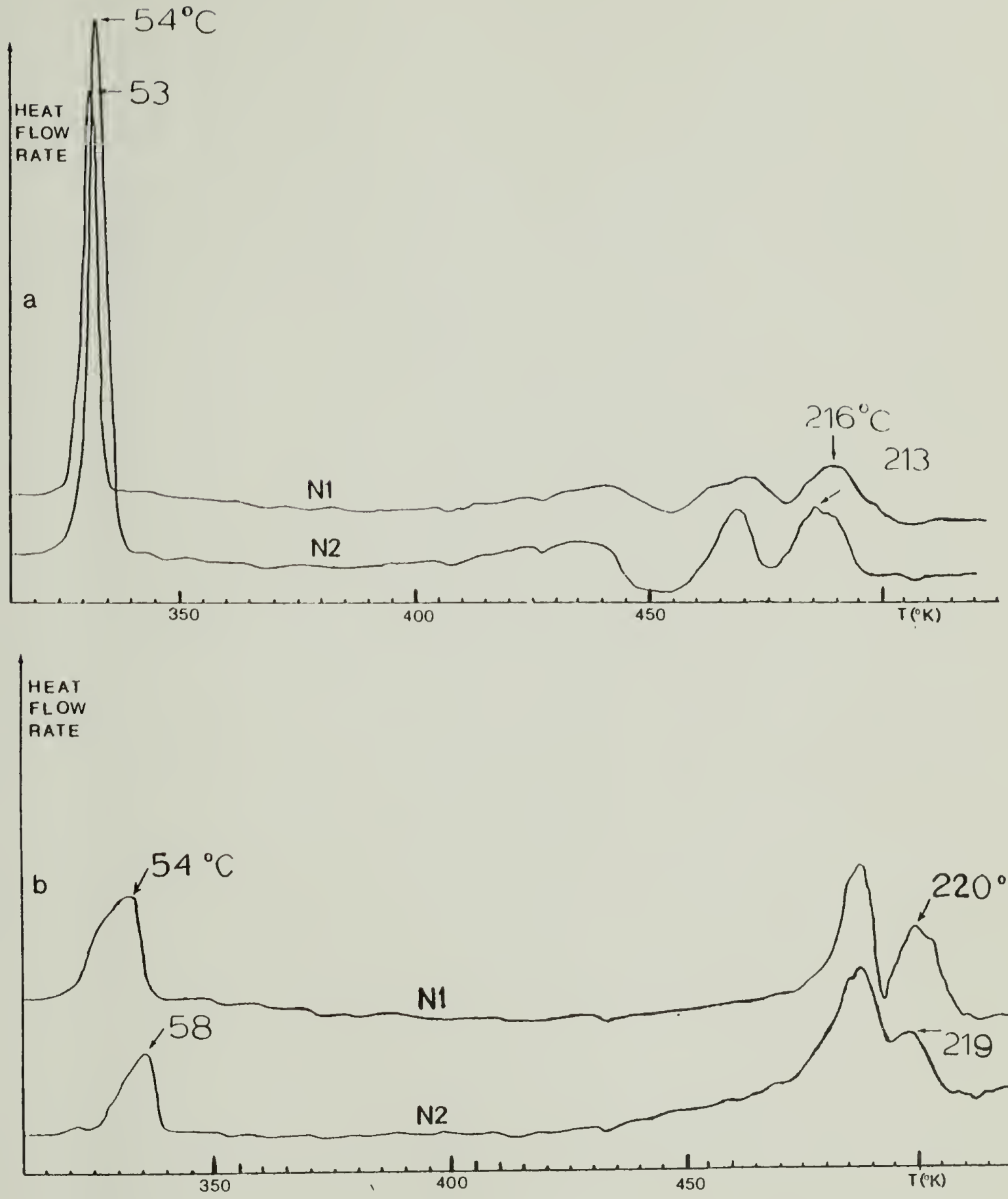

Figure 5.1-1. DSC scans of samples N1 and N2. (a) Mold surface portions show sharp soft segment melting peak and broad hard segment melting peaks. (b) Mold centerline portions show increased hard segment crystallinity and diminished soft segment crystallinity.

TABLE 5.1-1

SUMMARY OF EXPERIMENTAL DATA ON SAMPLES N1 and N2

		N1		N2	
		Center	Surface	Center	Surface
DSC Crystalline heats of fusion, (cal/g)*	(soft segment)	0.8	1.2	0.7	2.1
	(hard segment)	2.5	1.7†	2.5	0.8†
Interplanar d-Spacing (A) WAXS		4.50 4.09 3.81	-- 4.13 3.73	4.49 4.09 3.67	-- 4.17 3.81
Volume fractions** ± 10%	(spherulites)	0.93	0.20	0.83	0.03
	(globules)	0.04	0.35	0.12	0.53
	(matrix)	0.03	0.45	0.05	0.44
Average sizes of structures (μm), TEM	(spherulites)	33	35	20	20
	(globules)	8	10	4	6

*in cal. per gram of polymer. For pure soft segment[80] (100% crystallinity) ΔH_f=26.4 cal./g, and for hard segment[76] ΔH_f=35.5 cal.g.

**From optical and TEM micrographs. Area fraction equals volume fraction for random slices through random tridimensional phases.[82,83]

†Likely due to crystallization during DSC scan.

these values with the theoretical heat of fusion for the perfect 100% crystalline soft[80] and hard[76] segments one obtains the degree of crystallinity which varies from 5% (N2-C) to 14% (N2-S) for the soft segment, and from 5% (N2-S) to 16% (N2-C) for the hard segment. For samples N1-S and N2-S the exotherm observed in the range 170-185°C is likely due to hard segment crystallization taking place during the DSC scan.

The surface portions of the polymer exhibit a single soft segment melting peak at about 54°C and multiple hard segment melting peaks at approximately 195 and 215°C. Multiple hard segment melting peaks are consistent with reports of other workers.[15,29] The center portions of the polymer show a more concentrated hard segment domain melting at 210 to 220°C and a greatly diminished soft segment melting peak.

5.2 Wide Angle X-Ray Scattering

A summary of the WAXS data of samples N1 and N2 is shown on Table 5.1-1 and the traces in Figure 5.2-1a,b. The mold center portions show three distinct reflections at 4.50, 4.09 and 3.81Å (4.49, 4.07 and 3.67Å for N2-S). As shown in Figure 5.2-2, these soft segment crystalline reflections disappear upon heating the sample above the soft segment melting transition.

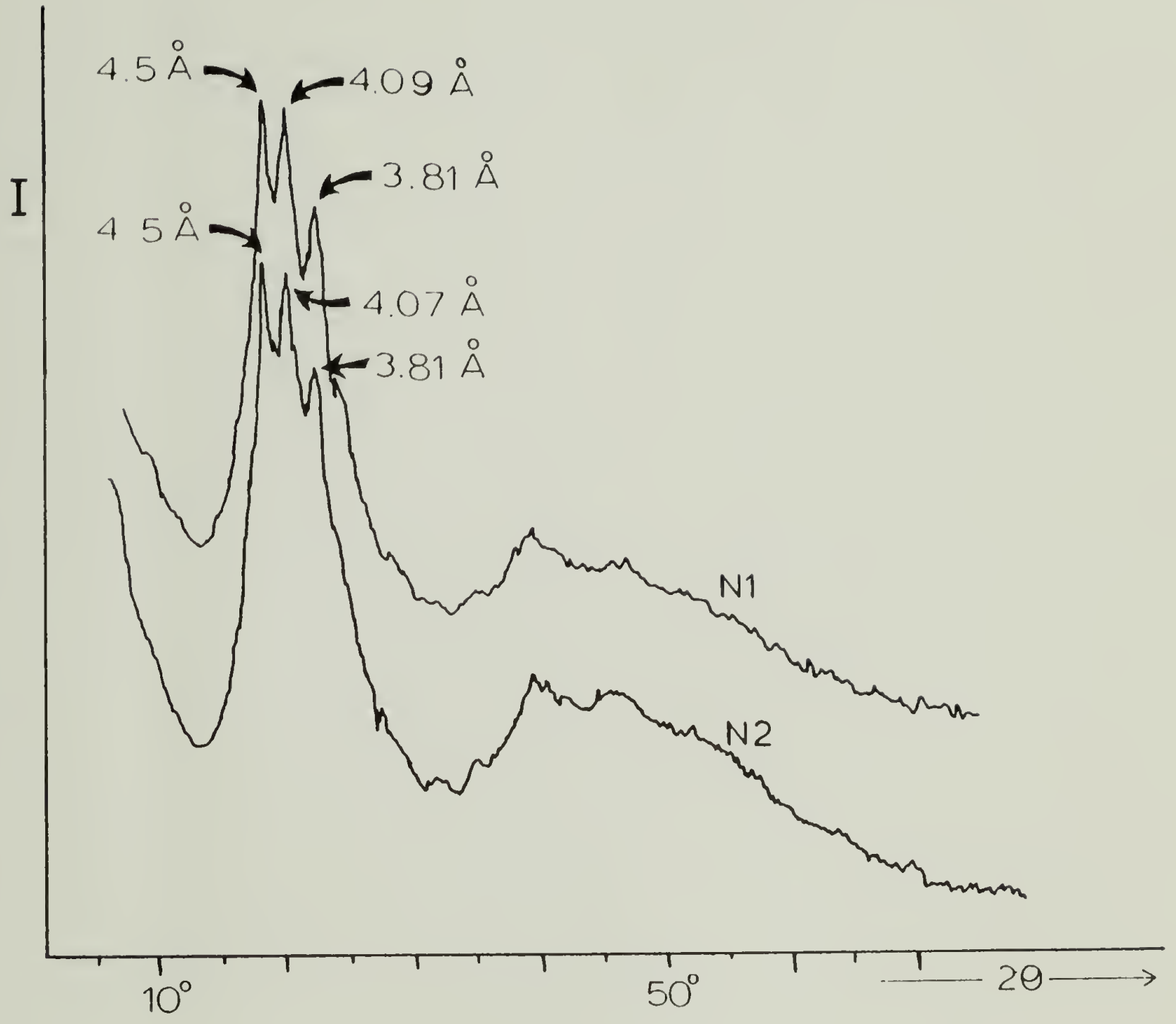

Figure 5.2-1a. WAXS scans of nonisothermal samples N1 and N2. Mold centerline portions.

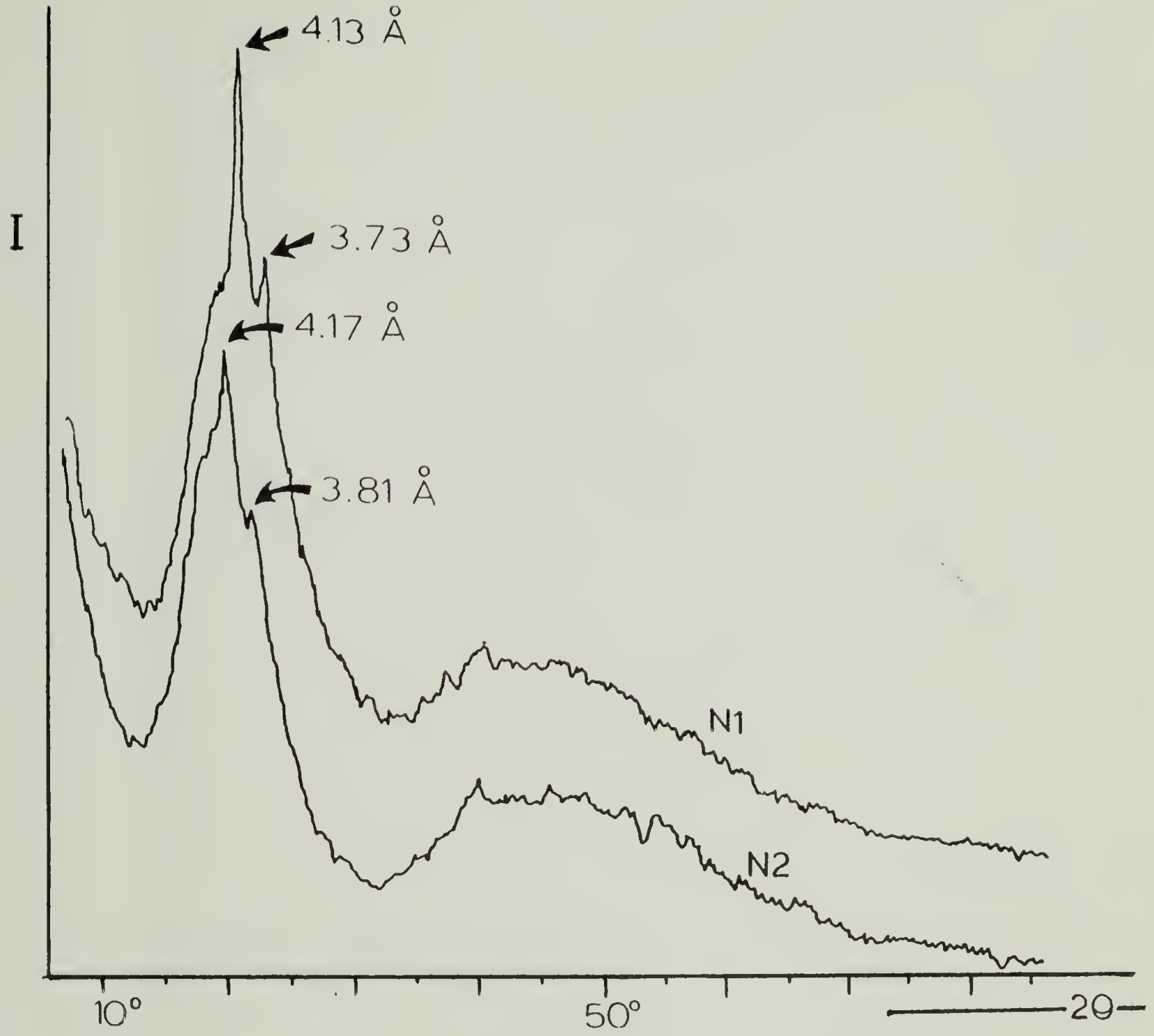

Figure 5.2-1b. WAXS scans of nonisothermal samples N1 and N2. Mold surface portions.

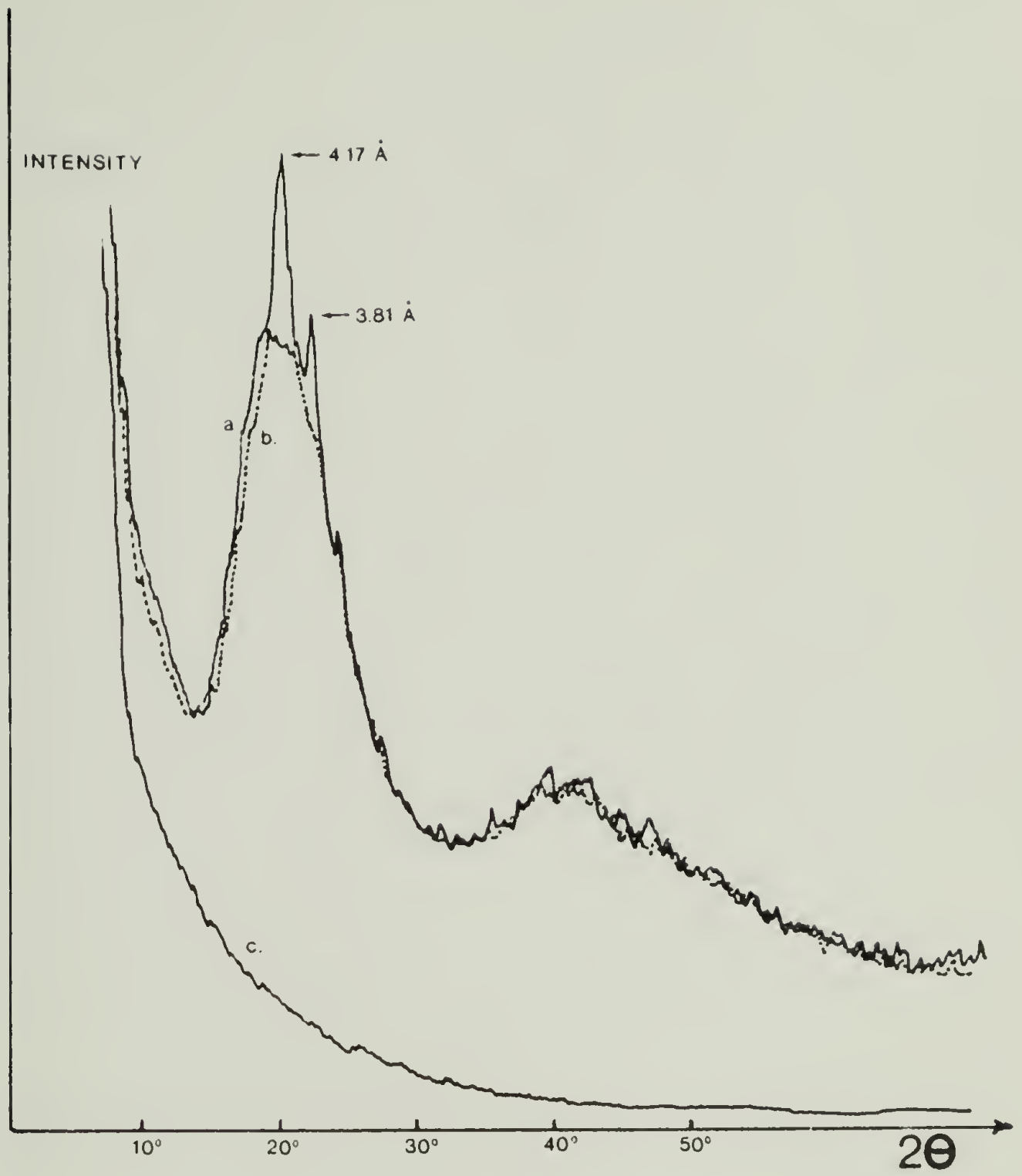

Figure 5.2-2. WAXS scans of sample N2-S. (a) Room temperature, (b) at 65°C (above soft segment melting transition), (c) background.

5.3 Transmission Electron Microscopy

Centerline slices of both N1 and N2 samples show spherulites of fibrous texture (see Figure 5.3-1a,b) reminiscent of hard segment-rich spherulites as observed by Schneider.[15] The average spherulite diameter is 30 μm and 20 μm for N1 and N2 samples, respectively. In addition, for the N2 sample there are occasional dense spherical structures or "globules" about 5 μm in diameter, in the featureless matrix between the spherulites and occasionally inside the spherulites as well.

In samples N1-S and N2-S the relative population of globules is significantly greater (diameters 6 to 10 μm) while the volume fraction of hard segment-rich spherulites is drastically diminished (see Figure 5.3-1c,d). The globules appear to have a featureless interior and are more electron dense than the matrix.

No soft segment-rich (PCP/MDI) spherulites were observed. The origin and nature of the novel globular structures will be discussed in Chapter VI.

5.4 Polarized Light Microscopy

The presence of hard segment-rich spherulites observed by TEM is confirmed by optical microscopy. Samples N1-C and N2-C (see Figure 5.4-1a,b and Appendix) show spherulites with very diffuse boundaries, normal extinction

Figure 5.3-1. Bright field TEM micrographs. (a) Sample N1-C showing interpenetrating hard segment spherulites. (b) Sample N2-C. Note presence of globules incompatible with both hard segment spherulites and soft segment-rich matrix.


a
1.0μm

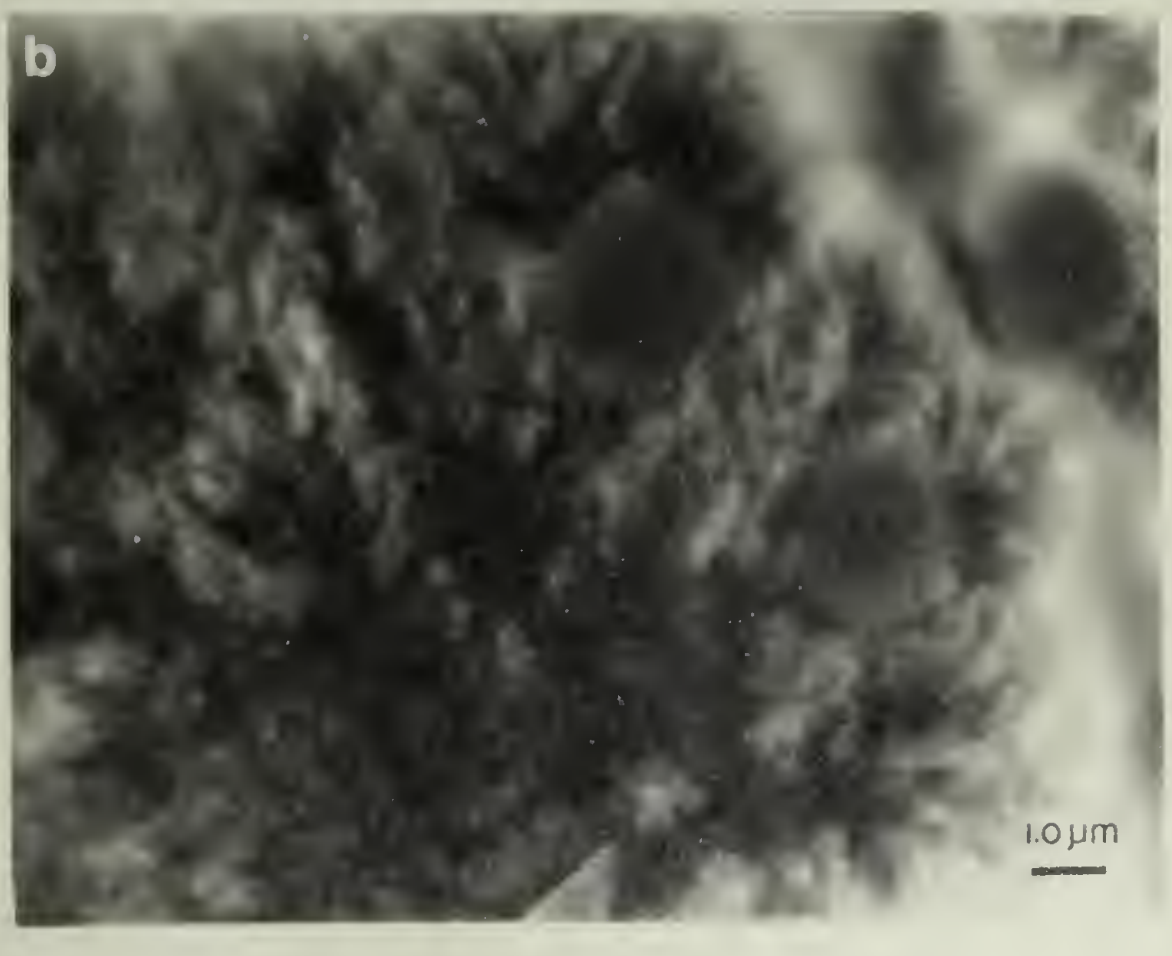
b
1.0 μm

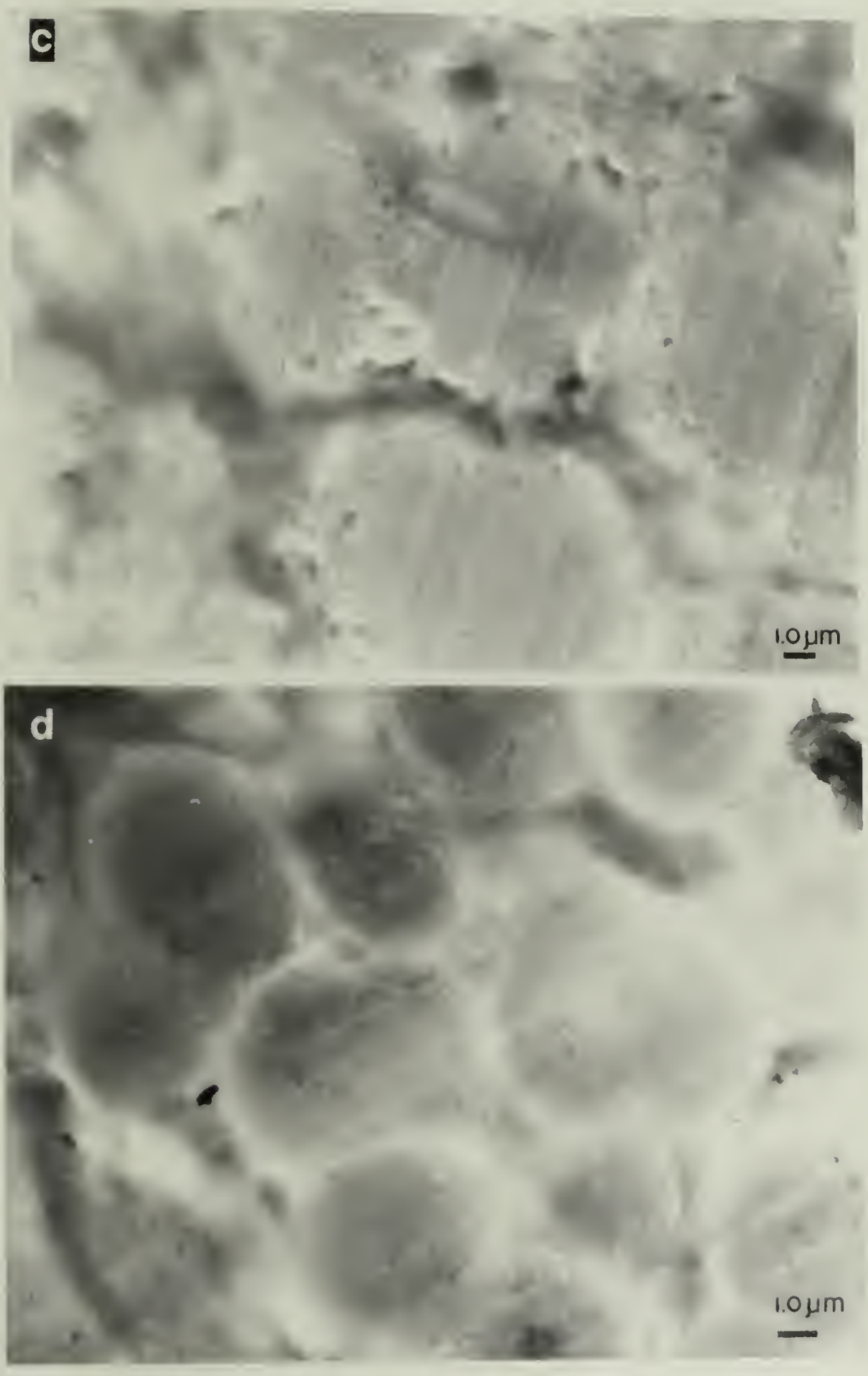

Figure 5.3-1. TEM bright field micrographs of microtomed sections, (c) N1-S and (d) N2-S exhibit densely populated globules immersed in a featureless matrix.

Figure 5.4-1a. Optical micrograph (under crossed) polars) of sample N1-C and schematic of structures. Note interpenetration of spherulites which complicates observation of individual entities.

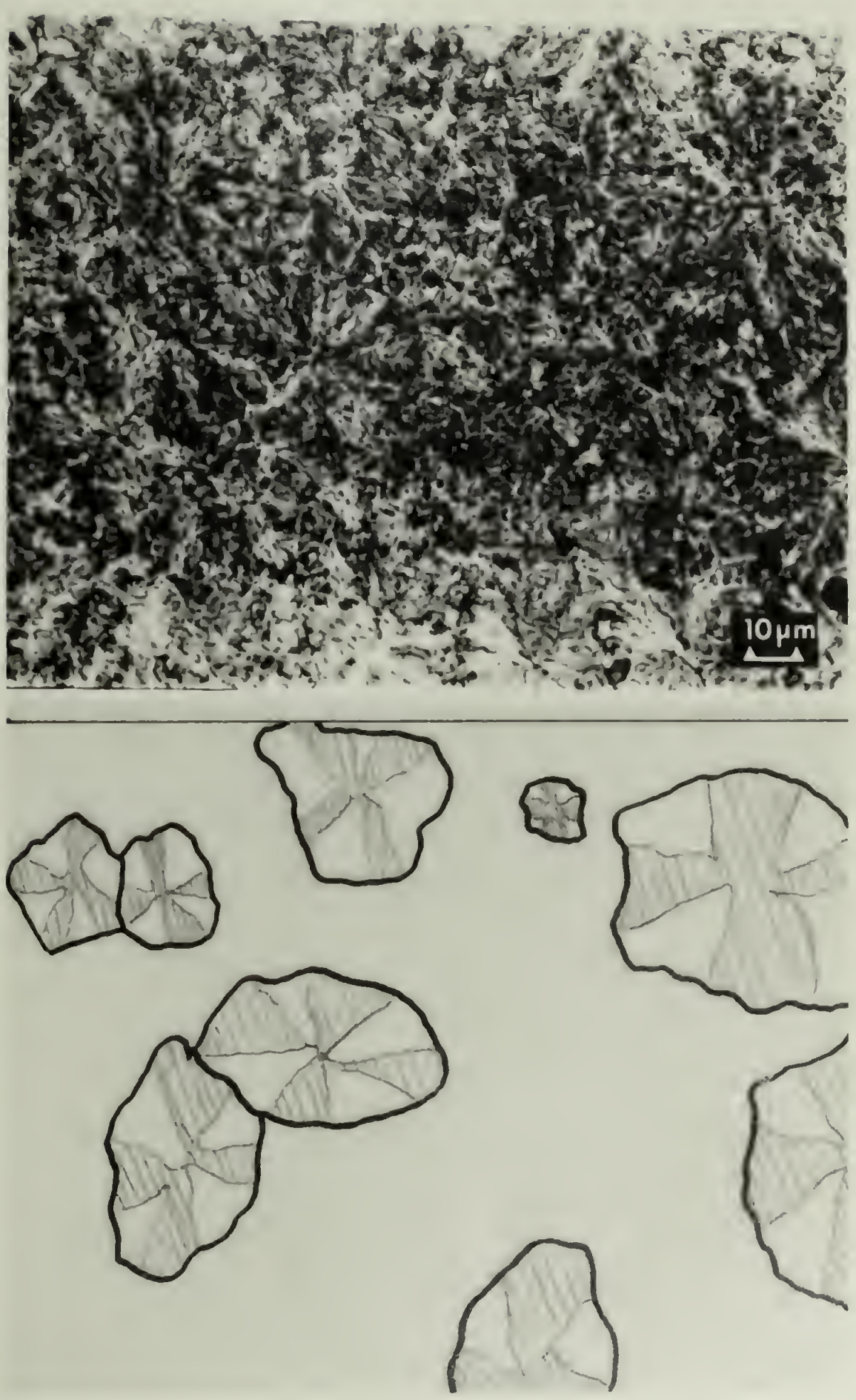
10µm

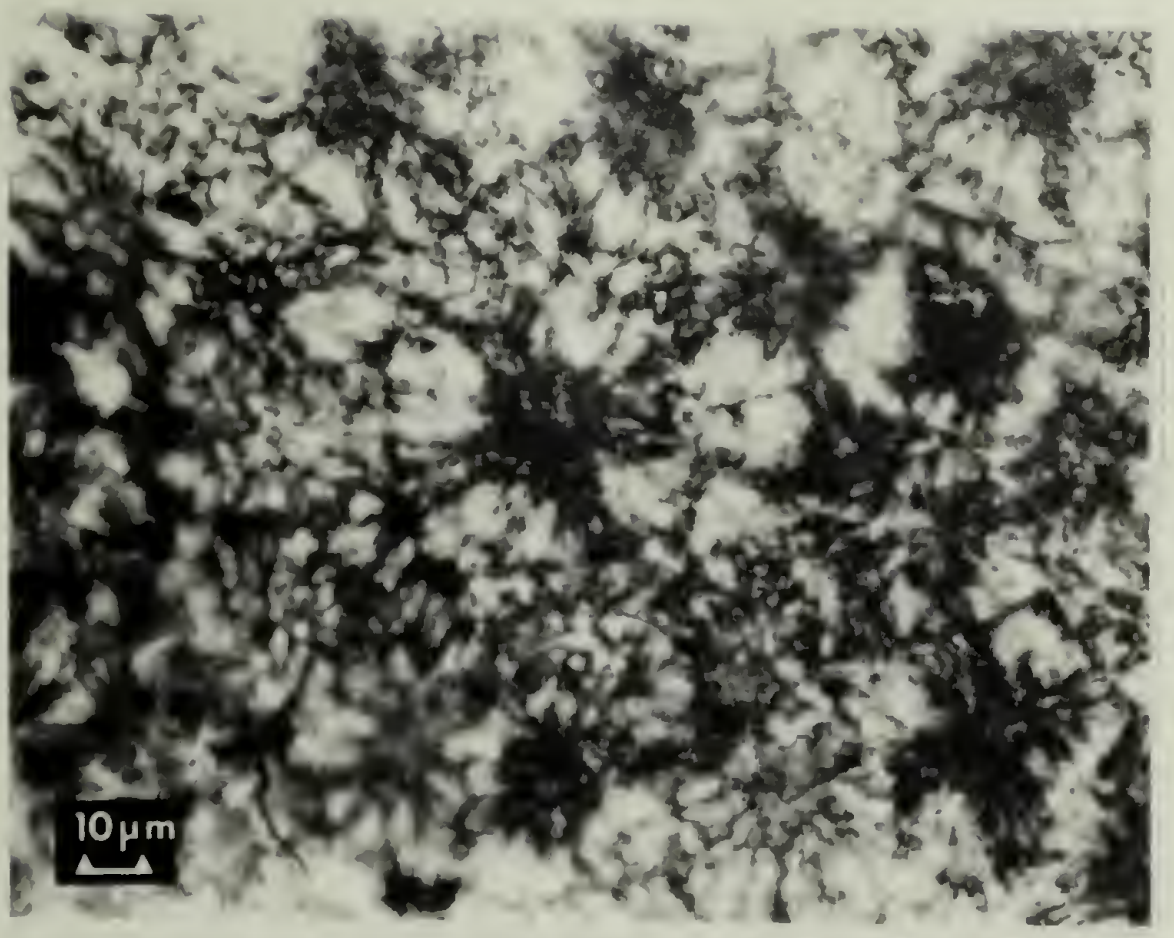

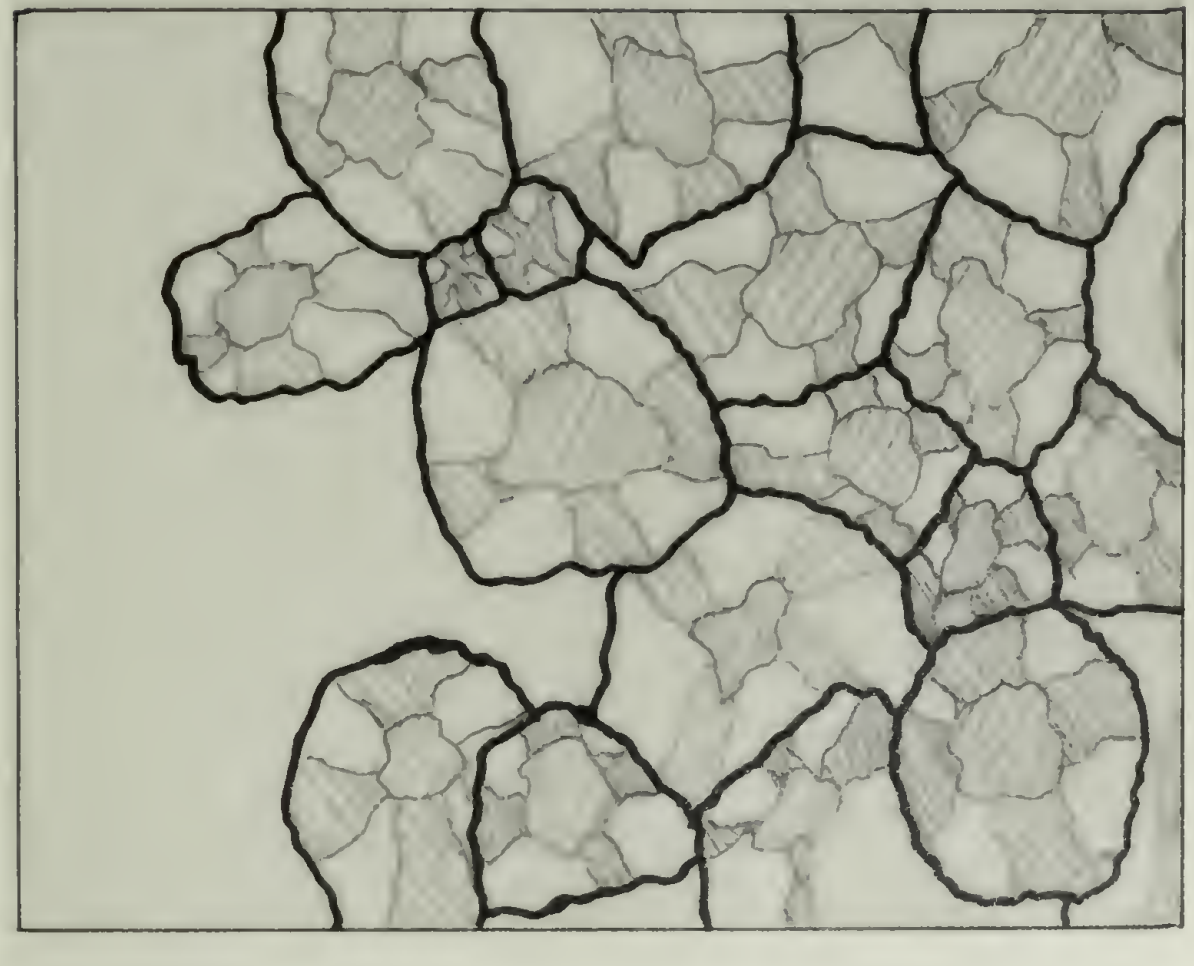

Figure 5.4-1b. Optical micrograph under crossed polars of sample N2-C showing spherulites with nonbirefringent centers of varying sizes and schematic of structures.

patterns (0°-90°) and negative birefringence. The interpenetration of hard segment-rich spherulites, shown in Figure 5.4-1a, hinder the visualization of individual spherulites. Samples taken from the mold surface (see Figure 5.4-1c,d) show that the hard segment-rich spherulite volume fraction has decreased substantially for the case of N1, and is essentially zero for N2. In addition, sample N2-S showed negatively birefringent maltese-cross patterns of about 100 μm in diameter. Both surface samples show the globules, previously seen by TEM, as weakly birefringent regions.

A hot stage experiment performed on N1-S is shown in the four sequential micrographs of Figure 5.4-2. A micrograph taken at 35°C shows 3 features: (i) zones of intense birefringence, (ii) small, well defined maltese-cross patterns, and (iii) zones of faint birefringence associated with the globules. Near the soft segment melting point (55°C) the intense birefringence due to the presence of soft segment organization has vanished and both the maltese-cross patterns and the globules are better defined. Upon further heating, the spherical structures begin to coalesce at approximately 150°C and their optical anisotropy vanishes. After annealing 10 minutes at 175°C, new hard segment-rich spherulites have nucleated in addition to the growth of already existing ones. Further heating to 220°C causes the melting of the hard segment-rich spherulites and renders the sample entirely isotropic. Interestingly, when the sample

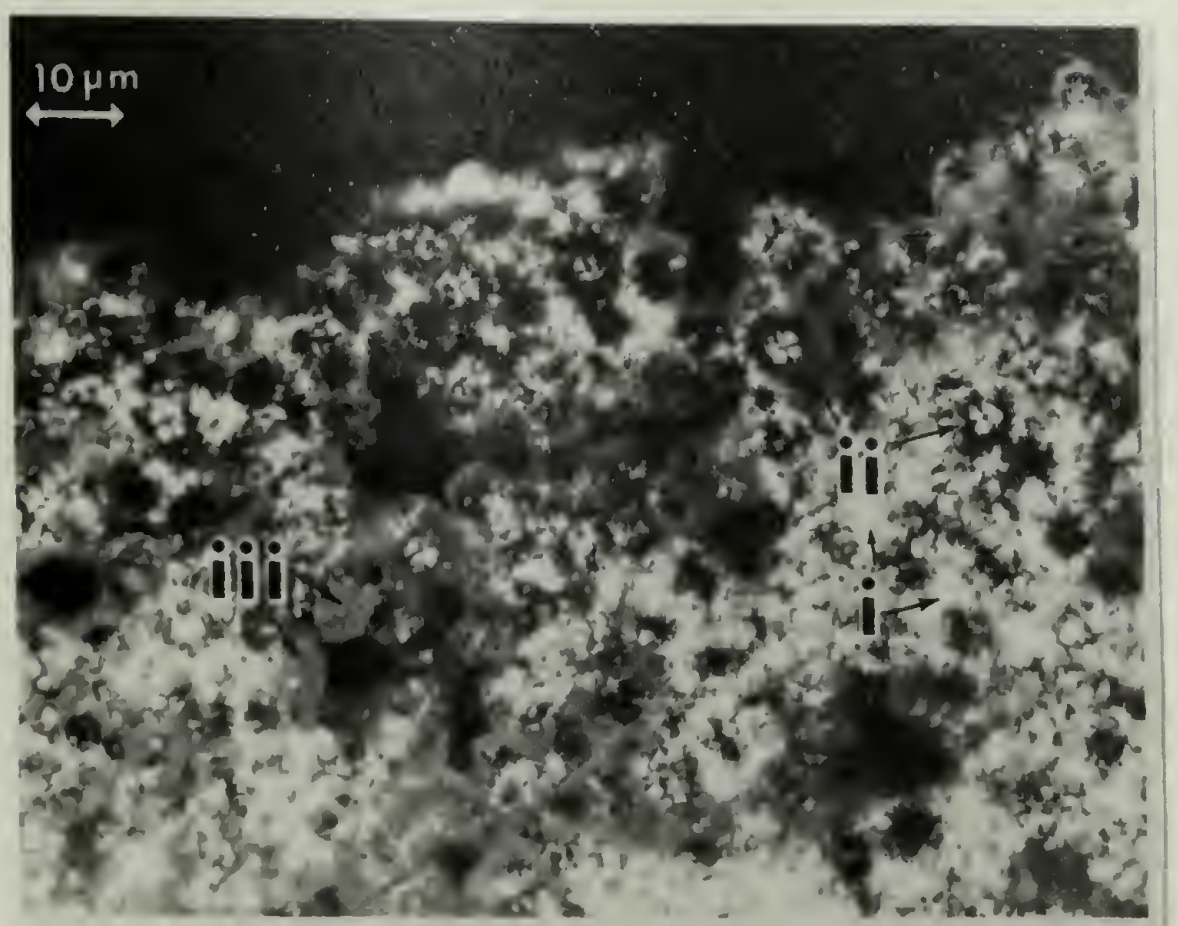

Figure 5.4-1c. Optical micrograph (crossed polars) of sample N1-S showing (i) intense soft segment birefringence, (ii) hard segment spherulites (maltese-cross patterns) and (iii) weakly birefringent globules.

Figure 5.4-1d. Optical micrograph under crossed polars of sample N2-S. Note presence of maltese cross pattern which vanishes at 53°C.

Figure 5.4-2. Heating experiment performed on sample N2-S. (a) 35°C, (b) 55°C. Soft segment birefringence has disappeared. Globules (i) and hard segment spherulites (ii) are clearly discernable. (c) At 150°C coalescence of globules and sample flow (arrow marking flow front). (d) At 175°C copious hard segment nucleation and spherulitic growth occurs.

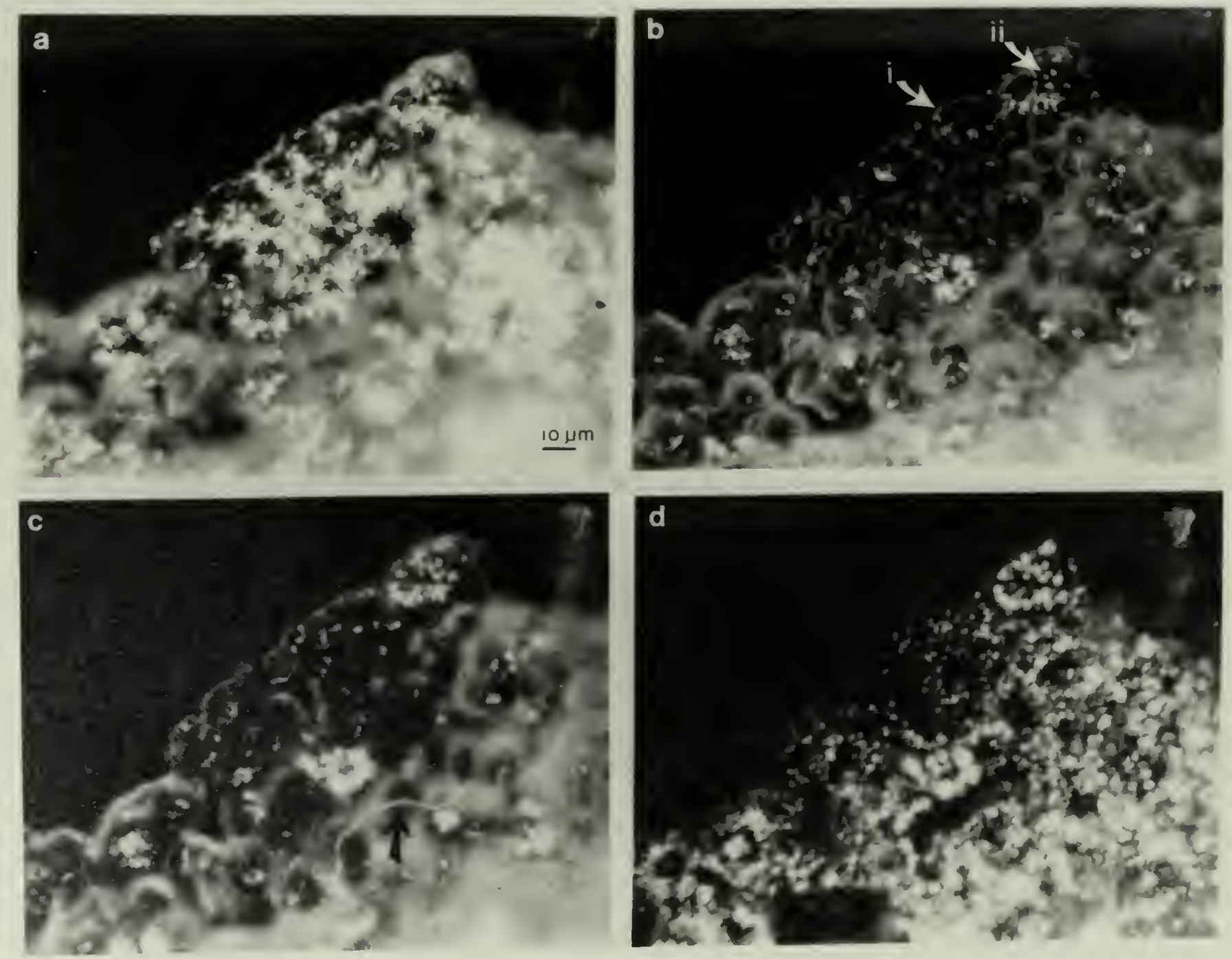
a
10 µm
b
i
ii
c
d

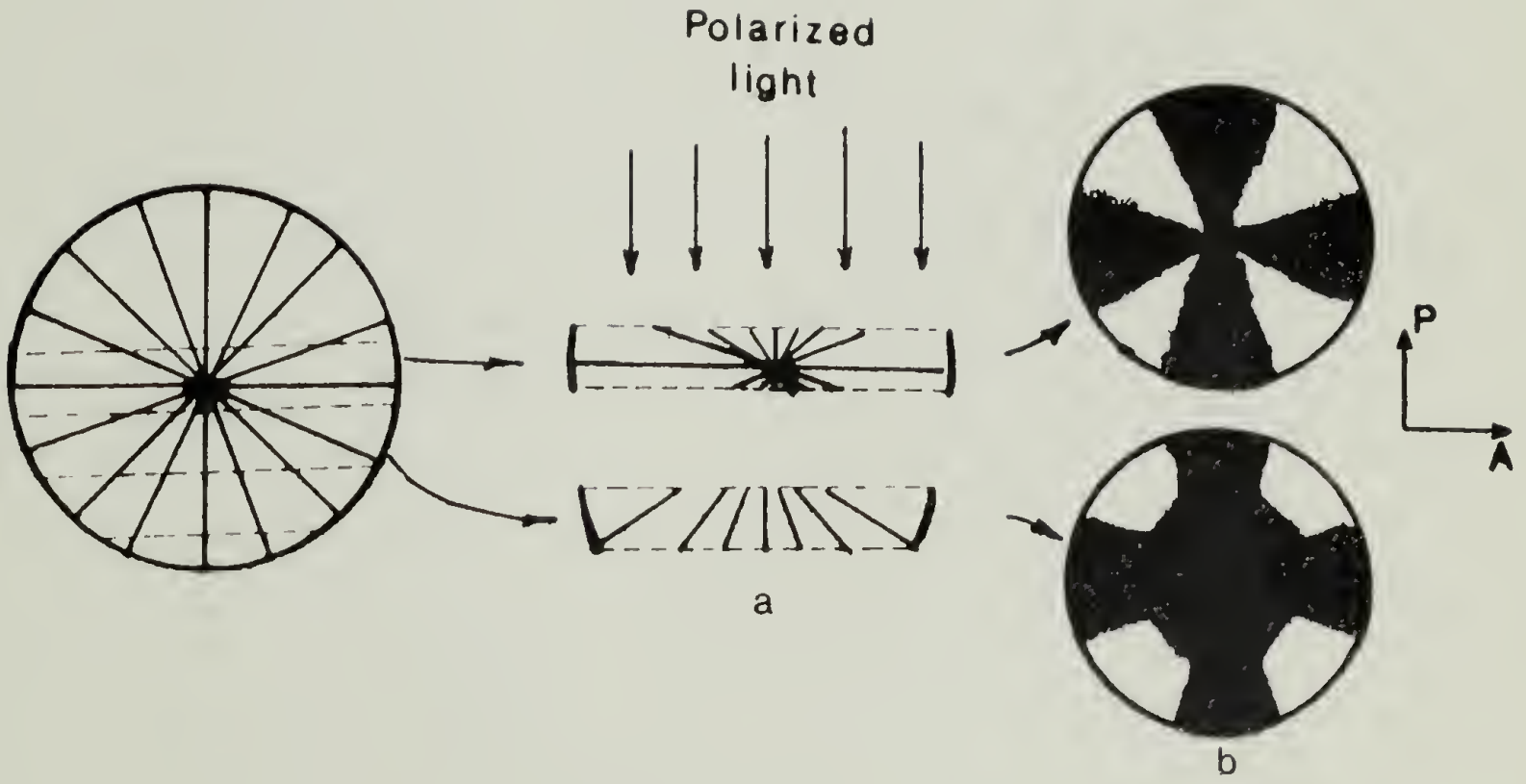

Figure 5.4-3. Schematic diagram of spherulite microtomed slices. (a) side view, (b) top view indicating origin of nonbirefringent centers.

is heated above the hard segment Tg promoting further appreciable crystallization, and later cooled down to room temperature, the birefringence due to soft segment organization is completely suppressed and the globules do not reappear.

The volume fractions of the different structures observed are given on Table 5.1-1.

5.5 Gel Permeation Chromatography

Lee and Macosko[78,86] have performed GPC experiments on the same N1 and N2 samples. Among their findings: (i) higher molecular weights are reached for samples reacted at higher temperatures (see Table 5.5-1); (ii) very large differences in molecular weight, roughly by a factor of two, can exist between the center and the surface of a sample subjected to a colder mold wall (N2); (iii) much of the difference in molecular weight between center and surface can be eliminated by heating the mold wall.

TABLE 5.5-1

MOLECULAR WEIGHT RESULTS[78,86]

Sample Designation	Intrinsic Viscosity (DMF)		GPC (THF)			Comments on THF Solution
	[η] (dl/g)	$\bar{M}v$	$\bar{M}n$	$\bar{M}w$	Poly-dispersity	
N1-C	0.359	21350	4260	9360	2.20	much insoluble
N1-S	0.362	21500	3540	9000	2.53	some sediment
N2-C	0.477	27500	--	--	--	much insoluble
N2-S	0.273	15500	4140	13660	3.3	--

C H A P T E R V I

DISCUSSION

The RIM samples N1 and N2 exhibit 4 distinct types of morphological structures:

- hard segment crystalline domains (and spherulites)
- soft segment crystalline domains
- surface and centerline globules
- noncrystalline matrix.

These structures show a strong positional dependence in the mold. Ordering of the hard segment is highest at the center of the mold and decreases at the surface. Conversely, soft segment crystallinity is highest at the surface and decreases at the center of the part. The globules are seen to be a significant fraction of the material near the surface but diminish near the centerline. The matrix volume fraction is small at the centerline but approaches 50% at the surface.

The variation in the type of structure from surface to centerline must be attributed to the different thermal history for each location, and subsequent molecular weight and segment distribution variations across the mold during the complex polymerization-phase separation-crystallization-solidification process.

The exothermic urethane reaction in conjunction with the poor thermal conductivity of the polymer mixture will result in an approximate adiabatic temperature rise at the mold centerline, whereas the surface region will remain approximately isothermal at the temperature set by the mold wall. The peak temperature at the centerline is nearly 100°C higher than the wall (see Figure 3.9-4). This centerline temperature is far above the Tm of the soft segment (55°C) but lies between the hard segment Tg and Tm (125 and 200°C respectively). Consequently, as polymerization proceeds and the hard segment sequence length builds to a sufficient size, hard segment agglomeration with subsequent crystallization and spherulite growth occurs. Because of the nature of the segmented chains, solidification (crystallization) of the longer hard segment sequences will dictate the agglomeration of the adjacent portions of the molecules containing the soft segment (see Figure 4.2-3). As well, noncrystallizable species (monomers, soft segment-rich molecules) must diffuse away from the growing spherulite. The reacting-solidifying system may be thought of as consisting of many component species, i.e., initially monomer and low molecular weight oligomers diminishing with reaction time as high molecular weight segmented polymer chains are formed. The mobility, compatibility and crystallizability of each of these species will depend on its respective sequence lengths and distributions as well as on the local

temperature history. When the local temperature drops below Tg of the hard segment, hard segment crystallization ceases and the mobility of the overall system greatly diminishes. The hard segment sequences near the surface, with essentially a low isothermal history, cannot aggregate and organize to form crystalline structures. Soft segment sequences do, however, have the required temperature history for their agglomeration and crystallization. Soft segment crystallinity is not as well organized as that of the hard segment--only large birefringent regions are visible via optical microscopy and no distinct spherulitic structures based on soft segment organization are seen. Well developed large scale soft segment organization is likely prevented by the hard segment rich regions which are immobile at the lower temperatures.

In addition to the featureless matrix spherical globules are observed both in N1 and N2 at the centerline, but predominantly at the surface. At the centerline these spherical regions are more electron dense than the surrounding matrix, have featureless interiors, do not appear to mutually coalesce, appear incompatible with both the hard segment-rich spherulites and the surrounding matrix. At the surface the globules are more volume filling and appear to be nearly equal in electron density with the matrix. If a sample (N2-S) containing such structure is dissolved in DMF and solution cast (3 hours at 50°C from 0.5% weight of

polymer in DMF) the globules completely disappear and volume filling hard segment-rich spherulites are observed, resembling spherulites seen in systems with same composition and different polymerization methods.[45] It is revealing that upon heating, hard segment crystallization takes place only after the globules have coalesced (circa 160°C). These appear to be feeding the growing hard segment-rich spherulites with crystallizable material (see Figure 5.4-2) and do not reappear upon cooling.

Taken as a whole, all the data suggest that the globules consist of a mixed phase, rich in glassy hard segment. Quite possibly the composition of the globules varies from surface to centerline. The detailed origin of these structures is not well understood at present but may be related to phase segregation occurring during polymerization[79,86] and nonuniform mixing of components.[62]

The present study indicates that under RIM conditions where large temperature gradients exist, distinct surface and centerline microstructures develop. Two structures on the scale of tens of microns, the hard segment based spherulites and the hard segment-rich glassy globules exist. Crystalline hard segment and soft segment domains on the scale of hundreds of Angstroms also occur, as well as a presumably mixed, noncrystalline (matrix) phase.

C H A P T E R V I I

CONCLUSIONS

7.1 Recapitulation

One goal of this thesis was to visualize hard segment domain structure in polyurethanes. We believe the staining technique has produced successful results. The preferential heavy atom tagging of the hard segments in films of solution cast PPO/MDI/BEDO polyurethane has permitted visualization of the phase separated microstructure. Hard segment domains have a fibrillar appearance. The matrix surrounding the fibrils is further comprised of a mixed phase of soft and unorganized hard segments, and a second predominantly soft segment phase. Because the solution casting process is rather slow the spherulites develop a radial variation of hard segment content. Slow spherulite growth enables the hard segment sequences to precipitate sequentially on the basis of their length, which leads to hard segment fibril branching during growth in order to accommodate the connecting soft segment units.

The second area of interest has been the characterization of polyurethane RIM morphology. This task, never previously undertaken, has yielded interesting results. Due to the exothermic nature of urethane polymerization and the

consequent development of mold temperature profiles as well as to the phase separation process that takes place during RIM polymerization, variables like molecular weight and segment distributions as well as type and size of morphological structures are strongly positionally dependent across a RIM part. By the same token, the physical properties of the material produced will be composite measures over the various structures.

Higher polymerization temperatures result in higher molecular weight polymer and promote better hard segment organization in the as-polymerized material. A new morphological feature, spherical structures, termed globules, are preferentially present near the mold surface. They are proposed to be regions of glassy hard segment-rich material which are unable to crystallize due to phase segregation during polymerization, low temperature and possibly insufficient mixing of components.

A multi-phased system was observed, with two scales of organization:

(i) on the order of 1-10 μm, corresponding to hard segment spherulites and hard segment-rich glassy domains.

(ii) on the order of 100Å, associated with hard segment spherulite fibrils and crystalline soft segment domains.

7.2 Generalizations and Possible Extensions of This Work

The ultimate goal of a morphological study lies in the elucidation of structure-property relationships of the materials investigated. Although this study has shed some light on the problems of phase separation and the influence of mold heat transfer conditions on the morphology of RIM polyurethanes, it represents only a start. The next step, namely the study of the relationships between morphology and physical and mechanical properties will help lead to the optimization of the RIM process. As previously discussed, high polymerization temperatures promote a higher degree of hard segment organization. The improved pseudocrosslinking action due to the presence of better formed hard segment domains should result in an increase in the modulus of the materials. Also, conditions favorable for hard segment organization will result in an amorphous soft segment matrix. This should bring about improved impact properties.

The conclusions of this work indicate that the presence of a steep temperature gradient across RIM parts has a severe effect on the morphology and molecular weight of the material. The development of temperature profiles can be diminished by maintaining the mold wall temperature at higher levels, making the system tend towards more isothermal behavior. In thick parts where heat buildup considerations cannot allow a hot mold wall, post-cure treatment at

suitable temperatures (e.g., 160-170°C) should help eliminate variations across the part.

Major points of interest still remain to be investigated, i.e., the study of orientation, mixing pattern morphology in relationship to impingement Reynolds number, as well as a more in-depth study including a variation in the ratio of reactants, catalyst concentration (gelation time), and post cure treatment.

Below we present specific suggestions for future study.

7.2-1 Crystallization kinetics of the pure hard segment MDI/BDO copolymer. In studying the solidification-crystallization process that takes place after RIM, we frequently encountered the problem of lack in basic knowledge on the kinetics of MDI/BDO crystallization. A study of this kind will provide insight into the relationship between temperature-time histories and the presence and size of hard segment crystalline structures, which at this moment are approached only qualitatively.

7.2-2 New polymer systems. (a) The presence of crystallinity in both soft (PCP/MDI copolymer) and hard (MDI/BDO copolymer) segments adds to the already complex interpretation of experimental data. The use of a polyether soft segment based on atactic poly(propylene oxide) which besides limiting the appearance of crystallinity to the hard segment,

would promote more complete phase separation due to its lower potential for hydrogen bond formation, is suggested.

(b) The increase in electron density provided to the hard segment phase by the heavy atom staining (OsO_4) of the unsaturated chain extender 1,4-butenediol (BEDO), has been shown in this study to be an extremely useful technique. The problem of visualizing mixing patterns and actual measurement of the striation thickness may be adequately studied by preparing a systematic series of RIM polyurethanes with varying compositions and impingement Reynolds numbers, based on the MDI/BEDO hard segment copolymer which can be later microtomed and stained with OsO_4.

7.2-3 Catalyst level and post cure treatments. Besides the variables already mentioned, the problems of catalyst concentration, which governs gel time of the reacting mixture, and post-cure treatment (annealing time and temperature and cooling rate to ambient temperature), should yield important information contributing to the optimization of RIM polyurethanes.

7.2-4 Additional experimental techniques. In addition to the experimental techniques used in this thesis, the following experimental techniques will aid in the morphological characterization.

(a) Small angle light scattering. To characterize spherulite size and optical anisotropy.

(b) Small angle x-ray scattering. To acquire further evidence of phase separation and average center to center spacing of hard segment phases.

(c) X-ray microanalysis. Samples of the specially prepared polyurethane PPO/MDI/BEDO after being exposed to the action of a staining agent (Cl_2) will help in providing mapping of the size and shape of the phase separated microstructures, as well as assessing the differential concentration of hard segment material in given areas of a sample. Provided that spatial resolution of the generated characteristic x-ray signal is smaller than the hard segment domain size or the average interdomain spacing, one can determine whether a given image contains chlorine and hence hard segment.

(d) Mechanical property measurement. Mechanical testing of RIM materials on the basis of mold location (skin-core) will contribute to the understanding of the structure property relationship. Stress-strain measurements, as well as flex modulus and sag--particularly at high temperatures (75°C)--are recommended.

(e) A further investigation on the appearance of nonbirefringent central regions in microtomed spherulitic polyurethanes should be pursued in a better understood crystalline polymer system. The gradual transition of nonbirefringence as well as its size should correlate to the position of the slice with respect to the spherulite center.

REFERENCES

1. S.L. Aggarwal, Polymer 17, 938 (1976). "Structure and Properties of Block Polymers and Multiphase Polymer Systems: An Overview of Present Status and Future Potential."

2. J.F. Beecher, L. Marker, R.D. Bradford, and S.L. Aggarwal, J. Poly. Sci. C26, 117 (1969). "Morphology and Mechanical Behavior of Block Copolymers."

3. D.J. Prepelka and J.L. Wharton, J. Cellular Plastics, 87 (1975). "Reaction Injection Molding in the Automotive Industry."

4. P.J. Cacciotti, J. Elastoplastics 5, 74 (1973). "Microcellular Urethanes in Automotive Exterior Parts."

5. F.W. Pahl, Soc. Auto. Eng. Meeting, Toronto, Oct. 1974, #741026. "Processing and Engineering of Polyurethane Technology for the Automotive Industry."

6. S.H. Metzger and D.J. Prepelka, J. Elast. and Plast. 8, 141 (1976). "Progress in RIM Technology."

7. D.J. Prepelka, Modern Plastics Encyclopedia 54, 356 (1977). "Reaction Injection Molding.

8. E. Broyer and C.W. Macosko, AIChE Journal 22, 268 (1976). "Heat Transfer and Curing in Polymer Reaction Molding."

9. E. Broyer, C.W. Macosko, F.E. Critchfield and L.R. Lawler, Polymer Eng. Sci. 18, 382 (1978). "Curing and Heat Transfer in Polyurethane Reaction Molding."

10. D.G. Leis, Modern Plastics Encyclopedia, McGraw-Hill 346 (1976). "Reaction Injection Molding."

11. J.D. Domine and C.G. Gogos, Soc. Plast. Eng. Tech. Papers 22, 274 (1976). "Computer Simulation of Injection Molding of a Reacting Linear Condensation Polymer."

12. S.C. Malguarnera and N.P. Suh, Polym. Eng. Sci. 17, 111 (1977). "Liquid Injection Molding System I. An Investigation of Impingement Mixing."

13. S.C. Malguarnera and N.P. Suh, Polym. Eng. Sci. 17, 116 (1977). "Liquid Injection Molding System II. Mechanical Design and Characterization of a RIM Machine."

14. C.L. Tucker and N.P. Suh, Soc. Plast. Eng. Tech. Papers 24, 158 (1978). "Impingement Mixing--A Fluid Mechanical Approach."

15. N.S. Schneider, C.R. Desper, J.L. Illinger, A.O. King, and D. Barr, J. Macro. Sci. B11, 527 (1975). "Structural Studies of Crystalline MDI-Based Polyurethanes."

16. S.B. Clough and N.S. Schneider, J. Macro. Sci. B2, 553 (1968). "Structural Studies on Urethane Elastomers."

17. R. Bonart, J. Macro. Sci. B2, 115 (1968). "X-Ray Investigations Concerning the Physical Structure of Crosslinking in Segmented Urethane Elastomers."

18. R. Bonart, L. Morbitzer, and E.H. Müller, J. Macro. Sci. B9, 447 (1974). "X-Ray Investigations Concerning the Physical Structure of Crosslinking in Urethane Elastomers. III. COmmon Structure Principles for Extensions with Aliphatic Diamines and Diols."

19. R. Bonart, L. Morbitzer, and G. Hentze, J. Macro. Sci. B3, 337 (1968). "X-Ray Investigations Concerning the Physical Structure of Crosslinking in Urethane Elastomers. II. Butanediol as Chain Extender."

20. I. Kimura, H. Ishihara, K. Saito, and H. Ono, Rpts. Prog. Polymer Phys. Japan 13, 205 (1970). "Property and Structure of Segmented Polyurethane. III. X-Ray Study on Orientation of Hard Segment."

21. R.R. Lagasse, J. Appl. Poly. Sci. 21, 2489 (1977). "Domain Structure and Time Dependent Properties of a Crosslinked Urethane Elastomer."

22. C.E. Wilkes and C.S. Yusek, J. Macro. Sci. B7, 157 (1973). "Investigations of Domain Structure in Urethane Elastomers by X-Ray and Thermal Methods."

23. S.L. Samuels and G.L. Wilkes, J. Polym. Sci. Symposium #43, 149 (1973). "The Rheo-Optical and Mechanical Behavior of a Systematic Series of Hard-Soft Segmented Urethanes."

24. I. Kimura, H. Ishihara, and H. Ono, Macromol. 7, 355 (1974). "Morphology and Deformation Mechanism of Segmented Poly(urethane ureas) in Relation to Spherulitic Crystalline Textures."

25. R.R. Lagasse and K.B. Wischmann, ACS Organic Coatings and Plastics Preprints 37, 501 (1977). "Castable Thermoplastic Urethane Elastomers. II. Structure Property Correlation."

26. S.B. Clough, N.S. Schneider, and A.O. King, J. Macro. Sci. B2, 641 (1968). "Small Angle X-Ray Scattering From Polyurethane Elastomers."

27. G.L. Wilkes and J.A. Emerson, J. Appl. Physics 47, 4261 (1976). "Time Dependence of Small Angle X-Ray Measurement on Segmented Polyurethanes Following Thermal Treatment."

28. S.L. Samuels and G.L. Wilkes, Polymer Letters 9, 761 (1971). "Anisotropic Superstructure in Segmented Polyurethanes as Measured by Photographic Light Scattering."

29. R.W. Seymour and S.L. Cooper, Macromol. 6, 48 (1973). "Thermal Analysis of Polyurethane Block Copolymers."

30. N.S. Schneider and C.S. Paik Sung, Polymer Engr. and Sci. 17:2, 73 (1977). "Transition Behavior and Phase Segregation in TDI Polyurethanes."

31. G.M. Estes, R.W. Seymour, and S.L. Cooper, Macro. 4, 452 (1971). "Infrared Studies of Segmented Polyurethane Elastomer. II. Infrared Dichroism."

32. M.F. Froix and J.M. Pochan, J. Poly. Sci. 14, 1047 (1976). "Phase Structure in a Polyurethane above Soft Segment Tg via Calorimetric and NMR Techniques."

33. R.A. Assink, J. Poly. Sci. 15, 59 (1977). "The Study of Domain Structure in Polyurethanes by NMR."

34. J.A. Koutsky, N.V. Hein, and S.L. Cooper, J. Poly. Sci. (Letters) 8, 353 (1970). "Some Results on Electron Microscope Investigations of Polyether-Urethane and Polyester-Urethane Block Copolymers."

35. G.L. Wilkes, S.L. Samuels, and R. Crystal, J. Macro. Sci. B10, 203 (1974). "Scanning and Transmission Electron Microscopy Studies on a Model Series of Spherulitic Segmented Polyurethanes."

36. I. Kimura, H. Ishihara, K. Saito, K. Tamaki, and H. Ono, Rpts. Prog. Polymer Phys. Japan 13, 209 (1970). "Property and Structure of Segmented Polyurethane. IV. Aggregation Structure of Hard Segments."

37. I. Kimura, H. Ishihara, and H. Ono, Macromol. Prepr. 1, 525 (1971). "Morphology and Deformation Mechanism of Segmented Polyurethanes in Relation to Spherulite Crystalline Texture."

38. P.J. Corish, Rubber Chem. Tech. 40(2), 324 (1967). "Fundamental Studies of Rubber Blends."

39. S.B. Clough and N.S. Schneider, U.S. Army Tech. Report 6777CM, Natick Labs, Natick, Mass.

40. R.F. Fedors, J. Poly. Sci. C(26), 189 (1969). "Cross-linked Block Copolymers."

41. D.J. Meier, J. Poly. Sci. C(26), 81 (1969). "Theory of Block Copolymers. I. Domain Formation in A-B Block Copolymers."

42. T. Indue, Polymer Letters 6, 75 (1978). "Electron Microscopic Texture of A-B Block Copolymers of Isoprene and Styrene."

43. E.B. Bradford and E. Vanzo, J. Poly. Sci. (A-1)6, 1661 (1968). "Ordered Structures of Styrene-Butadiene Block Copolymers in the Solid State."

44. S.L. Cooper, R.W. Seymour, and J.C. West, in Encyclopedia of Polymer Science, Suppl. Vol. 1, 521 (1976).

45. A.L. Chang and E.L. Thomas, ACS Adv. in Chem. #176, 31 (1979). "Morphological Structure of PCP/MDI/BDO Based Segmented Polyurethanes."

46. J. Blackwell and K.H. Gardner, Polymer 20, 13 (1979). "Structure of the Hard Segments in Polyurethane Elastomers."

47. L.L. Harrell, Jr., Macromolecules 2, 607 (1969). "Segmented Polyurethanes: Properties as a Function of Segment Size and Distribution."

48. Y. Chatani, Y. Okita, H. Tadokoro, and Y. Yamashita, Polymer J. 1, 555 (1970). "Structural Studies of Polyesters. III. Crystal Structure of Poly-ε-Caprolactone."

49. C.G. Seefried, Jr., J.V. Koleske, and F.E. Critchfield, J. Appl. Poly. Sci. 19, 2493 (1975). "Thermoplastic Urethane Elastomers. I. Effects of Soft Segment Variations."

50. S.L. Cooper and A.V. Tobolsky, J. Appl. Poly. Sci. 10, 1837 (1966). "Properties of Linear Elastomeric Polyurethanes."

51. R. Seymour, G. Estes and S. Cooper, Macromolecules 3, 579 (1970). "Infrared Studies of Segmented Polyurethane Elastomers. I. Hydrogen Bonding."

52. G. Estes, R. Seymour and S. Cooper, ACS Poly. Prepr. 11, 516 (1970). "Infrared Dichroism of Segmented Polyurethane Elastomers."

53. R. Seymour, G. Estes and S. Cooper, ACS Poly. Prepr. 11, 869 (1970). "Hydrogen Bonding in Segmented Polyurethane Elastomers."

54. C. Sung and N.S. Schneider, ACS Poly. Prepr. 15, 625 (1974). "Infra-Red Studies of Hydrogen Bonding in TDI Based Polyurethanes."

55. G.W. Miller, and J.H. Saunders, J. Poly. Sci. A1, 1923 (1970). "Thermal Analyses of Polymers. III. Influence of Isocyanate Structure on the Molecular Interactions in Segmented Polyurethanes."

56. H.K. Frensdorff, Macro. 4:4, 369 (1971). "Block-Frequency Distribution of Copolymers."

57. R.J. Cella, J. Poly. Sci. Symposium #42, 727 (1973). "Morphology of Segmented Polyester Thermoplastic Elastomers."

58. L.H. Peebles, Jr., Macromol. 9, 58 (1976). "Hard Block Length Distribution in Segmented Block Copolymer."

59. R.W. Lenz, Organic Chemistry of Synthetic High Polymers, Interscience Pub. Co., N.Y. (1967), p. 78.

60. T.H. Rogers and W.O. Sassman, J. Elast. and Plast. 6, 253 (1974). "Applications of Elastomeric Urethanes in Industrial Products."

61. L.J. Lee and C.W. Macosko, Soc. Plast. Engineers Tech. Papers 24, 151 (1978).

62. L.J. Lee, J.M. Ottino, W.E. Ranz and C.W. Macosko, Polym. Eng. Sci., Submitted. "Impingement Mixing in Reaction Injection Molding."

63. R.E. Fruzzetti, J.M. Hogan, F.J. Murray and J.R. White, Soc. Auto. Eng. Meeting, Detroit, Sept. 1977 Paper #770839. "Factors Affecting the Quality of Impingement Mixed RIM Urethanes."

64. E.B. Richter and C.W. Macosko, Polym. Eng. Sci. 18, 1012 (1978). "Kinetics of Fast (RIM) Urethane Polymerization."

65. S.D. Lipshitz and C.W. Macosko, J. Appl. Polym. Sci. 21, 2029 (1977). "Kinetics and Energetics of a Fast Polyurethane Cure."

66. F. Lopez-Serrano, M.V. Tirrell and C.W. Macosko, Department of Chemical Engineering and Materials Science, University of Minnesota. In preparation (1978).

67. Dong S. Huh and Stuart L. Cooper, Polymer Engr. and Sci. 11, 369 (1971). "Dynamic Mechanical Properties of Polyurethane Block Polymers."

68. K. Kato, J. Electron Microscopy (Japan) 19, 1 (1970). "Osmium Tetroxide Procedure as Applied to Synthetic Polymer Materials."

69. K. Kato, Polym. Eng. and Sci. 7(1), 38 (1967). "Osmium Tetroxide Procedure for Light and Electron Microscopy of ABS Plastics."

70. R. Criegee, Ann. Chem. 75, 522 (1936). "Osmic Acid Esters as Intermediate Products in Oxidation."

71. W. Stoeckenius and S.C. Mahr, Lab. Investigation 14(№6), 458 (1965). "Studies on the Reaction of Osmium Tetroxide with Lipids and Related Compounds."

72. Fieser and Fieser, Reagents for Organic Synthesis, J. Wiley and Sons (1967), pp. 759-764.

73. M.L. Evans, F.E. Critchfield and R.M. Gerkin, J. Cell. Plast., July, 235 (1976). "Factors Affecting the Modulus and Relaxation Properties of Liquid Reaction Molded Urethane Elastomers."

74. D.T. Grubb, J. Mats. Sci. 9, 1715 (1974). "Radiation Damage and Electron Microscopy of Organic Polymers."

75. E.L. Thomas and Y. Talmon, Polymer 19, 225 (1978). "Selective Electron Beam Etching of Multicomponent Polymer Systems."

76. W.J. MacKnight, M. Yang, and T. Kajiyama, Polymer Prep 9:1, 860 (1968). "Differential Scanning Calorimetry of Polyurethanes."

77. L.J. Lee and C.W. Macosko, Soc. Plast. Eng. Tech. Papers 24, 155 (1978). "Curing Studies on RIM (Reaction Injection Molding)."

78. L.J. Lee, University of Minnesota, Ph.D. Dissertation (1979).

79. A.E. Nesterov, T.E. Lipatova, K. Dusek, Z. Pelzbauer, M. Houska, J. Hradil and Y.S. Lipatov, Makromolecu-lare Chemie 52, 39 (1972). "Formation of Polyure-thane Networks Based on Poly(Propylene Glycol) and 4,4'-Diphenylmethane Diisocyanate."

80. V. Crescenzi, G. Manzini, C. Calzolaroli and C. Borri, Eur. Polym. J. 8, 449 (1972). "Thermodynamics of Fusion of Poly-β-Propiolactone and Poly-ε-Capro-lactone."

81. C.G. Seefried, Jr., J.V. Koleske, and F.E. Critchfield, J. Appl. Poly. Sci. 19, 2503 (1975). "Thermoplastic Urethane Elastomers. II. Effects of Variations in Hard Segment Concentration."

82. E. Underwood, Quantitative Stereology. Addison-Wesley Pub. Co. (1970), Chapter 2.

83. Proceedings of the Second International Congress for Stereology. H. Elias, E. Underwood, Ed., Springer-Verlag, N.Y. (1967), pp. 52, 53.

84. C.G. Seefried, Jr., J.V. Koleske, F.E. Critchfield, and J.L. Dodd, Polymer Engr. and Sci. 15, 646 (1975). "Thermoplastic Urethane Elastomers. IV. Effects of Cycloaliphatic Chain Extender on Dynamic Mechanical Properties."

85. A.L. Chang, University of Massachusetts, private communication.

86. M.V. Tirrell, L.J. Lee, C.W. Macosko, Am. Chem. Soc. Symp. Series, Submitted (1979). "Conversion and Composition Profiles in Polyurethane Reaction Molding."

A P P E N D I X

Some care must be exercised in the interpretation of light optical images of microtomed samples. Figure 5.4-1b reveals the appearance of hard segment-rich spherulites with nonbirefringent centers of varying sizes. This is in good agreement with previous observations by Schneider et al.,[15] and can be accounted for with the following rationale. We envision the spherulite as consisting of uniformly radiating structures (see Figure 5.4-3). The relative location of progressive microtomed slices with respect to the spherulite center will give rise to entirely different polarized light images. Assuming a normal birefringent spherulite, a slice containing the spherulite nucleus will display the conventional maltese-cross pattern, but as the slice is taken farther apart from the spherulite center it will be increasingly less birefringent and exhibit complete azimuthal extinction near its center since the slice is nearly uniaxial in that vicinity. The periphery of the slice will exhibit the normal maltese-cross (see Figure 5.4-3).